| REPORT DOCUMENTATION PAGE | Form Approved OMB No. 0704-0188 |
|---|---|

Public reporting burden for this collection of information is estimated to average 1 hour per response, including the time for reviewing instructions, searching existing data sources, gathering and maintaining the data needed, and completing and reviewing the collection of information. Send comments regarding this burden estimate or any other aspect of this collection of information, including suggestions for reducing this burden, to Washington Headquarters Services, Directorate for Information Operations and Reports, 1215 Jefferson Davis Highway, Suite 1204, Arlington, VA 22202-4302, and to the Office of Management and Budget, Paperwork Reduction Project (0704-0188), Washington, DC 20503.

| 1. AGENCY USE ONLY *(Leave blank)* | 2. REPORT DATE | 3. REPORT TYPE AND DATES COVERED |
|---|---|---|
| | 7.Jan.99 | THESIS |

**4. TITLE AND SUBTITLE**
COMPARISIONS OF OBSERVATIONS BY WSR-88D AND HIGH RESOLUTION MOBILE DOPPLER RADAR IN TORNADOES AND A HURRICANE

**5. FUNDING NUMBERS**

**6. AUTHOR(S)**
CAPT WINSLOW JENNIFER L

**7. PERFORMING ORGANIZATION NAME(S) AND ADDRESS(ES)**
UNIVERSITY OF OKLAHOMA

**8. PERFORMING ORGANIZATION REPORT NUMBER**

**9. SPONSORING/MONITORING AGENCY NAME(S) AND ADDRESS(ES)**
THE DEPARTMENT OF THE AIR FORCE
AFIT/CIA, BLDG 125
2950 P STREET
WPAFB OH 45433

**10. SPONSORING/MONITORING AGENCY REPORT NUMBER**
FY99-41

**11. SUPPLEMENTARY NOTES**

**12a. DISTRIBUTION AVAILABILITY STATEMENT**
Unlimited distribution
In Accordance With AFI 35-205/AFIT Sup 1

**12b. DISTRIBUTION CODE**

**13. ABSTRACT** *(Maximum 200 words)*

19990120 024

**14. SUBJECT TERMS**

**15. NUMBER OF PAGES**
109

**16. PRICE CODE**

| 17. SECURITY CLASSIFICATION OF REPORT | 18. SECURITY CLASSIFICATION OF THIS PAGE | 19. SECURITY CLASSIFICATION OF ABSTRACT | 20. LIMITATION OF ABSTRACT |
|---|---|---|---|
| | | | |

## Abstract

This study compares observations from the Doppler on Wheels (DOW) radar and the WSR-88D radars to identify any features that are important to forecasting that the WSR-88D may be missing. WSR-88D and DOW data were compared for the Dimmitt Tornado on 2 June 1995 (during VORTEX 95), the Rolla Tornado on 31 May 1996, and Hurricane Fran on 5-6 September 1996.

For Hurricane Fran, the reflectivity features and velocity features were compared. Small scale features in the wind field, believed to be sub-kilometer scale boundary layer rolls were discovered. It has been suggested that these are responsible for some of the small scale intense damage found in the aftermaths of some hurricanes. These rolls were also visible in the KLTX data but were not as well defined.

For the two tornado cases the strength (the difference between the maximum inbound velocity and the maximum outbound velocity) were examined. As expected the strength observed by the WSR-88D was about 50% less than that observed by the DOW. This was compared with predictions of Burgess (1993).

UNIVERSITY OF OKLAHOMA

GRADUATE COLLEGE

# COMPARISONS OF OBSERVATIONS BY WSR-88D AND HIGH RESOLUTION MOBILE DOPPLER RADAR IN TORNADOES AND A HURRICANE

A THESIS

SUBMITTED TO THE GRADUATE FACULTY

In partial fulfillment of the requirements for the

Degree of

MASTER OF SCIENCE

Jennifer Lynn Winslow
Norman, Oklahoma
1998

DTIC QUALITY INSPECTED 8

# COMPARISONS OF OBSERVATIONS BY WRS-88D AND HIGH RESOLUTION MOBILE DOPPLER RADAR IN TORNADOES AND A HURRICANE

A THESIS APPROVED FOR THE
SCHOOL OF METEOROLOGY

BY

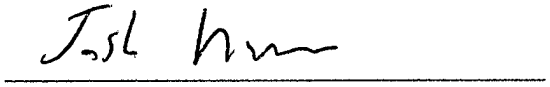

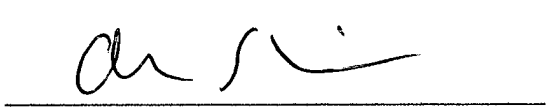

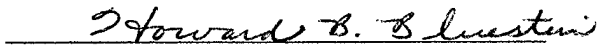

cCopyright by JENNIFER L. WINSLOW 1998
All Rights Reserved.

# ACKNOWLEDGEMENTS

First I would like to thank my committee Josh Wurman, Al Shapiro, and Howie Bluestein, for guiding me through the program. I would especially like to thank my advisor for giving me the opportunity to work with a data set that was the only one of its kind. I would like to thank the Air Force for funding me and providing me with the opportunity to continue my education.

I would like to thank the Staff of the School of Meteorology, including Nancy Agrawal, Celia Jones, Marcia Pallutto, and Alyssa Shulter. They are number one and no one at the school of would get through without them. A big thank to Tom Condo who constantly fixed the computers I managed to crash (not only my computer but the rest of the computers in the office as well).

I would like to thank my good friends who have put up with me these last two years and been there when I needed someone to talk to, especially Chris Stock, Eric Kemp, Steve Strum, and Chris Weiss. I would also thank Chris Weiss, Steve Strum, and Eric Kemp for proofreading my thesis for me. That could not have been fun, but it greatly improved the document. A thank you goes out to my officemates who had to put up with me, including Swarn Gill, Steve Mc Donald and Ed Alderman. I would like to thank the rest of my fellow graduate students. I have met some great people and take away some great memories.

I would like to thank my brother Jefferey who has always been there when I needed a friend. Most of all I would like to thanks my parents who have stood been behind me, even through my craziest of dreams. I believe my mother's comment was: "Chase tornadoes and hurricanes? WHY?" They also provided the moral support needed when things got tough (including the praying bear that was at my seminar and defense). Thank you both very much, I could not have made it through this program without you!

# TABLE OF CONTENTS


| | PAGE |
|---|---|
| 1. Introduction | 1 |
| 2. Hurricane Fran | 3 |
| 2.1. Introduction | 3 |
| 2.2. Hurricane Fran | 5 |
| 2.3. WSR-88D (KLTX) and Doppler on Wheels (DOW) | 6 |
| 2.4. Reflectivity | 9 |
| 2.5. Wind Field of Hurricane Fran | 12 |
| 2.5.1. Introduction | 12 |
| 2.5.2. Peak Wind versus Time | 13 |
| 2.5.3. Wind Direction versus Height | 17 |
| 2.5.4. Wind Direction versus Time | 18 |
| 2.6. Rolls | 19 |
| 2.6.1. Introduction | 19 |
| 2.6.2. General Description of Rolls | 21 |
| 2.6.3. Amplitude of Rolls | 21 |
| 2.6.4. Wavelength of Rolls | 26 |
| 2.6.5. Dependence on Wind Speed | 28 |
| 3. Tornadoes | 32 |
| 3.1. Introduction | 32 |
| 3.2. Dimmitt | 35 |
| 3.3. Rolla | 39 |
| 4. Conclusions | 44 |
| 4.1. Hurricane Fran | 44 |
| 4.2. Tornadoes | 46 |

# List of Figures


| FIGURE | | PAGE |
|---|---|---|
| 2.1 | Location of Doppler on Wheels (DOW and the Wilmington WSR-88D (KLTX) during Hurricane Fran 5-6 September 1996..... | 48 |
| 2.2 | KLTX and DOW reflectivity at 1908 UTC..... | 49 |
| 2.3 | Rain band approaching the DOW about 2136 UTC..... | 50 |
| 2.4 | Rain band in DOW reflectivity field and hour before eye passage..... | 51 |
| 2.5 | The eye of Hurricane Fran as it passes to the east of KLTX..... | 52 |
| 2.6 | Eye of Hurricane Fran in DOW reflectivity field..... | 53 |
| 2.7 | Weak rain band in eye of Hurricane Fran..... | 54 |
| 2.8 | DOW peak wind versus time for 1.0-3.0 degree scans..... | 55 |
| 2.9 | DOW peak wind versus time for 5.0-20.0 degree scans..... | 56 |
| 2.10 | DOW peak wind versus time for inbound and outbound sides..... | 57 |
| 2.11 | KLTX peak wind versus time for 1.0 degree scan for inbound and outbound sides..... | 58 |
| 2.12 | KLTX peak wind versus time for 10.0 degree scan for inbound and outbound sides..... | 59 |
| 2.13 | Peak wind versus time for inbound side of KLTX and the DOW using the 1 degree scan..... | 60 |
| 2.14 | DOW wind direction versus height at 2059 UTC..... | 61 |
| 2.15 | DOW wind directon versus height at 2038 UTC..... | 62 |
| 2.16 | KLTX wind direction versus height at 2131 UTC..... | 63 |
| 2.17 | KLTX wind direction versus height at 2331 UTC..... | 64 |
| 2.18 | KLTX wind direction versus height at 0102 UTC..... | 65 |

2.19 DOW and KLTX wind direction versus time at 1 km..... 66

2.20 KLTX and DOW wind direction versus time at 5 km..... 67

2.21 Boundary layer rolls in DOW velocity field during Hurricane Fran..... 68

2.22 Schematic representation of boundary layer rolls..... 69

2.23 DOW roll amplitude versus time for the inbound side..... 70

2.24 DOW roll amplitude versus time for inbound and outbound sides using the 1.0 degree scan..... 71

2.25 DOW roll amplitude versus time for the inbound and outbound sides using the 5.0 degree scan..... 72

2.26 KLTX roll amplitude versus time for the inbound side..... 73

2.27 KLTX roll amplitude versus time for the outobund side..... 74

2.28 KLTX roll amplitude versus time for the inbound side using the 2.0 degree scan..... 75

2.29 KLTX and DOW roll amplitude versus time for the outbound side using the 2.0 degree scan..... 76

2.30 DOW wavelength versus time for the inbound side..... 77

2.31 DOW wavelength versus time for the outbound side..... 78

2.32 DOW and KLTX wavelength versus time for the outbound side using the 1.0 degree scan..... 79

2.33 KLTX wavelength versus time for the inbound side..... 80

2.34 KLTX wavelength versus time for the inbound and outbound sides..... 81

2.35 KLTX wavelength versus time for the outbound side..... 82

2.36 DOW peak wind versus roll amplitude for the inbound side using the 3.0 degree scan..... 83

2.37 Peak wind versus roll amplitude for inbound side using the 5.0 degree scan..... 84

2.38 DOW peak wind and roll amplitude versus time for the inbound side using the 2.0 degree scan..... 85

2.39 DOW peak wind and roll amplitude versus time for the inbound side using the 5.0 degree scan..... 86

2.40 DOW roll amplitude and peak wind versus time for the outbound side using the 1.0 degree scan..... 87

2.41 KLTX peak wind versus roll amplitude for the inbound side using the 3.0 degree..... 88

2.42 KLTX peak wind and roll amplitude versus time for the inbound side using the 1.0 degree scan..... 89

2.43 KLTX peak wind and roll amplitude versus time for the outbound side using the 1.0 degree scan..... 90

3.1 Illustration of the Radar Horizon and Aspect Ratio Problems for radar... 91

3.2 The Dimmitt Tornado observed by the KLBB and DOW..... 92

3.3 DOW strength versus time for the 0.0 degree scan..... 93

3.4 DOW strength versus time for the 1.0 degree scan..... 94

3.5 DOW strength versus time for the 12.0 degree scan..... 95

3.6 DOW strength versus time for the 14.0 degree scan..... 96

3.7 DOW strength versus time for the 18.0 degree scan..... 97

3.8 KLBB strength versus time for the 1.5 degree scan..... 98

3.9 KLBB strength versus time for the 4.3 degree scan..... 99

3.10 Reflectivity from the Roll Tornado..... 100

3.11 DOW strenght versus time for the 0.5 degree scan..... 101

3.12 DOW strength versus time for the 2.0 degree scan..... 102

3.13 DOW strength versus time for the 3.0 degree scan..... 103

3.14 KDDC strength versus time for the 0.5 degree scan..... 104

3.15 KAMA strenght versus time for the 1.0 degree scan..... 105

3.16 KAMA strength versus time for the 0.5 degree scan..... 106

4.1 Relation of beam width to vortex size..... 107

## Abstract

This study compares observations from the Doppler on Wheels (DOW) radar and the WSR-88D radars to identify any features that are important to forecasting that the WSR-88D may be missing. WSR-88D and DOW data were compared for the Dimmitt Tornado on 2 June 1995 (during VORTEX 95), the Rolla Tornado on 31 May 1996, and Hurricane Fran on 5-6 September 1996.

For Hurricane Fran, the reflectivity features and velocity features were compared. Small scale features in the wind field, believed to be sub-kilometer scale boundary layer rolls were discovered. It has been suggested that these are responsible for some of the small scale intense damage found in the aftermaths of some hurricanes. These rolls were also visible in the KLTX data but were not as well defined.

For the two tornado cases the strength (the difference between the maximum inbound velocity and the maximum outbound velocity) were examined. As expected the strength observed by the WSR-88D was about 50% less than that observed by the DOW. This was compared with predictions of Burgess (1993).

# 1. Introduction

The following was a comparison study between the high resolution mobile "Doppler on Wheels" (DOW) radar and the National Weather Service WSR-88D. The DOW has the ability to get close to weather event rather than having to wait for the weather to come to it; the resolution of the data collected was finer when the radar was closer to the event, making the DOW a useful research tool.

It was hoped that the results of the study will aid the identification of small-scale and potentially dangerous weather events on radar and thus help in the forecasting of such events. The spacing of the current 88-D network often results in few tornado observations close to the nearest radar. The farther away a tornado (or other weather feature) was from the radar, the coarser the data resolution will be and the harder it was to identify significant characteristics. By comparing the data collected by the DOW and the 88-D radars, it is hoped that features that are resolved at great distance from the latter and their evolution might provide clues about tornado formation and intensity.

By looking at high resolution DOW data from a hurricane, it is hoped that the identification of small-scale features that might be missed by the 88-D can be documented. One result of this work was that sub-kilometer boundary layer rolls have been discovered in the data recorded by the DOW during Hurricane Fran. These are believed to be responsible for the gustiness at the surface during hurricanes and possible the damages found in the aftermath of some hurricanes.

Chapter 2 will discuss Hurricane Fran, including the sub-kilometer boundary layer rolls. First, the history of Hurricane Fran will be described, followed by the features of the two radars and the scanning strategies used. Features in the reflectivity and velocity fields, for each radar will then be discussed and compared. Finally, the rolls discovered in the wind field will be documented, including how the amplitude and wavelength changed with time and their dependence on wind speed.

Chapter 3 will describe the Dimmitt and Rolla tornadoes as viewed by the DOW and 88-D radars. Differences between the inbound and outbound peak velocities and how they change with time will be described. Finally the results from both the hurricane and tornado studies will be discussed in Chapter 4.

# 2. Hurricane Fran

## 2.1. Introduction

Many studies of hurricanes have been conducted using Doppler radar, both ground based and airborne. Hurricane Fran was the first hurricane studied using the Doppler on Wheels (DOW). Some of the studies done with Doppler radar include a study of Hurricane Hortense in the Caribbean (Bennett, 1997), Hurricane Opal in the Gulf of Mexico ( Schneider et al. 1997), and Typhoon Herb in Taiwan (Lee, 1997). Many studies have also been conducted using airborne Doppler radar, including the study of eyewall characteristics (Marks and Dodge, 1997), Mesoscale and convective scale features (Jorgensen, 1984), and vertical motions in hurricanes (Jorgensen, 1985).

Many of the studies of hurricanes have focused on the tornadoes produced. Gentry (1983) found that the tornadoes are generally F0 or F1 (Ahrens, 1994), but an F2 or F3 can occasionally occur. These tornadoes can also occur during any time of the day, however, they most often occur between the hours of 1200 and 1800 LST. Hodanish, Spratt, and Sharp (1983) studied the velocity and reflectivity patterns associated with hurricane spawned tornadoes. They studied four tropical cyclones with winds of 17 $ms^{-1}$ or greater. Their study included 20 tornadoes, 16 of which occurred in the outer rain bands and the remaining were found in the eyewall. The tornadoes in the outer rain band were associated with oval shaped cells with reflectivity values of 50-60 dBZ. In the velocity data, the associated mesocyclones had an average core diameter of 3.2 km.

It was hoped that tornadoes from Hurricane Fran could be studied using the high resolution DOW velocity and reflectivity fields. However, only one tornado was reported in the south coastal region of North Carolina. This tornado was F0 on the Fujita scale (Ahrens, 1994) and occurred in Lumberton North Carolina, which was over 110 km from the DOW (well beyond the range of the DOW). Still, both the rain band at the beginning of the period and the eyewall were examined for the features described by Hodanish, et al (1997), but no mesocyclones were found.

The advantage the DOW has over WSR-88D radar is the high resolution of the data and the mobility. The DOW can be deployed to the location of landfall and not have to wait for a hurricane to make landfall close enough for observation. Hurricane Fran was the first hurricane that was observed by the DOW, airborne Doppler, and WSR-88D radars. Dodge et al (1997), did a study investigating the "three dimensional wind fields in Hurricane Fran" using marine stations, drifting buoys, WSR-88D and airborne Doppler radars. One goal was to determine "differences in onshore and offshore flow". Cline (1997) also studied the wind field of Hurricane Fran.

In the current study the reflectivity and velocity fields for KLTX were compared to those from the DOW. Because the DOW was able to collect high-resolution reflectivity and velocity data, this was an opportunity to compare the two data sets obtained by the two radars during Hurricane Fran, looking for potentially important and dangerous small-scale features that the 88-D radars may be missing. It is hoped that this information will be helpful to radar operators and forecaster when looking at future landfalling hurricanes.

## 2.2. Hurricane Fran

On 22 August 1996, a tropical wave emerged from the West Coast of Africa and by 23 August, developed into a tropical disturbance and moved west at about 7.7 $ms^{-1}$. Not until 27 August did this disturbance evolve into Tropical Storm Fran, located about 1700 kilometers east of the Lesser Antilles. The effects of Hurricane Edouard might have impeded the storm's development, which was only about 1400 km to the west-northwest of Fran. Fran became a hurricane on 29 August at 0000 UTC, when it was roughly 740 kilometers northeast of the Leeward Islands (NHC, 1996).

On 30 August, Fran weakened to below hurricane strength and moved northwest at about 2.5 $ms^{-1}$, again because of the influence of Hurricane Eduoard. By 31 August, Fran was again a hurricane and moved west-northwest at 5.1 $ms^{-1}$, tracking about 185 kilometers northeast of the Bahaman Islands. By 4 September, Fran was a category 3 hurricane (on the Saffir-Simpson scale) and reached its strongest intensity by 5 September, with peak surface winds of 54 $ms^{-1}$and a central pressure of 946 mb (NHC, 1996).

At 0030 UTC on 6 September, Hurricane Fran made landfall on the North Carolina coast near Wilmington, with wind speeds near 51 $ms^{-1}$. After landfall, Fran moved north at about 7.7 $ms^{-1}$, eventually reaching Southern Ontario and becoming extratropical on 9 September 1996 (NHC, 1996).

## 2.3. WSR-88D (KLTX) and Doppler on Wheels (Mobile Doppler Radar)

The Doppler on Wheels (DOW) is a 3cm wavelength Doppler radar mounted on a truck bed. This radar was designed at the University of Oklahoma (OU) in conjunction with the National Oceanic and Atmospheric Administration's National Severe Storms Laboratory (NSSL), the National Science Foundation sponsored National Center for Atmospheric Research (NCAR), and the Center for Analysis and Prediction of Storms (CAPS). It was designed to study events that were difficult to resolve with the current 88-D network (events that happen infrequently, very close to the ground, or on short time scales). These events include tornadoes and hurricanes. For example, tornadoes are small-scale phenomenon and are difficult to resolve with the current 88-D network unless they occur very close to a radar site. This is not likely because some of the radar sites are separated by distances of over 200 km. Fortunately the DOW is able to travel to the tornadoes and obtain data from a range of just a few kilometers. Tornadoes also occur on time scales of several minutes, but the current scanning strategy for the 88-D radars allow a full volume scan to be completed every five minutes, providing very poor temporal resolution of the tornado (Wurman et al., 1997).

The DOW employed a 1.83 meter diameter antenna, which resulted in a beam width of 1.2 degrees. The gate length of the DOW, in the range of 37.5 – 300 m, combined with the narrow beam width resulted in resolution volumes of 64m x 64m x 75m at a range of 3 km. For both the Rolla and Dimmitt tornadoes, the DOW used gate lengths of 75 m, and during Hurricane Fran, 75, 150, and 225 meter gate lengths

were used. The pulse repetition frequency for the DOW was typically 2000Hz, which resulted in Nyquist interval of $32ms^{-1}$ (Wurman et al., 1997).

The KLTX WSR-88D radar is a stationary operational Doppler radar used by the National Weather Service (NWS) forecast office in Wilmington, North Carolina, and is part of the national WSR-88D network. The KLTX radar is a 10 cm wavelength radar with a 0.96 degree beam width (Alberty and Crum, 1991).

The DOW was driven from Norman Oklahoma to South Carolina to intercept Hurricane Fran 4-5 September 1996. The DOW was redeployed to the Wilmington, North Carolina International Airport when the forecasted track changed. The DOW was then deployed on a taxiway of the airport. This put the DOW 10 km west of the coastline, 54 km northeast of KLTX (Figure 2.1), and in the path of the eye of Hurricane Fran (Wurman and Winslow, 1998). The DOW collected data on Hurricane Fran from 1900 UTC on 5 September until 0230 UTC on 6 September. The time period for this study was from 1900 to 0130 UTC, which includes several hours prior to eye passage through 45 minutes after eye passage. The time recorded by the DOW was UTC time plus four hours. The DOW was also not oriented due north, therefore, all directions obtained by the DOW had to be corrected (the correction factor was –110 degrees).

As Hurricane Fran was the first DOW hurricane intercept, experiments were necessary to determine the best sampling strategies. For this reason, both the scanning strategy and the resolution (by changing the gate lengths) varied throughout the period. Early in the period, each volume scan was completed approximately every 480 seconds. The volumes scans consisted of only the lower elevation angle

scans, including 0.0, 1.0, 2.0, 3.1, 4.1, and the 5.0 degree elevation angles. From 1949 to 1954 UTC, only the 10.0 and 20.0 degree elevation angles were taken. There was then a gap in the data from 1954 to 2034 UTC. After 2037 UTC, full volume scans were completed approximately every 360 seconds and consisted of the following elevation angles: 0.1, 1.2, 2.0, 3.1, 5.1, 10.1, and 30.1. For a nearly 40 minute period from 2154 to 2231 UTC, only the 1.0 and 2.0 degree elevation angles were taken. This was also the time period when an intense rain band was approaching the DOW. After 2233 UTC, the DOW continued the full volume scans (with another break in data 2230-2301 UTC) until 0055 UTC on 6 September. From 0057 to 0059 UTC only the 10.0 and 20.0 degree scans were taken as another small-scale feature in the reflectivity field moved through. Between 0043 UTC and the end of the period (0129 UTC) the full volume scans were again taken.

Apart from changing the scanning strategy, the DOW was also able to change the resolution of the data collected by modifying the gate length. Three different gate lengths were used during Hurricane Fran: 225, 150 and 75 meter gates. The 75 meter gate length was used for five periods and provided the highest resolution. The first of these was from 2349-2354 UTC, which corresponded to the time period of only 10.0 and 20.0 degree scans. This time period, however, did not coincide with any specific feature in the reflectivity or velocity fields. The second period of high resolution data did not correspond to a change in scanning strategy, or specific patterns in velocity or reflectivity, but the third period of high resolution data collection was just after a strong rain band had passed the radar. The last two periods of high resolution data collection were conducted because of interesting features in the reflectivity field.

Between 2355-0002 UTC a rain band was approaching and during the 0120-0126 UTC period (6 September) there was another rain band approaching the DOW, after the passage of the eye wall.

Unlike the DOW, the KLTX radar had a very consistent scanning strategy. The KLTX radar performed 360 degree scans the entire period, with a full volume scan consisting of the following elevation angles: 0.5, 1.5, 2.4, 3.3, 4.3, 5.2, 6.2, 7.5, 8.7, 10.0, 12.0, 14.0, 16.7, 19.5. There were no changes in gate length (therefore no changes in data resolution). It took the KLTX radar approximately 300 seconds to complete each volume scan.

**2.4. Reflectivity**

At the beginning of the period (about 1900 UTC on 5 September), Hurricane Fran was approximately 160 kilometers south-southeast of KLTX and about 180 kilometers due south of the DOW. The eye, over 50 km across at this time, was visible in the KLTX radar data (Figure 2.2a). Also visible on the KLTX radar was a large rain band approaching from the southeast (Figure 2.2b). The discontinuous rain band had reflectivities above 40 dBZ and embedded cells with reflectivities over 50 dBZ.

The DOW reflectivity at this time was characterized by a broad area of heavy rain, with occasional heavier cells moving in from the east (Figure 2.2c). The reflectivity throughout this period was about 45 dBZ with the individual cells over 50 dBZ. One of the strongest cells during this time period first became visible in the DOW reflectivity field about 10 kilometers east of the radar, with a maximum reflectivity over 50 dBZ. This was a very well defined cell and it moved directly

toward the radar at a speed of over 22 $ms^{-1}$. By 1911 UTC, the cell was only 4.7 kilometers from the radar and still very well defined with reflectivity near 50 dBZ. This cell moved over the radar at approximately 1914 UTC and attenuation became very problematic at this point (Figure 2.2d). Several other slightly weaker cells moved over the radar from the east with similar speed before 2043 UTC.

The large-scale rain band passed over the DOW by 1928 UTC and moved over KLTX by 1931 UTC. As the heavy rain moved over the DOW, the attenuation problem again became evident. As the radar dome became coated with water, the range at which signals could be detected drastically decreased. Because of this, the reflectivity field was useless while the rain band was over the DOW, and many of the small-scale features during the rain band passage were not visible. The rain band moved past both radars by 2011 UTC, at a time when there was a gap in the DOW data.

At 2136 UTC, two large rain bands were visible on radar the first about 27 km to the southeast of the radar, and the other behind it about 39 km southeast of the radar (Figure 2.3). These moved across the airport at 2154 and 2221 UTC respectively. The second rain band, the stronger of the two, had a maximum reflectivity of about 40 dBZ. As the first rain band moved over the radar at 2138 UTC, the second rain band seemed to lose some of its definition due to attenuation. At this point the second and stronger, rain band was almost 35 km from the radar. At 2142 UTC the heaviest rain moved past the radar and the second rain band was again clearly visible. The rain band was about 30 kilometers away with a maximum reflectivity of 40 dBZ. The reflectivity increased slightly as it approached the radar

to about 45 dBZ, probably due to better sampling as the band moved closer rather than an increase in strength. Both of these rain bands were visible in the KLTX data as well.

By 2333 UTC, a very intense thin line of high reflectivity moved over the DOW (Figure 2.4). The rain band was first visible on the edge of the radar at 2310 UTC (Figure 2.4a), about 26 kilometers to the south with a maximum reflectivity of 35 dBZ. At this time a rain band was approaching the radar with reflectivities of 45 dBZ. The first rain band moved through and a second stronger rain band showed up much more clearly. By 2321 UTC, the strong rain band was very well defined and about 13 km from the radar, with a maximum reflectivity of 53 dBZ (Figure 2.4b). The rain band also was visible on the higher scans (both 10.0 and 20.0 degree elevation scans). The rain band was very narrow (only about 1-2 kilometers wide at 2322 UTC) but appeared to get wider (about 4 kilometers wide) by 2327 UTC (Figure 2.4c) before it reached the radar. At this point it still had a maximum reflectivity of 51 dBZ. By 2333 UTC, the rain band was over the radar and the maximum reflectivity had decreased to 40 dBZ because of attenuation (Figure 2.4d). The rain bands continued to pass over the radar until after 0000 UTC. This was visible in the KLTX data as a very thin line to the north of the high reflectivity in the forward eye wall (Figure 2.5a). The eye at this time was also visible in the KLTX data located about 64 kilometers south of the DOW.

By 0036 UTC 6 September, there was evidence of a very large ill-defined eyewall in the radar data about 13 kilometers south of the DOW moving north (Figure 2.6). Only part of the eye was visible. One explanation for this, was that the storm

was already starting to decay as it made landfall. But some studies have suggested "most storms with strong convective rainbands have incomplete eyewalls" (Schneideret al, 1997). As discussed previously, at least on strong rain band was visible in the KLTX data during the period. The forward eye wall h exhibited rapidly decreasing reflectivity with height. The maximum reflectivity was only about 40 dBZ in the 10.0 degree scan. At 0045 UTC, the eye passed over the radar with no back eye wall visible, however, some regions of higher reflectivity (about 50 dBZ) were present in the eastern eye wall. The leading edge of the eye had passed KLTX to the east by 0027 UTC.

After eye passage, the last interesting observed feature in the reflectivity pattern was a very weak rain band (Figure 2.7). Reflectivities were only about 25 dBZ and appeared first in the 0104 UTC scan (Figure 2.7a). It was a very wide band and moved toward the radar from the southwest, passed over the radar by 0112 UTC, and appeared to intensify as it approached. The tail end of the line, about 15 km to the east of the radar, had the greatest development and by 0112 UTC there were a couple of cells with maximum reflectivities near 50 dBZ. These were also visible in the KLTX data as weak linear features in the eye, but did not extend above 2.4 kilometers in height.

## 2.5. Wind Field of Hurricane Fran

### 2.5.1. Introduction

The peak wind was found in the inbound and outbound regions of each elevation angle in each volume scan. The peak wind was found by zooming in on the region of highest wind and manually selecting the largest value. Inbound and

outbound patterns were examined separately since the inbound winds were straight off the ocean and not modified, but the outbound winds had experienced longer trajectories over land. The peak wind was plotted versus time for all elevation angles 1.0 degree through 30.0 degrees (1.0, 2.0, 3.0, 5.0, 10.0, 20.0 and 30.0 degrees).

The wind direction was found by noting the location of the zero line and adding 90 degrees to get the direction of the wind. The 30.0 degree scan was used this because it sampled the highest levels of the hurricane without becoming attenuated. The directions were extracted by hand for 0.2-0.5 km, every 0.1 km and every 0.5 km from 0.5 to12 km (when available). These directions were plotted versus height each half hour for the period 1911-0124 UTC. The wind direction was plotted versus time at 0.5 km and 1-10 km (every km). The data for KLTX was analyzed in the same manner as the DOW data.

### 2.5.2. Peak Wind versus Time

The patterns are fairly similar for all elevation angles (Figures 2.8 and 2.9). At the beginning of the period, all the scans showed that the peak wind speed started to increase at 2055 UTC on 5 September and continued until it reached its peak about 2300-2335 UTC. In most scans the peak wind was steady until 0030 UTC. The peak winds started to decrease slightly about 15 minutes prior to the eye passage and decreased dramatically right after eye passage until the end of the observational period at 0130 UTC. Before 2055 UTC the wind speeds were about 45 $ms^{-1}$ and by 2130 UTC the wind speeds increased to about 55 $ms^{-1}$. The lowest elevation angles had peak winds of about 60-62 $ms^{-1}$while the upper elevation angles had peak winds about 56 $ms^{-1}$. This was due to the fact that the upper elevation angle wind

observations contained a vertical component and thus did not measure the true horizontal wind. The minimum winds in most elevation angles occurred in the last 30 minutes and were about 35 $ms^{-1}$.

For the 3 and 5 degree elevation angles there was a decrease in wind speed from about 55 $ms^{-1}$ to 40 $ms^{-1}$ during the time period 1911 to 2055 UTC. After 2055 UTC, both exhibited the same pattern as the rest of the scans. This pattern was not evident in the upper elevation angles or the elevation angles below 3 degrees.

The general pattern of the outbound velocities was very similar to the inbound velocity pattern but the timing and amplitude are different (Figure 2.10). In most scans, the dramatic increase in wind speed for the outbound winds began about 2149 UTC, compared to 2055 UTC for the inbound side. The outbound velocities reached their peak about 0000 UTC, compared to 2300 to 2330 UTC for the inbound side. The outbound pattern lagged the inbound pattern by about 30-60 minutes because the hurricane was approaching from the south, so the eye and the peak winds reached the inbound side before the outbound side. The outbound winds dropped off dramatically after 0000 UTC, immediately after reaching the peak, but the inbound velocities remained at their peak of 60 $ms^{-1}$for about an hour. This was because the hurricane was weakening as it came ashore and the peak winds finally reached the outbound side. The inbound velocities increased by about 20 $ms^{-1}$ but the outbound peak velocities only increase by about 10-15 $ms^{-1}$, because the inbound velocities were over the ocean and the outbound velocities were over land and were therefore slightly modified by frictional effects. The peak winds for the lower elevation angles were both about 60 $ms^{-1}$ but the peak wind for the upper elevation angles (above 10.0

degrees) was less for the outbound region (47-53 $ms^{-1}$ for outbound compared to 56 $ms^{-1}$ for inbound). This was possibly because the upper level scans did not measure true horizontal wind but had some vertical component as well.

The KLTX maximum inbound and outbound wind velocities were plotted in the same fashion (Figure 2.11 and 2.12). For all elevation angles, the inbound wind velocities were fairly steady at about 52 $ms^{-1}$ before 2130 UTC. All reached their peak wind speed of about 55-59 $ms^{-1}$ between about 2230 and 2300 UTC, remaining steady in most scans for about 60 minutes from 2300 to 0000 UTC. All elevation angles showed a rapid decrease in maximum wind speeds of about 10-20 $ms^{-1}$, between 2359 and 0029 UTC. The winds were steady or very slowly decreasing in the last 60 minutes in all scans and the minimum wind speeds were reached in these 60 minutes. The lower and mid-level elevation angles had a minimum in the wind speed of about 40- 44 $ms^{-1}$. The 20.0 degree elevation angle had a minimum in the maximum wind speed of about 35 $ms^{-1}$. Again the upper elevations had lower peak wind speeds because they did not measure true horizontal wind but included a vertical component.

The outbound pattern of maximum velocities exhibited similar patterns as the inbound velocities but the magnitudes were much less (Figures 2.11 and 2.12). All scans had fairly steady wind speeds from 1931 to 2200 UTC, around 47 $ms^{-1}$, compared to the inbound 52 $ms^{-1}$. All elevation angles reached their peaks about 2227-2300 UTC with a magnitude of about 54 $ms^{-1}$, which was much less than the inbound velocities of 57 $ms^{-1}$. This was because the eye of the hurricane passed to the east of KLTX and therefore the inbound side was closer to the center of

circulation than the outbound side. All scans had a sharp decrease in wind speeds between the hours of 2359 and 0029 UTC and all reached their minimum wind speeds in the last 60 minutes. Afterwards, all winds speeds were steady or slowly increasing in the last 30 minutes. The minimum wind speed for most of the scans was about 33-38 $ms^{-1}$, which was also much less than the inbound speed.

The general patterns for the DOW and KLTX peak wind speeds, were similar, but the magnitude and timing were different because of the location of the radars (Figures 2.13). Both had fairly steady wind speeds at the beginning of the period, an increase in peak wind speeds in the middle of the period, and were followed by a sharp decrease in peak wind speeds at the end of the period. In most scans, the DOW lagged KLTX by 60-90 minutes. Because the KLTX radar was to the southwest of the DOW and the hurricane approached from the south, the peak winds reached KLTX before they reached the DOW and the winds decreased at KLTX before they decreased at the DOW. The magnitude of the changes was also much less for KLTX than for the DOW. The peak winds speeds for KLTX only increased about 10 $ms^{-1}$, but the DOW-measured increase in peak wind speed was much more dramatic with a magnitude of over 20 ms-1. The decrease at the end of the period had the same magnitude for both radars, but the peak winds for KLTX decreased gradually over the last 120 minutes, whereas the peak winds from the DOW dropped off drastically in the last 30 minutes. Again location was the prime reason. The eye went directly over the DOW, but passed 20 kilometers to the east of KLTX; therefore the winds did not get as strong and the changes were more gradual.

### 2.5.3 Wind Direction versus Height

Wind direction was plotted versus height in half-hour time steps from 2042 to 0031 UTC. Data before 2042 UTC and after 0031 UTC were missing. All wind versus height profiles throughout the period 2042-0031 UTC showed a very sharp veering with height in the lowest kilometer (Figures 2.14 and 2.15). This veering was 30 to 50 degrees in magnitude and occasionally extended up to 3 km. Most profiles had steady or slightly veering winds above 3 km and below 10 km. All times showed a sharper veering again above 10 km.

The winds veered sharply with height in the lowest two kilometers of the atmosphere because the balance of forces was different at the surface than it was for the upper levels. In the middle and upper troposphere, due to the relative absence of friction (the effects of friction are usually negligible), the winds flowed parallel to the isobars in a counterclockwise circulation around the hurricane. But in the boundary layer, friction was important and acted to slow the winds. When the net wind speed decreased the centrifugal force was no longer enough to balance the pressure gradient force, causing the wind to turn to the left. Therefore, as height increased and friction became less of a factor the winds more closely followed the isobars and the wind veered with height (Holton, 1992).

The KLTX radar had a similar profile of wind direction with height compared to the DOW in the early part of the period, but during the latter part of the period the KLTX radar profile was much more interesting. Before 2030 UTC KLTX had sharp veering winds with height below 2 km (like the DOW) with a fairly steady direction in the middle levels, and veering winds above 10 km. This was during the time when

the hurricane was well south of both radars and both radars were in relatively the same environments with respect to the storm. However, as time went on the storm moved directly toward the DOW and to the east of KLTX, confining veering winds to the lowest and highest levels, with backing winds in the middle levels. By 2031 UTC (Figure 2.16), there was a small amount of backing winds present around 6 km. The magnitude of this backing was only about 15 degrees and only about 2 km deep. But by 2331 UTC (Figure 2.17), which was about 45 minutes before the eye passed to the east of KLTX, this backing extended from 2 kilometers to almost 7 kilometers and was about 30 degrees in magnitude. 45 minutes after the eye of the hurricane passed to the east of the radar (0102 UTC) the backing occurred throughout the profile except for the lowest kilometer, where the strong veering with height still existed (Figure 2.18).

### 2.5.5 Wind Direction versus Time

Wind direction was plotted as a function of time for each kilometer from 1 km to 10 km (Figures 2.19 and 2.20), and for all heights the pattern was the same. The wind direction was steady out of the east before 2038 UTC, since the eye of the hurricane was still well south of the radar. After 2038, the winds started to veer slightly as Hurricane Fran moved closer toward the coast. The winds veered sharply at all levels about 15 minutes prior (0031 UTC) to the eye passing over the DOW and continued to veer sharply until the end of the period (about 0130 UTC) as the eye passed by and moved north of the DOW.

For KLTX the pattern of wind direction with time (Figures 2.19 and 2.20), as expected, was very different than that of the DOW. The eye was still well offshore

before 0031 UTC and like the DOW, the KLTX wind direction was steady out of the east. In the lowest levels the winds started backing about 2131 UTC with the sharpest turning occurring between 0002 UTC and the end of the period. This was about 30-60 minutes before the winds measured by the DOW started veering. This was because the KLTX radar was located south of the DOW's latitude, thereby closer to the storm. The leading edge of the eye was actually passing to the east of KLTX by 0015 UTC (about 30 minutes before it went past the DOW). The KLTX wind direction backed with time, whereas the DOW wind direction veered with time. The KLTX winds backed with time as the eye passed to the east, but the eye went directly over the DOW. At KLTX the upper levels showed the same backing of the winds as the eye passed, but the winds started backing about an hour earlier at 6 kilometers; above 7 kilometers, the winds were backing throughout the entire time period (1930-0130 UTC). All of these wind directions were taken from the 20.0 degree scan. Therefore as the height increased, the distance from the radar increased, and the distance to the storm decreased. Therefore, at 7 kilometers in height, one would expect the winds to back sooner.

## 2.6 Rolls

### 2.6.1 Introduction

In the DOW velocity data from Hurricane Fran, small-scale features embedded in the large-scale wind flow were discovered (Figure 2.21). These features were regions of very high wind velocity immediately adjacent to regions of low velocity winds. It was proposed by Wurman and Winslow (1998) that these features were axially horizontal rolls. It was theorized that the regions of very high velocity

near the surface were high momentum air brought to the surface from above, and that the immediately adjacent low velocity regions (the other half of the vertical circulation) were low momentum air being brought aloft from the surface (Figure 2.22). It was also proposed that these rolls were possibly responsible for some of the damage from hurricanes and the much of the surface gustiness.

To study these rolls, the amplitude and wavelength were analyzed verses time and compared to the peak wind. The amplitude was defined as the difference between the high velocity band and the adjacent low velocity band. The amplitude of the rolls was obtained manually by examining at the most well defined rolls in each scan. The two were subtracted to find the maximum peak to peak roll amplitude. The vertical extent of these rolls was also noted. The maximum roll amplitude was then plotted with time. The KLTX analysis was conducted in the same manner and the roll amplitude was plotted with time. This procedure was done for the elevation angles 1.0, 2.0, 3.0, and 5.0.

The wavelength of the rolls was obtained manually by examining at the most well defined rolls. As many rolls as possible were sampled, to obtain the average wavelength. For the DOW data, it was possible to sample more rolls than for the KLTX data because the rolls were better defined. For the 5.0 degree elevation angle for KLTX data, rolls were not well defined. Therefore, often only one wave was sampled.

The roll amplitude, height of maximum roll amplitude, and wave length of rolls were then compared with the maximum wind speed. The roll amplitude was

also compared with reflectivity, which was obtained by noting the reflectivity at the same location as the rolls, not the average reflectivity of the entire field.

### 2.6.2 General Description of Rolls

The rolls were best defined in the lower elevation scans and decrease in definition as the elevation angle and thus the altitude increases. For example, the rolls were still very well defined throughout the period in the 1.0, 2.0, and 3.0 degree scans, but the rolls were not always easily found in the 5.0 degree scan. During the periods 2300-0000 UTC and 0100-0124 UTC, the rolls were not very well defined in the 5 degree elevation scan. However, the rolls were visible in 5 degree scan at 2235 and 0000 UTC. These corresponded to the scans where the gatelength was decreased, thereby providing higher resolution.

The KLTX data showed much the same pattern as the DOW data. The rolls were much better defined in the lowest scan, but unlike the DOWs, the rolls were not well defined in the 1.0 degree scan. It was difficult at certain times to detect any rolls in the 2.0, 3.0, and 5.0 degree scans.

### 2.6.2 Amplitude of Rolls

For the DOW, the general pattern of roll amplitude versus time was similar for all DOW elevation angles on the inbound side, but there were slight differences between the lowest (1.0 and 2.0 degree) elevations and the middle (3.0 and 5.0 degree) scans (Figure 2.23). In the lowest two scans (1.0 and 2.0 degrees), the roll amplitude slowly started to increase about 1930 UTC. The sharpest increase in both scans occurred between 2149 and 2234 UTC, with an immediate decrease in roll amplitude over the next 60 minutes. The roll amplitude once again increased sharply

between 2334 and 0027 UTC, about 60 minutes prior to eye passage and slowly started decreasing at 0027 UTC, which was about 15 minutes prior to the eye passing the DOW.

There were two apparent differences between the 1.0 and 2.0 degree scans, both of which were due to missing data. Both showed a decrease in roll amplitude starting at 2234 UTC, but the magnitude of the decrease was larger in the 1.0 degree scan. Also, the roll amplitude reached a minimum at 2334 UTC in the 1 degree elevation angle scan, which was 30 minutes after the 2.0 degree scan. Unfortunately, the 2334 UTC volume was missing the 2.0 degree scan, so the exact time of the minimum amplitude was uncertian. The other difference between the two occurred at the end of the period. The 1.0 degree scan showed steady roll amplitude after 0027, but the 2.0 degree showed an immediate drop off in roll amplitude after 0028 UTC. Since the 1.0 degree scan at 0130 UTC and the 2.0 degree scan at 0100 were missing, it was uncertian whether this difference was significant.

The 3.0 and 5.0 degree scans were similar to the lower scans, without the double peak. The roll amplitude was steady before 2127 UTC in both the 3.0 and 5.0 degree scans. In the 5.0 degree scan, the roll amplitude started to increase about 2130 UTC and the roll amplitude in the 3.0 degree scan started to increase about 20 minutes later at 2150 UTC. But since the 2127 UTC 3.0 degree scan was missing, this apparent difference may again be just due to missing data. The increase in roll amplitude was slow at first, then increases dramatically about 45 minutes prior to eye passage (which was about 30 minutes after the start of the second dramatic increase in

the 1.0 and 2.0 degree scans), reaching its peak about 15 minutes prior to eye passage. The roll amplitude immediately decreased after the peak until the end of the period.

The outbound pattern was different from the inbound pattern in the lowest two scans (the 1.0 and 2.0 degree scans)(Figures 2.24 and 2.25), but was very similar to the middle level scans (3.0 and 5.0 degrees). The outbound 1.0 and 2.0 degree scans had an increase in roll amplitude starting from 1930 to 2030 UTC and both reached their peak about 2304 UTC (Figure 2.24). This was about 30 minutes after the inbound data reached its peak in roll amplitude. Like the inbound data, the outbound side showed a decrease in roll amplitude within an hour of eye passage, but the outbound decrease occurred 30 minutes after the inbound, and the magnitude was much smaller. Like the inbound data, the 1.0 degree scan showed steady roll amplitudes right after eye passage, but the 2.0 degree scan showed a dramatic decrease in roll amplitude after eye passage. Similar to the case of with the inbound data, this feature was again due to the missing data points.

The patterns for the outbound 3.0 and 5.0 degree scans were very similar to the inbound scans(Figure 2.25). After 2100 UTC, the roll amplitude began to increase slightly as the storm approached, even though the hurricane was still well off shore, at about 45 minutes prior to eye passage, the roll amplitude in the 3.0 and 5.0 degree scans, both inbound and outbound, increased dramatically. The roll amplitude then decreased dramatically after eye passage. In the 3.0 and 5.0 degree scans the timing was very similar. The magnitudes were very similar for the 5.0 degree scan, but in the 3.0 degree scan the magnitudes were much larger for the inbound side.

The amplitudes were comparable between the inbound and outbound sides, with the inbound amplitudes being slightly larger. The outbound maximum amplitudes were about 21-24 $ms^{-1}$, compared to the inbound amplitudes of 23-27 $ms^{-1}$. The 5.0 degree scan had a peak amplitude of 33 $ms^{-1}$. But all scans, both inbound and outbound, reached their peak roll amplitude at about 0030 UTC. The minimum amplitudes were much less in the outbound scans (1-7 $ms^{-1}$), compared to the inbound minimum roll amplitudes of 7-10 $ms^{-1}$.

For the inbound side of KLTX, the roll amplitude magnitudes were similar in all scans, but the pattern with time varied greatly (Figure 2.26). The minimum roll amplitude was about 9 $ms^{-1}$and the maximum was 16-21 $ms^{-1}$. All elevation angles showed a slight increase (about 5 $ms^{-1}$) in amplitude in the first hour of the period followed by a slight decrease in roll amplitude of the same magnitude from 1957 to 2057 UTC. Most scans exhibited a minimum in roll amplitude at this time. There was then a significant increase in roll amplitude in all scans after this time, but the timing varied with elevation angle. In the lowest scan, the increases in roll amplitude started at about 2057 UTC. The 2.0 degree scan started 30 minutes later, followed by the 3.0 and 5.0 degree scans 30 minutes after that. The timing of the peaks also varied greatly with elevation angle. The peaks in the roll amplitude occurred 15 minutes prior to eye passage for the 1.0 degree scan and almost 2 hours prior to eye passage for the 3.0 degree scan. The lowest two scans were steady after eye passage, while the upper two scans had a decrease in roll amplitude in the last 30 minutes of data.

For the outbound scans of KLTX (Figure 2.27), the magnitude was very similar to the inbound, but the pattern with time was more consistent between scans. The maximum amplitudes ranged from 16-19 $ms^{-1}$and the minimum amplitudes ranged from 6-9 $ms^{-1}$. All scans exhibited a slight increase in roll amplitude in the first 30 minutes of the period followed by a decrease of the same magnitude. The roll amplitude again started to increase in the upper two scans at about 2127 UTC and in the lower two scans 30 minutes later. All but the 2.0 degree scan reached their peak at about 15 minutes prior to eye passage and all scans had a dramatic decrease in roll amplitude as the eye passed by KLTX. All scans also had an increase in roll amplitude in the last 30 minutes of the period, well after eye passage.

There were two main differences between the KLTX and the DOW roll amplitude (Figures 2.28 and 2.29). The magnitude of roll amplitudes and their changes in the DOW were much greater than the KLTX pattern with time for the DOW lags the roll amplitude with time pattern for KLTX.

The first difference was due to the fact that the roll amplitude and its changes with time were much greater in the DOW data than in the KLTX data. The first difference was due to the fact that the hurricane passed directly over the DOW, while the closest point of approach to KLTX was 30 kilometers to the east. The rolls measured by the DOW generally had a maximum amplitude about 23-27 $ms^{-1}$in the inbound data and about 21-24 $ms^{-1}$in the outbound. The outbound magnitudes were slightly less because the outbound data were over land and therefore modified by friction, whereas the inbound side was still over the ocean. This same pattern was evident in the peak wind velocities as well. The minimum values for roll amplitude

for the DOW were about 9 $ms^{-1}$ for the inbound and about 5-7 $ms^{-1}$ for the outbound side. This resulted in a total range of about 20 ms-1 and in some cases the range was even greater. But for KLTX, the total range was generally less that 10 $ms^{-1}$. The maximum roll amplitudes were about 16-20 $ms^{-1}$, which were much less than the DOW maximum roll amplitudes, but the minimum roll amplitudes were about 9 $ms^{-1}$, which were about the same as the DOW minimum roll amplitudes.

The timing of the changes in the roll amplitude was also different for the two radars. In general, the rolls measured by the KLTX radar reached their peak about 30 to 90 minutes before eye passage on the inbound side and 30 to 60 minutes before eye passage on the outbound side, before the rolls in the DOW data reached their peak. The rolls in the KLTX data started to decrease in amplitude about 30 to 60 minutes prior to the DOW, since the eye passed KLTX about 30 minutes prior to passing over the DOW.

### 2.6.3 Wavelength of Rolls

The inbound pattern of wavelength versus time in the DOW data was similar for all elevation angles (Figure 2.30). The wavelength started to increase by 2149 UTC and peak in wavelength occurred about 2304 UTC, which was well before the passage of the eye. However, this time did seem to correlate with the time in which the peak wind reached its maximum. The peak in wavelength was immediately followed by a decrease of the same magnitude. The wavelength decreased slowly as the eye passed and until the end of the period. The maximum wavelength for the inbound side was between 800 and 1000 meters and the minimum was about 500 meters.

The data on the outbound side exhibited no definite pattern in wavelength that was common to all elevation angles (Figure 2.31). The wavelength started to increase for all scans about 2055 UTC, which was about 60 minutes before the increase on the inbound side, but the peak in wavelength was reached at different times in each scan. The magnitude was about the same on the outbound side as the inbound side, with about 1000 meters as the maximum wavelength and 500 meters for the minimum wavelength.

Unlike the peak wind and the roll amplitude, the wavelength pattern with time was just as amplified in the KLTX data as it was in the DOW data (Figure 2.32). The magnitudes for both inbound and outbound sides were similar to the DOW wavelengths, with a maximum of about 1000 meters and a minimum of about 400 meters. The wavelength started to increase in all inbound scans at about 2258 UTC (Figure 2.33), which was about an hour before the DOW. The wavelengths reached their maximum for KLTX about the time the eye passed KLTX. The DOW reached its maximum about 2 hours prior to eye passage. There was a sharp decrease in wavelength 30-60 minutes after the eye passed.

The outbound pattern was very similar to the inbound (Figures 2.34 and 2.35). There was a sharp increase in wavelength starting at 2258 UTC. The maximum wavelength was reached 15 minutes prior to the eye passing KLTX, which was again very different from the DOW pattern. The wavelengths then decreased sharply as the eye passed to the east of KLTX.

There was some correlation in the KLTX data between the roll amplitude and the wavelength of the rolls and it was most pronounced in the outbound data. The

best correlation was in the 1.0 degree elevation scan (in both the inbound and outbound data). For the 1.0 degree elevation scan the peak in roll amplitude and the peak in wavelength both occurred at 2359 UTC. Both decreased dramatically immediately afterwards and both were steady in the last 30 minutes. In the upper scans, the peak in roll amplitude occurred before the peak in wavelength by as much as 90 minutes. There did not seem to be the same correlation in the DOW data, as the peaks in wavelength and roll amplitude occured at different times.

### 2.6.4 Dependence on Wind Speed

The roll amplitude was compared with the peak wind using two different methods. The roll amplitude was first plotted directly against the peak wind with a scatter plot (Figures 2.37 and 2.38). Then, both the peak wind and the roll amplitude were plotted with time and compared. The scatter plots had only a weak positive correlation between roll amplitude and peak wind, but the comparison of both with time had a strong positive correlation.

When comparing peak wind and roll amplitude directly, there was a weak positive correlation on the inbound side and there was no correlation at all in the 5 degree scan (Figures 2.36 and 2.37). However, the outbound side had a slightly better correlation. The 1.0, 2.0, and 3.0 degree scan on the inbound side, had a weak positive correlation between peak wind and roll amplitude. Peak wind speeds of about 43 $ms^{-1}$ correlated to a roll amplitude of about 10 $ms^{-1}$ and peak wind speeds of about 58 $ms^{-1}$ roughly corresponded to a roll amplitude of about 20 $ms^{-1}$. However, the 5 degree scan showed a roll amplitude of about 15 $ms^{-1}$ for wind speeds 44-56 $ms^{-1}$

$^{1}$. With wind speeds at about 58 $ms^{-1}$ the roll amplitude varied from 5 $ms^{-1}$ to almost 30 $ms^{-1}$. The outbound side showed a slightly stronger correlation.

When comparing the chronological trends of peak wind and roll amplitude (Figures 2.38-2.40), there was a strong correlation for both the inbound and outbound sides for the DOW. For all scans on the inbound side, there was a strong positive correlation between the pattern of peak wind and roll amplitude with time. However, the roll amplitude lagged the peak wind by about 60 minutes. For most scans, there was a sharp increase in peak wind starting at about 2056 UTC. This was followed by a sharp increase in roll amplitude starting at 2149 UTC. About 2150 UTC, the peak winds were steady or only slightly increasing, and about 60 minutes later the roll amplitudes had the same tendencies. The 5 degree scan (Figure 2.39) had a more gradual increase in peak winds than the lower scans and the roll amplitude had the same pattern as the peak wind. All scans show a rapid decrease in the peak wind and the roll amplitude at the same time, starting just before the eye passed the DOW.

The outbound pattern still had a strong correlation between the pattern of roll amplitude and the peak wind with time, but there was no lag between the two (Figure 2.40). The 5.0 degree scan was the best example and showed both the roll amplitude and peak wind started to increase about 2151 UTC. The increase in both was gradual at first, with the sharpest increase in both roll amplitude and peak wind occurring about 60 minutes prior to eye passage. But like the inbound side, both the peak wind and roll amplitude decreased sharply as the eye passes the DOW.

Looking at a scatter plot for the KLTX data, there was very little correspondence between roll amplitude and peak wind, if any (Figure 2.42). There

was also not as much change in roll amplitude in the KLTX data as there was in the DOW data.

The inbound and outbound sides of KLTX were very similar to the outbound side of the DOW. The correlation was strong in the lower two elevation scans, but was not as strong in the 3.0 and 5.0 degree scans (the rolls were also not very well defined in the 3.0 and 5.0 degree scans). Both the inbound and outbound side of KLTX (Figures 2.42 and 2.43) had patterns similar to the outbound side of the DOW in that the increases in roll amplitude occurred at the same time and the roll amplitude did not lag the peak wind as it did in the DOW inbound data. For KLTX, the roll amplitude and the peak wind started to increase at about 2158 UTC. The peak winds then leveled off or were only slightly increasing, with an accompanying increase in roll amplitude. Both the roll amplitude and the peak wind rapidly decreased as the eye passed KLTX. Both the peak wind and the roll amplitude increased slightly in the last 30 minutes of the period (an hour after eye passage) in the outbound data. This feature did not show up in the inbound KLTX data or any of the DOW data.

One of the main differences between the peak wind in the two radars was the fact that the peak wind pattern was not as amplified in the KLTX data as it was for the DOW data. This was also true for the roll amplitude, as the roll amplitude was much greater for the DOW than for KLTX.

The inbound side of the DOW data showed a slight correlation between wind speed and wavelength after the middle of the period. The 1.0 degree scan did not seem to show any correlation, but the 2.0, 3.0, and 5.0 degree scans all showed the sharpest increase in wavelength about an hour after the sharpest increase in peak wind

speed. The peak wind speed was steady at its peak for about an hour or more, but the wavelength decreased dramatically about an hour before the peak winds dropped off. The DOW outbound side showed the same slight correlation for all scans except the 3.0 degree scans (which had no dominant pattern of wavelength). Unlike the inbound side, however, the most dramatic increase in wavelength led the increase in peak wind speed by a 30 to 60 minutes. The most dramatic increase in peak wind speed was at about 2149 UTC and the most dramatic increase in wavelength started at about 2125 UTC. The dramatic drop in wavelength also occurred before the dramatic drop in peak wind speed by about 30 minutes at the end of the period.

For the inbound KLTX data, the 1.0 and 2.0 degree scans (the only two that had a definite pattern in wavelength versus time) had almost a negative correlation with peak wind speed. For both the 1.0 and 2.0 degree scans, the sharpest increase in wavelength occured at 2328 UTC, which was the same time as the sharpest decrease in peak wind speed. The same was not true for the outbound data. The sharpest increase in wavelength occurred between 2258 and 2359 UTC. The peak wind did not increase during this period but for both the wavelength and the peak wind there was a dramatic decrease after 2359 UTC.

# 3. Tornadoes

## 3.1. Introduction

Before the Doppler network was in place, warning for tornadoes using conventional radar were based on signatures in the reflectivity field, such as the hook echo and the Bounded Weak Echo Region (BWER). The hook echo is an appendage from a horizontal thunderstorm echo and is often associated with tornadoes. However, this feature was found to have a moderate false alarm rate when used to warn for tornadoes (Burgess, 1991). In three quarters of the tornadoes reported, the hook echo was absent; and in the remaining cases was not visible until after the tornado was on the ground. The BWER is found when looking at a vertical cross-section of reflectivity and is defined as a region of relatively weak reflectivity surrounded by high reflectivity. The BWER was found to be a good indicator of a supercell thunderstorm, which is the type that produces most of the strong and violent tornadoes; however, it was not an indicator of the tornado itself.

With the advent of the Doppler radar and the installation of the Doppler network in the early 1990's, real time velocity data as well as reflectivity data are available. Doppler radars only measure the motion directly towards and away from the radar (the radial component). Therefore, a rapid circulation (such as a tornado) is detected by identifying a strong couplet of inbound and outbound velocities.

Using this information, several algorithms were developed for the WSR-88D radars to aid in warning for tornadoes. These include the Tornado Vortex Signature (TVS) and the mesocylcone signature. The TVS is characterized by extreme shear greater than 0.05 $s^{-1}$ and large vertical extent to the shear. The mesocyclone signature

is actually a measure of the parent rotation (the mesocyclone) above cloud base. It has been found in studies, that the mesocyclone appears over 10 minutes before the tornado touches down. As this circulation strengthens and comes down to the surface, weak tornadoes may form. The strongest tornadoes occur when the mesocylcone strengthens and the TVS appears and moves down toward the ground. It is estimated that the use of the TVS can lead to warning times of 10 minutes or more.

But even with Doppler radar, there are several limitations in detecting tornadoes. The first is the radar horizon problem (Figure 3.1a), which is due to the fact that the radar beam does not bend with the curvature of the earth. The further the beam is from the radar, even at a 0.0 degree elevation angle, the higher the radar beam is above the ground. For this reason, at medium and long distances (greater than 80 km from the radar) the circulation measured is above the cloud base. Therefore, for even the lowest elevation angles, the circulation detected is the mesocyclone and not the tornado itself, because the tornado is only defined below cloud base.

The second limitation is the aspect ratio problem (Figure 3.1b). As the radar beam travels away from the radar, the beam widens and therefore the ability to detect the vortex depends on the size of that vortex and the beam width at that distance. For a vortex that is larger than the beam width (aspect ratio is less than one), the vortex will be detected by the radar. For an aspect ratio near two, the vortex will only be detected for certain viewing angles. If the vortex is much smaller than the beam width, the vortex will not be detected by the radar at all. According to Burgess

(1991), this last case "approximates the typical sampling condition for an operational radar scanning an average sized tornado at moderate range".

Because of the aspect ratio problem and the radar horizon problem, the maximum range in which a TVS will be detected is generally less than 100 km (for both the Rolla and Dimmitt tornadoes, the closest WSR-88D radars were over 100 km away). The TVS signature has even less range (less than 20 km) for very narrow tornadoes. Therefore at ranges greater than 100 km, detection and warning has to be based on the mesocyclone signature.

But the same limitations exist for the mesocyclone signature. Because of the radar horizon problem, the radar beam is above 4 km at a range of 200 km, with even the lowest elevation angle. Therefore, there is no information available for the low-level mesocyclone. This is a problem because studies have shown the tornadoes form when the mesocyclone stretches toward the ground. Also the peak rotation may be underestimated at long distances due to beam averaging.

The final problem with forecasting tornadoes using the mesocylcone signature is that the mesocyclone is the parent circulation and not the tornado itself. Not every mesocyclone produces a tornado; in fact, Burgess (1991) suggests that on average, only between 30 and 50% of mesocyclones produce tornadoes.

With this in mind, an attempt was made to compare the data from the WSR-88D radars and the data from the DOW for the Rolla and Dimmitt tornadoes. The comparison was made using the observed strength of the tornado, or in the case of the WSR-88D, the observed strength of the mesocyclone.

### 3.2. Dimmitt

On 3 June 1995, a tornado occurred near the town of Dimmitt, Texas in the Texas panhandle. The DOW (Figure 3.2a and b) observed this tornado from a distance of 3-5 kilometers, for about twelve minutes during the mature and decaying stages. During this twelve minute period (from 0103 to 0116 UTC 3 June 1995), six full volume scans and two partial volume scans were completed, which included the following elevation angles: 0.0, 1.0, 2.0, 4.0, 6.0, 8.0, 10.0, 12.0, 14.0, and 18.0 degrees. The tornado and parent storm were sampled from the surface to a height of 1 kilometer (Wurman et al, 1996).

After finding the strong inbound/outbound couplet indicative of the tornado, the difference between the maximum inbound and maximum outbound was calculated. In the lower scans (Figures 3.3 and 3.4), the difference ranged from a maximum of 130-140 $ms^{-1}$ to a minimum of about 100 $ms^{-1}$. The upper levels (above 500 meters) however had a much greater range, with a maximum difference of 125-140 ms-1 and a minimum of 75-85 $ms^{-1}$ (Figures 3.5-3.7). The 14.0 and 18.0 degree scans (approximate altitude of 800 meters and 1 kilometer, respectively), showed only a maximum of 128 $ms^{-1}$ and 125 $ms^{-1}$ respectively and a minimum of 68 $ms^{-1}$ and 75 $ms^{-1}$. Most of the scans showed the peak difference at the beginning of the period (before 0107 UTC) and the minimum at the end of the period (about 0116 UTC). This was because the tornado was sampled during its mature and dying stages.

Most of the scans had a decreasing trend in strength throughout the period 0105-0116 UTC, but the specific pattern changed with each scan. The 0.0 degree scan (Figure 3.3) showed a decrease from 130 $ms^{-1}$ to 98 $ms^{-1}$ between 0105 and 0107

UTC. There was then an increase of about 7 $ms^{-1}$ by 0112 UTC, followed by a decrease at the end of period. The 1.0 degree scan (Figure 3.4) showed a decreasing trend throughout the period. The difference started out at its maximum value at 0105 UTC and decreased until 0110 UTC. Then there was a period when the differences were fairly steady (between 0110 and 0114 UTC), and it finally decreased again in the last minute of data. The 12 degree scan (Figure 3.5) was fairly steady in the first minute, decreased rapidly between 0108 and 0113 UTC, becoming steady again at the end of the period (Gill, 1998).

The Lubbock, Texas WSR-88D Doppler radar (KLBB) also observed the Dimmitt tornado, but with much lower the spatial and temporal resolution than the DOW (Figure 3.2c and d). The KLBB radar did however sample more of the tornadic life cycle than the DOW did. The Dimmit tornado was first visible in the KLBB radar data at about 0042 UTC (about 22 minutes before the DOW observed the tornado). The tornado was last noticeable in the KLBB radar data at about 0114 UTC (which was about two minutes before the end of the DOW data and the death of the tornado

The DOW had much better spatial and temporal resolution than the 88-D, because the tornado was over 100 kilometers from the KLBB radar. The 88-D completes a volume scan every five minutes compared to every 40 seconds with the DOW. The 88-D was using a gate length of 250 meters and the DOW used a gate length of 70 meters. The WSR 88-D had a beam width of 0.96 degrees. Therefore when this beam was over 100 kilometers away from the radar, the beam had spread out to more than 1.7 kilometers (the DOW was only 5 kilometers from the tornado

and the beam had only spread out to 104 meters). Also, the lowest height the 88-D could sample at that distance (even using the lowest elevation angle of 0.5 degrees) was about 800 meters. This was the highest that the DOW was able to scan. This means that the 0.5 degree scan in the KLBB data and the 18.0 degree scan (Figure 3.7) for the DOW were the only scans sampling comparable heights. In the KLBB radar, the 1.5, 2.4, 3.3, and 4.3 degree scans corresponded to heights of 2.6, 4.4, 6.2 and 8.0 kilometers above the ground. The circulation was visible on some 5.2 degree scans but above this, the radar beam was above the storm due to the distance and the curvature of the earth. Therefore, the Dimmitt storm was only sampled at 800 meters, 2, 4, 6, and 8 kilometers.

The distance from the radar not only affected the spatial resolution of the data but also the temporal resolution. The 88-D completed a volume scan every five minutes, but because there were fewer data points available only the first five scans were usable (only the first two minutes of the volume scan). For example, the DOW was able to observe the tornado until its death at 0116 UTC, but the Lubbock radar missed the last two minutes of the tornado's life cycle. This was because the 4.3 degree scan occurred at 0114 and the next 0.5 degree scan did not occur until 0117 UTC (a full minute after the death of the tornado).

The same analysis was that performed on the KLBB data was also done on the DOW data. After the velocity couplet was found, the difference between the maximum inbound and maximum outbound was calculated and plotted with time (Figures 3.8 and 3.9). Both the maximum and the minimum differences were much less than what the DOW measured. For all scans of the LBB radar, the maximum

difference was only 50-60 $ms^{-1}$ compared to 120-140 $ms^{-1}$ observed by the DOW. The minimum was also much less, 20-40 $ms^{-1}$ compared to 70-110 $ms^{-1}$. This was because the radar beam had spread out to over 1.7 kilometers, which was greater than the tornado itself.

All scans in the KLBB data showed an increase in the difference between the maximum outbound and maximum inbound between 0047 and 0057 UTC. The increase was about 20-40 $ms^{-1}$. All scans except the 3.3 degree and the 4.2 degree scans reached the maximum difference at this time and started decreasing. The 3.3 degree scan only slowly increased between 0058-0109 UTC and the 4.3 degree continued to increase until 0104 UTC. The 0.5 -2.4 degree scans (Figure 3.8) decreased after 0058 UTC, but the upper scans did not start to decrease until after 0104 UTC.

Comparing the 18 degree scan for the DOW and the 0.5 degree scan for KLBB (both were about 800 meters above ground), the DOW showed a dramatic decrease in the difference (130 to 90 $ms^{-1}$) between 0105 and 0113 UTC. KLBB also showed a decrease during this period, but the decrease only lasted until 0107 UTC, after which, the difference leveled off. The DOW showed a leveling off as well but it did not start until 0111 UTC, this continued until 0113 UTC, when it again decreased until the end of the period.

KLBB showed the same trends as the DOW, but the timing appeared slightly different. KLBB appeared to level off 4 minutes before the DOW, but there were no observations from KLBB after 0107.

### 3.3. Rolla

The DOW observed the Rolla, Kansas Tornado on 31 May 1996 in southwest Kansas (Figure 3.10a and b). Data was collected from a distance of approximately two kilometers for 10-15 minutes. Only the low level scans (0-3 degrees) were taken, meaning that the storm was only sampled to a height of 200 meters above the ground. This also means that the temporal resolution was greater than for the Dimmitt tornado, since each shallow volume scan was completed in about 20 seconds. A total of 23 volumes scans were taken with a four minute gap in data from 2254 to 2258 UTC.

The data was analyzed in the same manner as the Dimmitt tornado data and the difference between the maximum outbound and maximum inbound velocities were plotted with time for each elevation angle. The maximum difference ranged from 68 ms-1 to 85 $ms^{-1}$, which was much less than in the Dimmitt tornado. The minimum difference ranged from 43-50 $ms^{-1}$. There was not much change in the difference with height, but the storm was only sampled to a height of 200 meters. In all the scans but the 0.0 degree scan, the minimum difference occurred between 2252 and 2254 UTC. The 1.0 and 3.0 degree elevation angle scans showed a second peak of the same magnitude around 2300 UTC, and the 2.0 degree scan showed the primary peak occurring at 2301 UTC.

The pattern of the difference with time was very similar for all scans, except for the 0.0 degree scan. All scans above 0.0 degrees showed an increase in the difference between the maximum outbound velocities and the maximum inbound velocities starting at 2250 UTC with the peak at 2254 UTC. The 1.0 degree scan

reached its peak at 2252 UTC, decreased slightly at 2253 UTC and again reached another peak at 2254 UTC. The magnitude of the increase was greatest for the 1.0 degree scan with an increase of 27 $ms^{-1}$. The upper scans had a magnitude of 12-17 $ms^{-1}$. In all scans the peak was immediately followed by a decrease in magnitude of 18-27 $ms^{-1}$. All scans again showed a strengthening from 2259 to 2301 UTC. For the 0.5 and 1.0 degree scans (Figure 3.11), this increase reached a peak that was less than the previous peak. For the 2.0 degree scan (Figure 3.12), the second peak was the larger of the two and the in the 3.0 degree scan (Figure 3.13), the second peak was the same magnitude of the first peak. All scans showed a sharp decrease in the last minute of data as the tornado dies.

The Rolla tornado was also observed by both the Dodge City, Kansas (KDDC) 88-D radar (Figure 3.10c and d) and the Amarillo, Texas (KAMA) 88-D radar (Figure 3.10e and f). Both radars observed the tornadoes at levels well above the DOW scanning levels. The KAMA and the KDDC radars had the same problems observing the Rolla tornado that the KLBB radar had observing the Dimmitt tornado. The temporal and spatial resolution were much lower than in the DOW data and the 88-D radar sampled above the levels that the DOW sampled. The height problem was even more amplified in the Rolla case because the DOW only took shallow volume scans and only sampled up to a height of 150 meters.

The KDDC radar was approximately 170 kilometers from the tornado. Rotation was first noticeable in the data at about 2228 UTC, which was almost 23 minutes before tornado touchdown. The rotation was last visible at 2316 UTC, which was about 18 minutes after the dissipation of the tornado. Because the storm was

over 170 kilometers from the radar, the storm was only visible on the 0.5, 1.5, and 2.4 degree scans, since the radar beam was above the storm at this distance for the other scans. These scans corresponded to heights of 1.4, 4.4, and 7.1 kilometers, respectively. As a result, the 88-D was not even sampling the tornado itself but was observing the upper level circulation.

The KAMA radar was over 200 kilometers away and therefore sampled even higher levels of the storm than the KDDC radar did. Only the 0.5 and the 1.5 degree elevation angle scans were usable because for the other scans, the radar beam was again above the storm. The circulation was visible on two of the 2.4 degree scans. The 0.5 and 1.5 degrees scans corresponded to heights of 1.5 and 5.1 kilometers, respectively. Therefore we see once again that the radar was looking at the upper level circulation and not the tornado. A circulation was visible in the data at 2225 UTC, about 25 minutes before tornado touchdown, and was last seen about 2316 UTC, about 18 minutes after the dissipation.

Both KAMA and KDDC, like KLBB, completed a volume scan every 5 minutes. This resulted in very poor temporal resolution; in fact. In the lifetime of the tornado, the KAMA radar completed only 3 volume scans and the KDDC radar completed only two volume scans.

The spatial resolution of the data was even less for the Rolla tornado than it was for the Dimmit tornado, since the tornado was further from the radars. Rolla was about 170 kilometers from the KDDC radar and the beam had spread out to over 2.8 kilometers. The radar beam from the KAMA radar had spread out to over 3.4

kilometers when it was sampling the Rolla storm (over 200 kilometers from the radar).

The difference between the maximum outbound and maximum inbound for KDDC velocities was plotted with time. The maximum occurred about 2251 UTC in all scans and was about 45 $ms^{-1}$ for the 0.5 degree scan and about 50 $ms^{-1}$ for the 1.5 degree scans. The values were much less for the 88-D radars than the DOW values, again due to the spread of the radar beam. The minimum values in the KDDC data were about 15-20 $ms^{-1}$.

The circulation was evident in the KDDC data from 2228 to 2314 UTC. There was a sharp increase in this circulation from 2245 to 2251 UTC (right before tornado touchdown). This was followed by a dramatic decrease from 2251 to 2302 UTC (the life time of the tornado)(Figure 3.14).

This pattern was very different from the DOW data and the reason may be twofold. The DOW data showed an increase in circulation from 2250 to 2254 UTC, then a decrease from 2254 to 2259 UTC. The KDDC data showed a decrease throughout this period, but there were only 3 data points during this period, so the increase may have occurred between the two observation points, and therefore may have been missed. Also, the two radars were sampling at two different heights. The DOW was sampling below 150 meters and was measuring the tornado itself, but the KDDC radar was sampling the upper level circulation. Therefore, the upper level circulation increased dramatically right before tornado touchdown (approximately 2251 UTC). After 2251 UTC, KDDC showed a sharp decreasing trend while the DOW had an increasing trend, indicating that the upper level circulation was dying as

the tornado completed its life cycle. The DOW data also had a slight restrengthening of the tornado from 2259-2300 UTC. The KDDC radar missed this feature completely because there were no observations between 2257 and 2302 UTC.

The data from the KAMA radar was much the same as that from the KDDC radar. The values for the difference between the maximum outbound and the maximum inbound velocities were much less than those from the DOW. The maximum values were 30-40 $ms^{-1}$, which was even less than the KDDC values, but the Amarillo radar was also further away from the storm. The 1.5 degree scan for KAMA (Figure 3.15), like the KDDC data, showed an increase in circulation during 2236-2250 UTC, right before touchdown. KAMA also showed a decrease in circulation during the lifetime of the tornado and again, like the KDDC radar, missed the restrengthening of the tornado during the period 2259–2300 UTC due to the temporal resolution.

The 0.5 degree scan for KAMA (Figure 3.16), which corresponded, to a height of 1.5 kilometers, showed a very different pattern than the 1.5 degree KAMA scan (or any of the KDDC scans). The 0.5 degree scan showed an increase in circulation during the entire life time of the tornado, then a sharp decrease after this time. However, the 1.5 degree scans also missed the restrengthening of the tornado.

# 4. Conclusions

## 4.1 Hurricane Fran

This study compared the reflectivity and velocity fields of Hurricane Fran measured by the KLTX 88-D radar and the Doppler on Wheels. The sub-kilometer boundary layers rolls were also studied and compared. The resolution was much greater in the DOW data than in the KLTX data and it was hoped that small-scale features may be better identified in the DOW data.

The main difference in the reflectivity pattern was the scale. The KLTX radar had a much greater range, and during the entire period (1900-0130 UTC), the eye was visible in the KLTX reflectivity. The large scale rain bands were also clearly visible in the KLTX reflectivity pattern. The range for the DOW was only about 40 km during most of the observations and even less when heavy rain was over the DOW. As a result, the rain bands were also visible in the reflectivity field from the DOW but appeared like a broad area of rain. The rain bands could not be entirely seen. The eye was also not visible in the DOW data until about 15 minutes before it passed over the DOW. The DOW however, had much better resolution, with the smaller scale features clearly visible in the data. There were several cells embedded in the large-scale rain bands that were not well resolved in the KLTX data, but were in the DOW data. There were also several very thin high reflectivity lines that passed over the DOW, that were not as well resolved in the KLTX data.

Some of the differences in the wind field were due to the locations of the radar and some were due to differences in resolution. The eye of the hurricane passed to the east of KLTX and went over the DOW. As a result, the winds backed sharply at KLTX, starting about an hour before eye passage, while the winds veered sharply for the DOW. The wind direction with height was also different between the two radars because of the difference in location with respect to the eye of the hurricane. The winds veered with height for both locations in the lowest 2 km for both radars, but the upper level winds were steady or veered slightly in the DOW data. For the KLTX radar, the winds backed above 2 km starting about 2 hours before eye passage.

The differences in the peak wind were likewise due to both location and resolution. The peak winds were less for the KLTX radar then were measured by the DOW, partly due to the fact that the eye went 30 km to the east of KLTX, while passing right over the DOW. But because the DOW had much greater resolution than KLTX, the DOW did a much better job resolving the wind field. Because of this, the KLTX radar underestimated the peak winds. This had important implications for the forecasting of peak winds based on the radar.

There was a very strong positive correlation between the roll amplitude and the peak wind. Both the peak wind and the roll amplitude (for both radars) sharply increased about an hour before eye passage, then both sharply decreased starting right before eye passage. Because of this strong correlation between the peak wind and the roll amplitude and the fact that the KLTX underestimated the peak wind speed, the KLTX radar also underestimated the maximum roll amplitude. This is important because it was theorized that the rolls may be responsible for much of the gustiness at

the surface and some of the major damage found in the aftermath of hurricanes. The wavelengths of these rolls ranged from 500 to 1200 meters, which was the same scale of some of the damage paths found after some hurricanes make landfall.

There was no apparent correlation between roll amplitude and reflectivity, and there were only slight correlations between peak wind and wavelength and roll amplitude and wavelength. The peak wind and roll amplitude patterns were much less amplified in the KLTX data, than in the DOW data. But the wavelength pattern over time was just as amplified in the KLTX data.

### 4.2 Tornadoes

The data from the WSR-88D and DOW radars were compared for the Rolla and Dimmitt tornadoes. In both cases the aspect ratio problem and the horizon problem were evident and in both cases the WSR-88D underestimated the strength of the rotation.

Because of the aspect ratio problem mentioned before, at middle and large distances from the vortex a radar will underestimate the strength of a vortex. Burgess (1993) presented calculations relating the aspect ratio (the ratio of the size of the beam at a certain distance from the radar to the size of the vortex being observed) to the percentage of the rotation that would be observed by the radar (Figure 4.1).

For the Dimmit Tornado, the DOW was about 5 km from the tornado and with a beam width if 1.2 degrees. In this case the aspect ratio was 0.42 and according to Burgess (1993), should be observing about 90% of the rotation. The peak velocity difference across the measured by the DOW at 900 meters was 126 $ms^{-1}$ implying a true difference of about 140 $ms^{-1}$. The Lubbock radar had a beam width of 0.96

degrees and was over 100 km from the tornado. The aspect ratio in this case was 7.0 and according to Burgess, KLBB should have observed only 30% of the rotation. The peak measured by KLBB was about 47 $ms^{-1}$ or about 33%.

The same procedure was done for the Rolla Tornado case. The DOW was only about 3 km from the tornado with a beam with of 0.96 degrees, giving an aspect ratio of 0.05. According to Burgess, the DOW should be observing very close to 100% of the strength of the vortex. KDDC was over 170 km from the tornado and the aspect ratio was 3 and should be estimating about 60% of the rotation or about 42 $ms^{-1}$. The peak for KDDC was about 43 $ms^{-1}$. KAMA was over 200 km from the tornado and had an aspect ratio of 3.6 and should be estimating 45% of the rotation. KAMA actually observed peak velocities of 42 $ms^{-1}$, about 60%, of the DOW or "true" strength.

Burgess' predictions (1993) of the relation between the aspect ration and the observed vortex strength were very similar to what was observed in the Dimmitt and Rolla Tornado cases. For the Dimmitt Tornado, Burgess' predictions of only observing30% of the rotation were very close. Even though the radars were much farther from the tornadoes in the Rolla case, the tornado itself was much larger than the Dimmitt tornado and according to Burgess the KDDC radar and the KAMA radars should have been observing 60 and 45% of the rotation. Even though the DOW and the WSR-88D radars observed the tornado at two different levels, the estimations were very close.

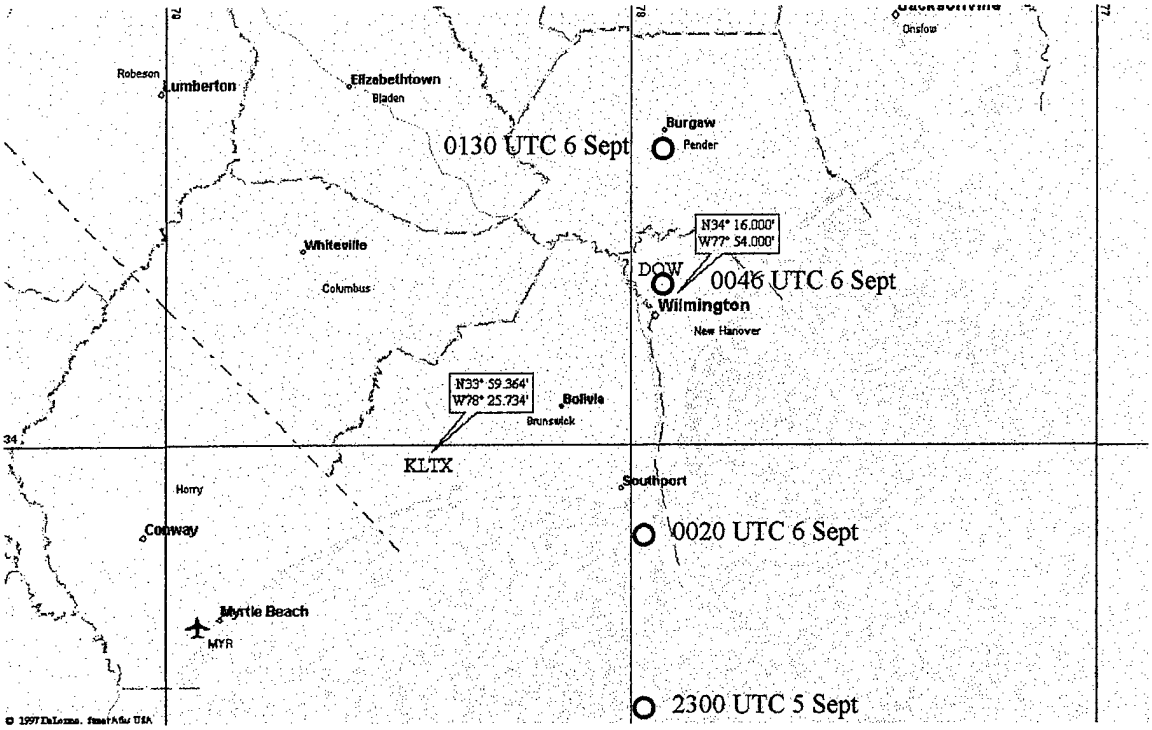


**Figure 2.1** Location of Doppler on Wheels (DOW) and the Wilmington WSR-88D (KLTX) during Hurricane Fran 5-6 September 1996

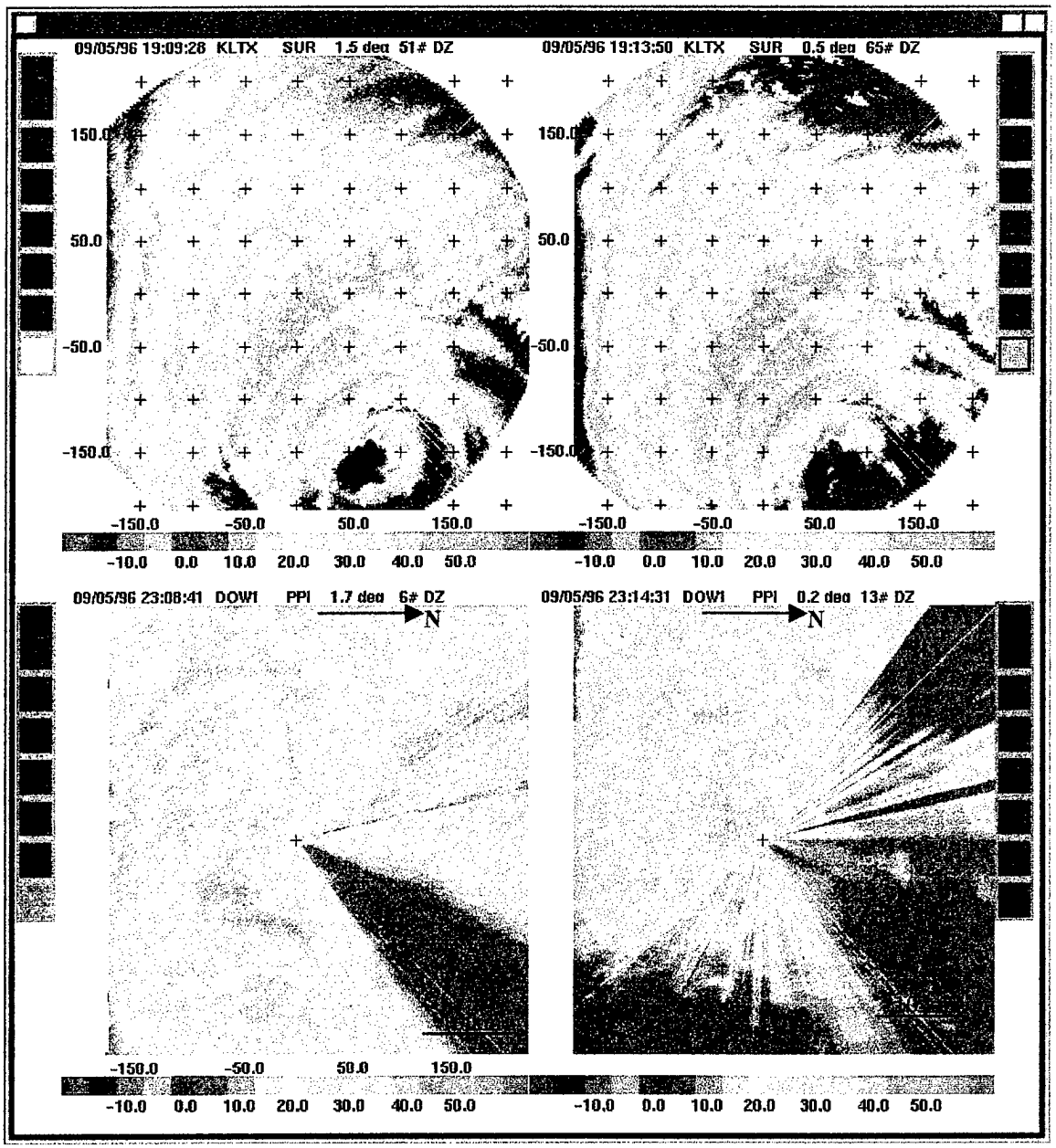


**Figure 2.2** KLTX and DOW reflectivity at 1908 UTC (a. is the upper left, b. is the upper right c. is the lower left and d. is the lower right).

a. KLTX reflectivity: Eye of Hurricane Fran 160 kilometers to the southeast of the radar.
b. Large rain band in Hurricane Fran approaching KLTX.
c. DOW reflectivity: large area of heavy rain with imbedded cells, with some attenuation.
d. One of the imbedded cells over the DOW causing attenuation.

Note: UTC (DOW time is four hours ahead of UTC e. g. 2308 DOW time is 1908UTC).

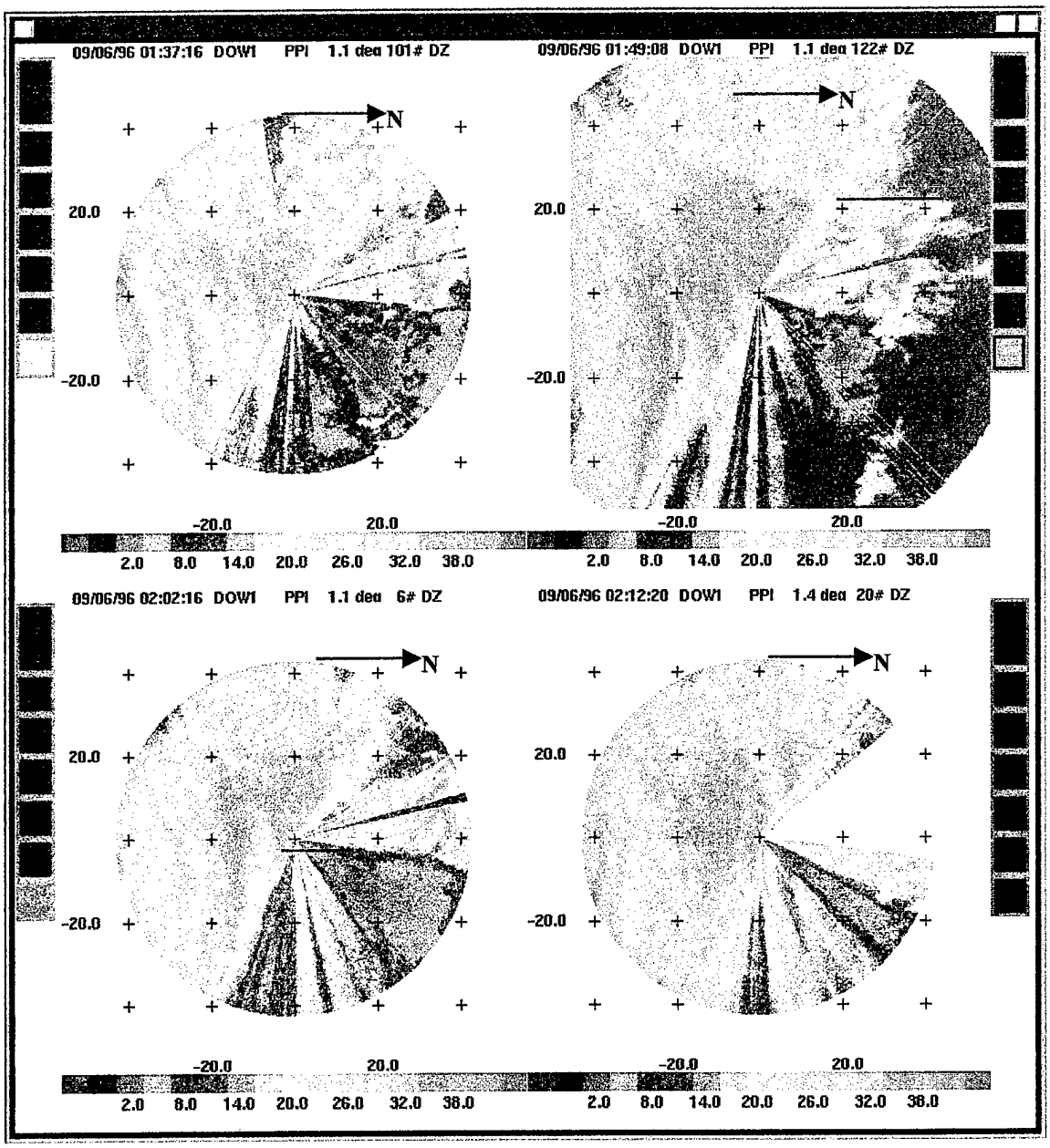


**Figure 2.3** Rain band approaching the DOW about 2137 UTC on 5 September 1996 1908 (a. is the upper left, b. is the upper right c. is the lower left and d. is the lower right).

a. Three rain bands visible, one over the radar and two to the south-southeast.
b. Strong rain band approaching the DOW.
c. Strong rain band approaching the DOW.
d. Strong rain band over the DOW.

Note: UTC (DOW time is four hours ahead of UTC).

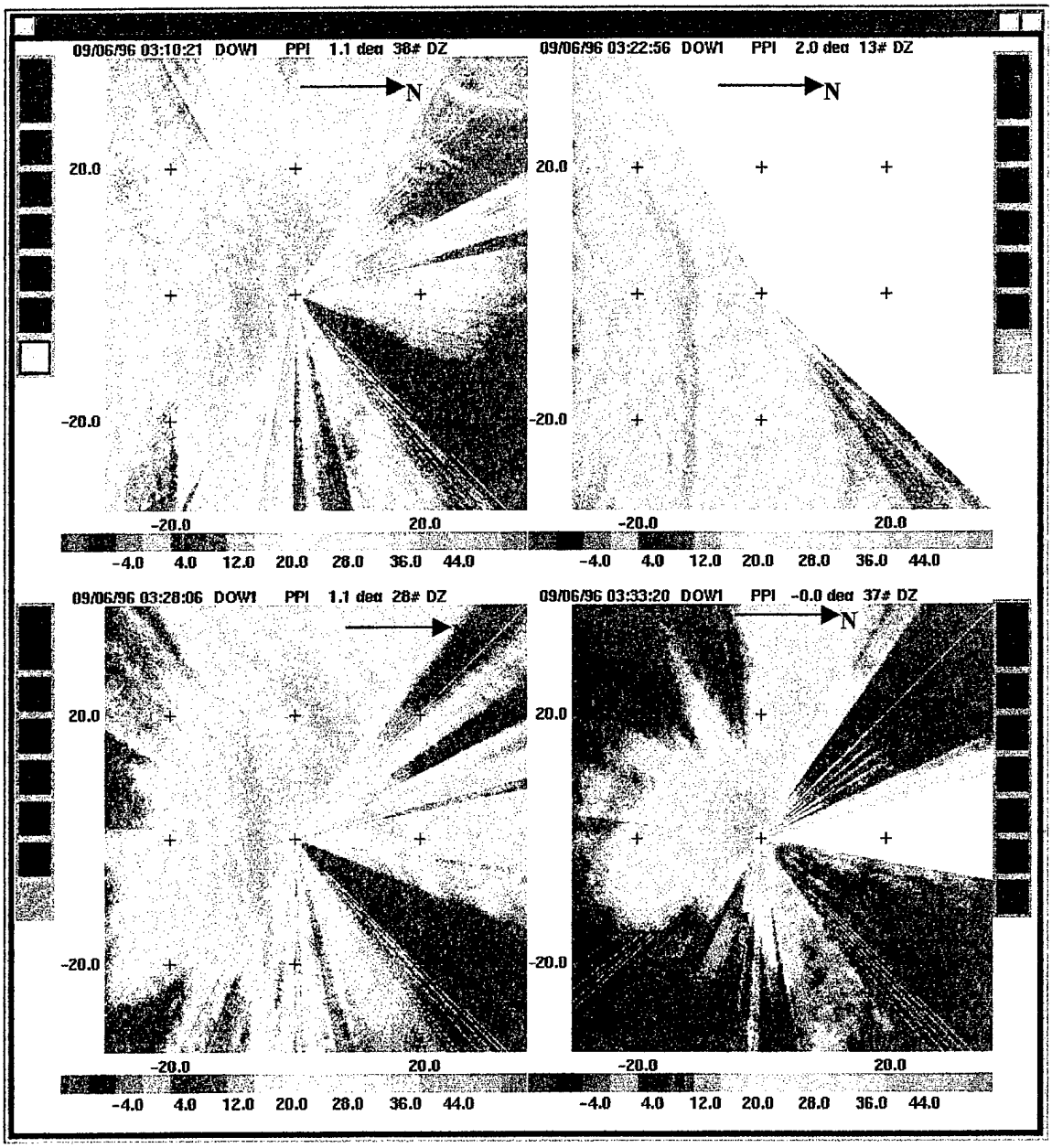


**Figure 2.4** Rain band in DOW reflectivity field an hour before eye passage (a. is the upper left, b. is the upper right c. is the lower left and d. is the lower right).

a. Rain band approaching radar and thin intense line visible at edge of radar.
b. This line clearly visible approaching radar.
c. Thin line approaching radar.
d. Thin line over radar causing attenuation.

Note: UTC (DOW time is four hours ahead of UTC).

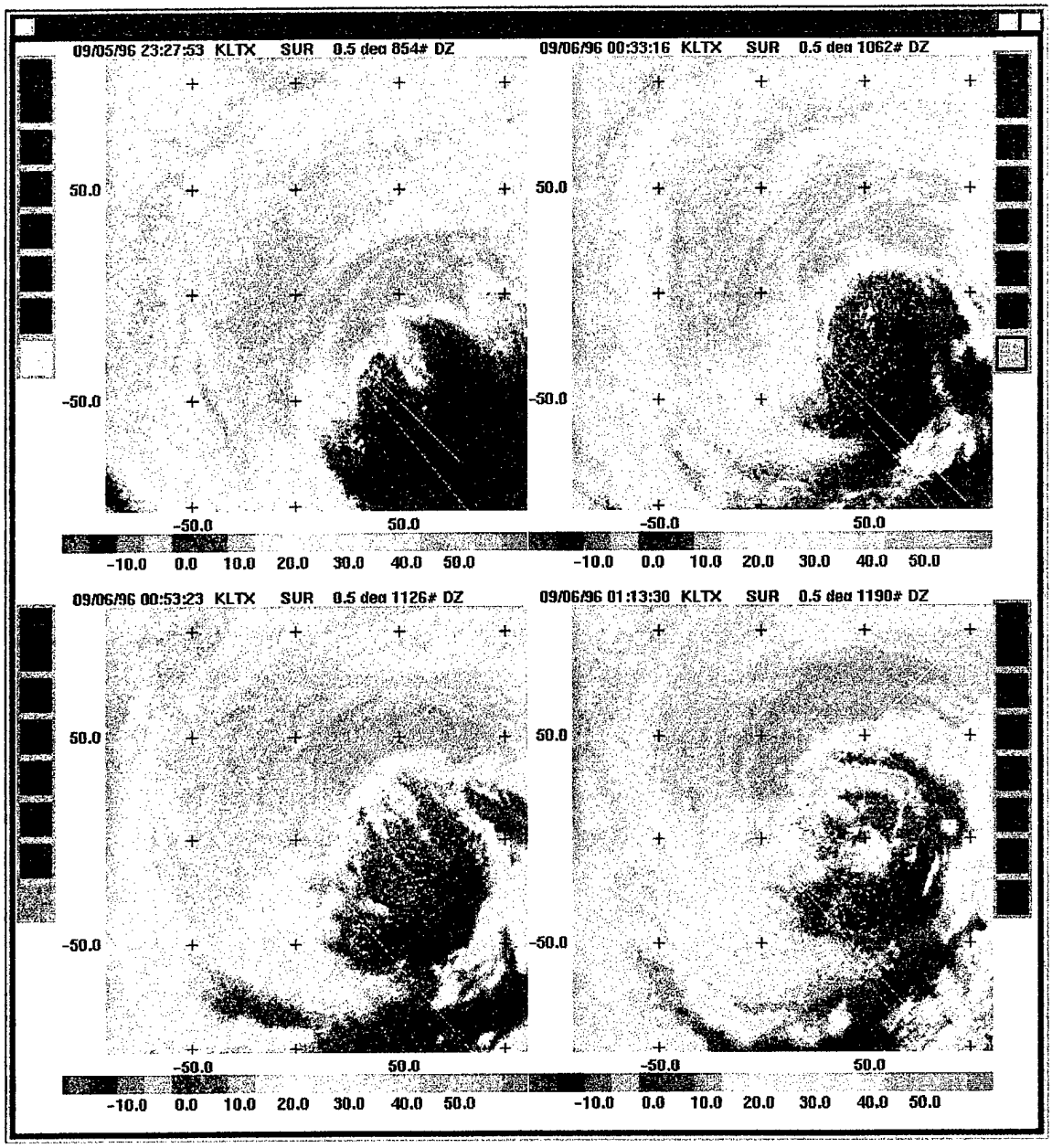


**Figure 2.5** The eye of Hurricane Fran as it passes to the east of KLTX (a. is the upper left, b. is the upper right c. is the lower left and d. is the lower right).

a. Thin line approaches the DOW.
b. Rain bands starting to form in the eye of Hurricane Fran.
c. Rain bands developing in the eye and approaching the DOW.
d. Rain bands in the eye and over the DOW.

Note: UTC (DOW time is four hours ahead of UTC).

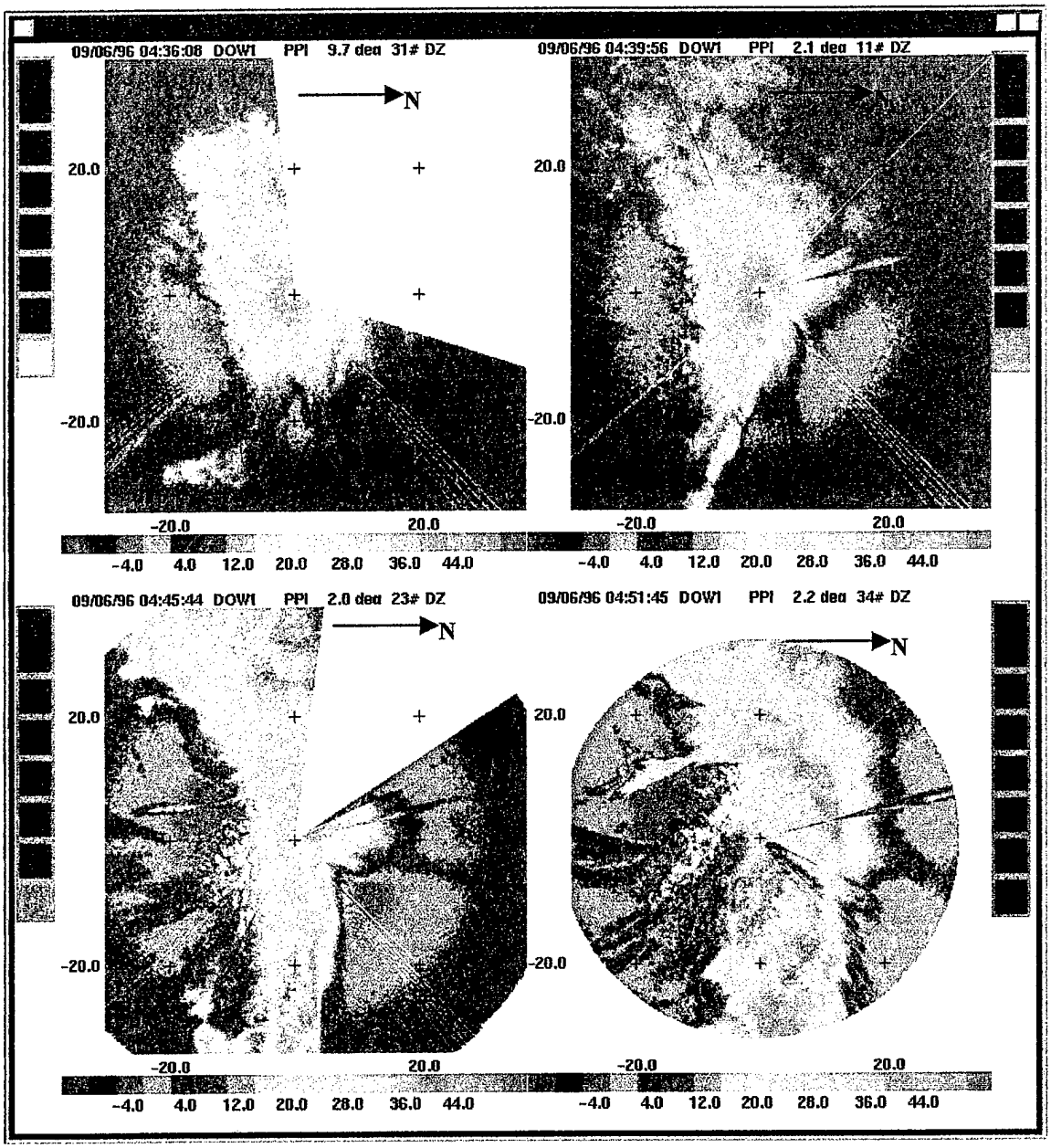


**Figure 2.6** Eye of Hurricane Fran in DOW reflectivity field (a. is the upper left, b. is the upper right c. is the lower left and d. is the lower right).

a. Eye first visible in reflectivity field.
b. Eye approaching the DOW from the south.
c. Forward eye wall over the DOW.
d. Eye over the DOW. Weak rain bands forming in the eye.

Note: UTC (DOW time is four hours ahead of UTC).

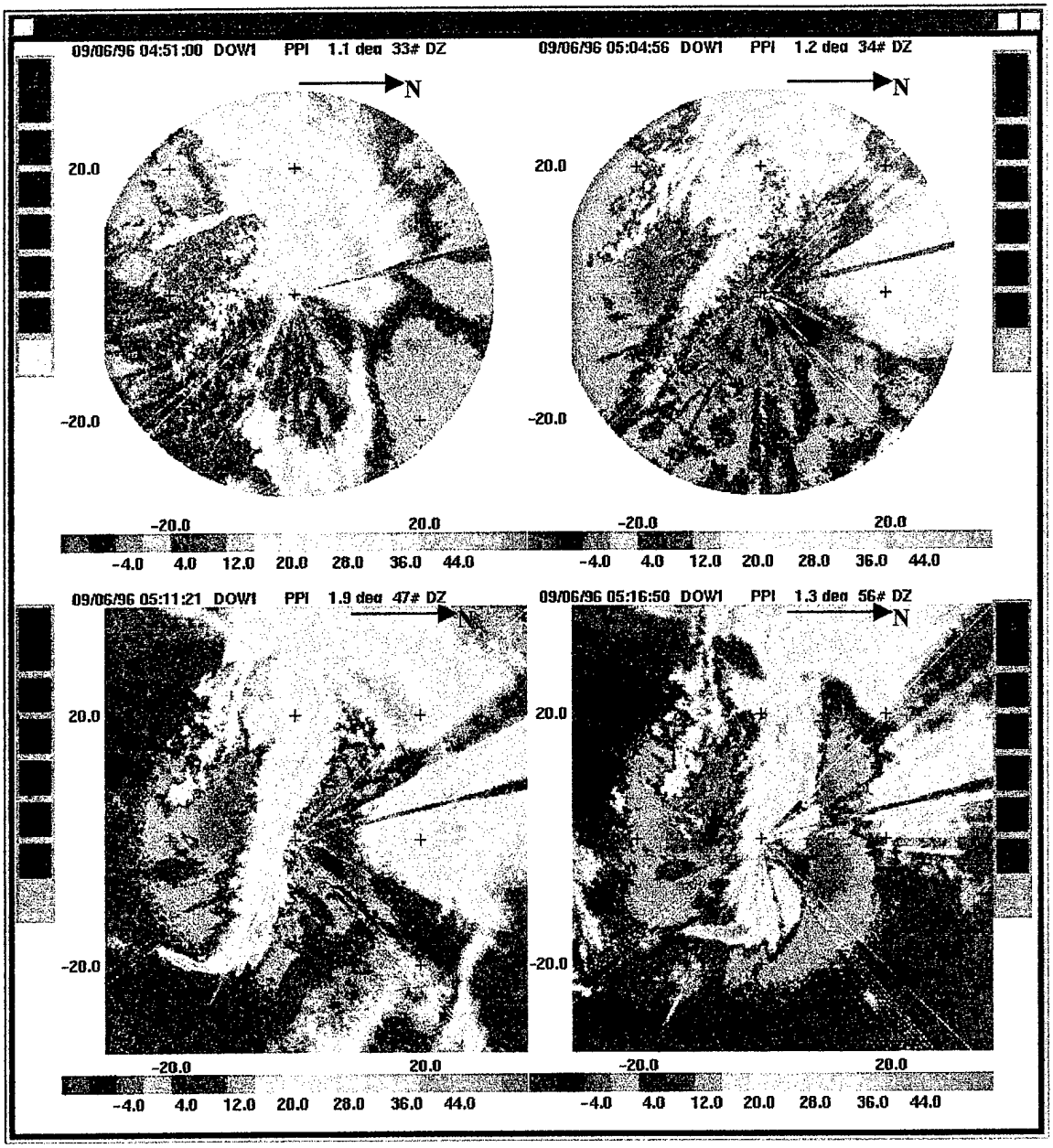


**Figure 2.7** Weak rain band in eye of Hurricane Fran (a. is the upper left, b. is the upper right c. is the lower left and d. is the lower right).

a. Weak rain band just to the southwest of the DOW.
b. Rain band starting to develop as it approaches DOW.
c. Rain band just to south of DOW.
d. Developing rain band passing DOW.

Note: UTC (DOW time is four hours ahead of UTC therefore 2308 DOW time is 1908UTC).

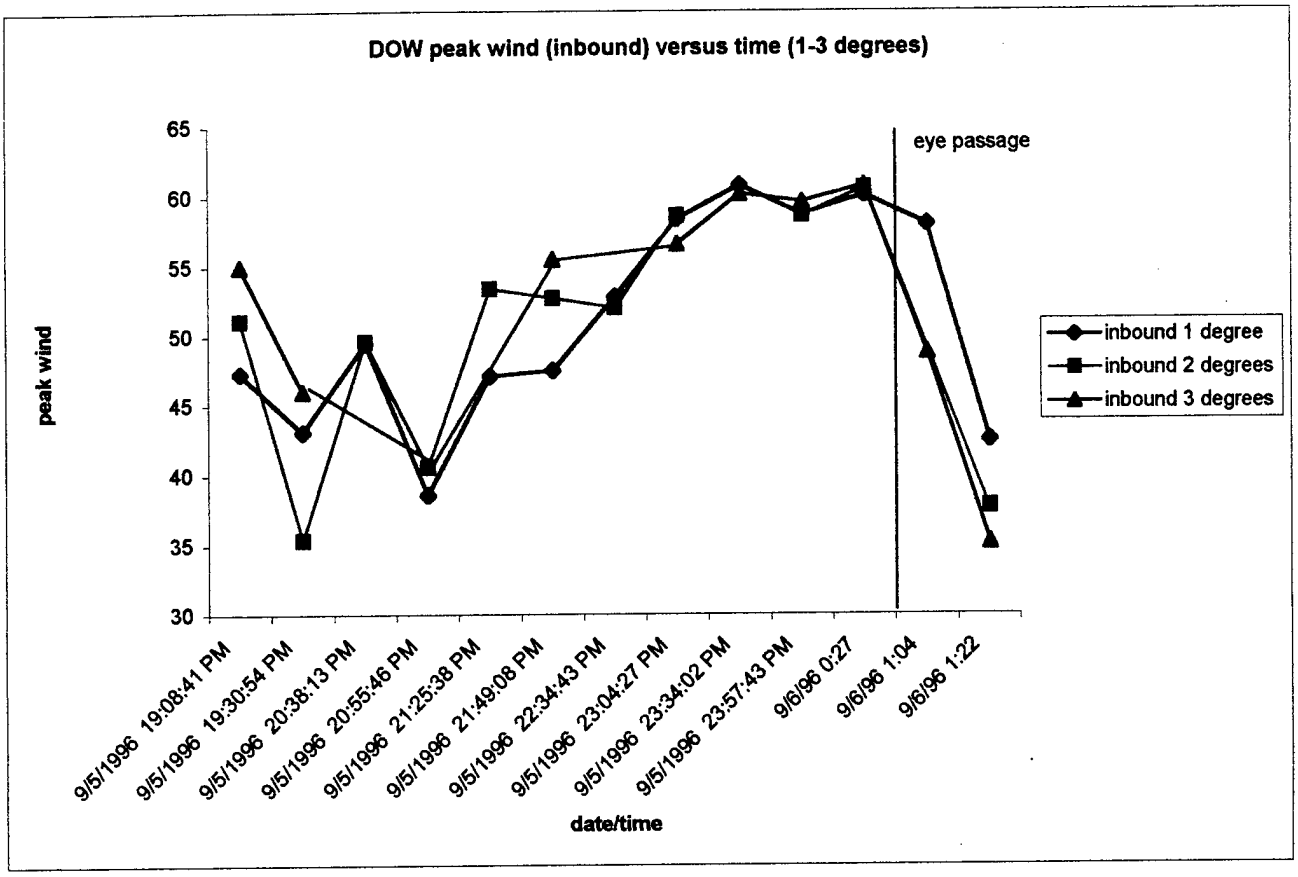


**Figure 2.8** DOW peak wind ($ms^{-1}$) versus time for the 1.0, 2.0, and 3.0 degree elevation angle scans.

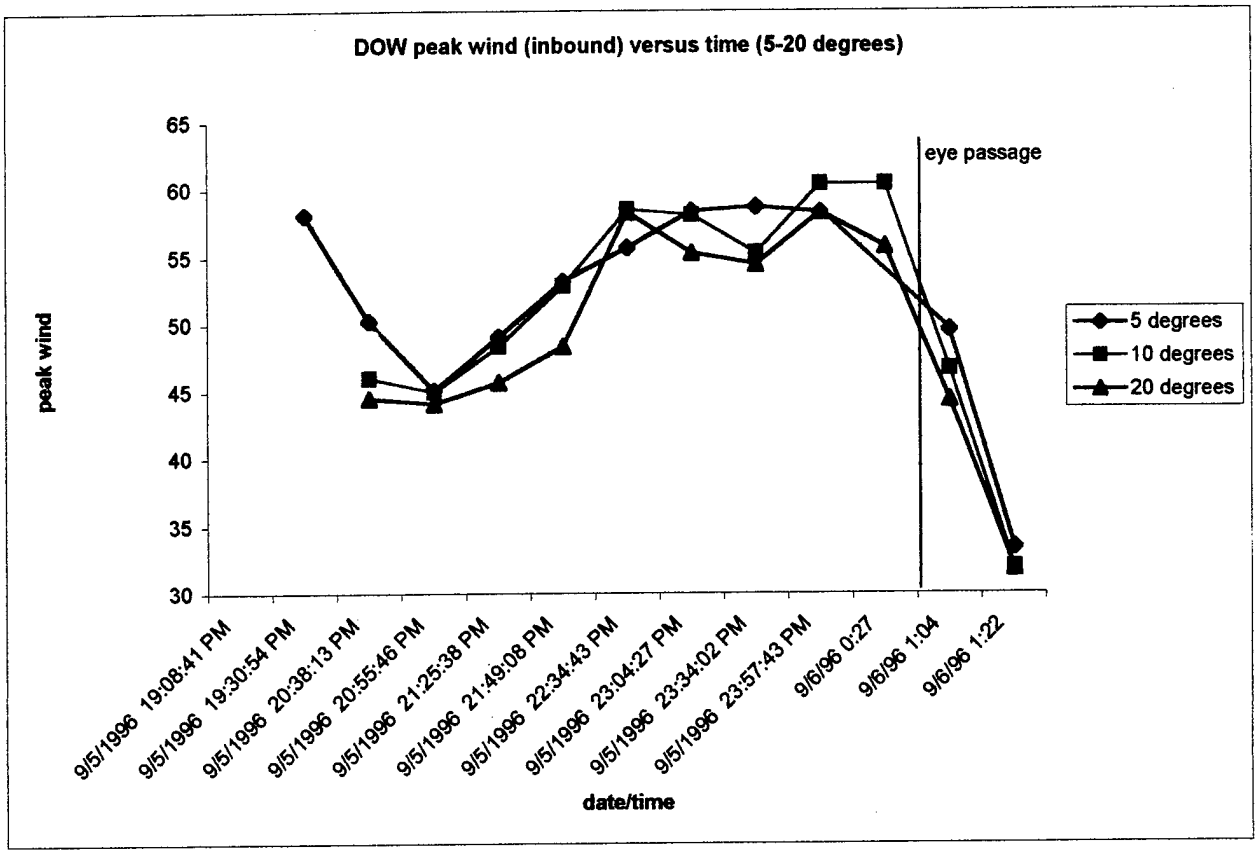


**Figure 2.9** DOW peak wind ($ms^{-1}$) versus time (UTC) for the 5.0, 10.0, and 20.0 degree elevation angle scans.

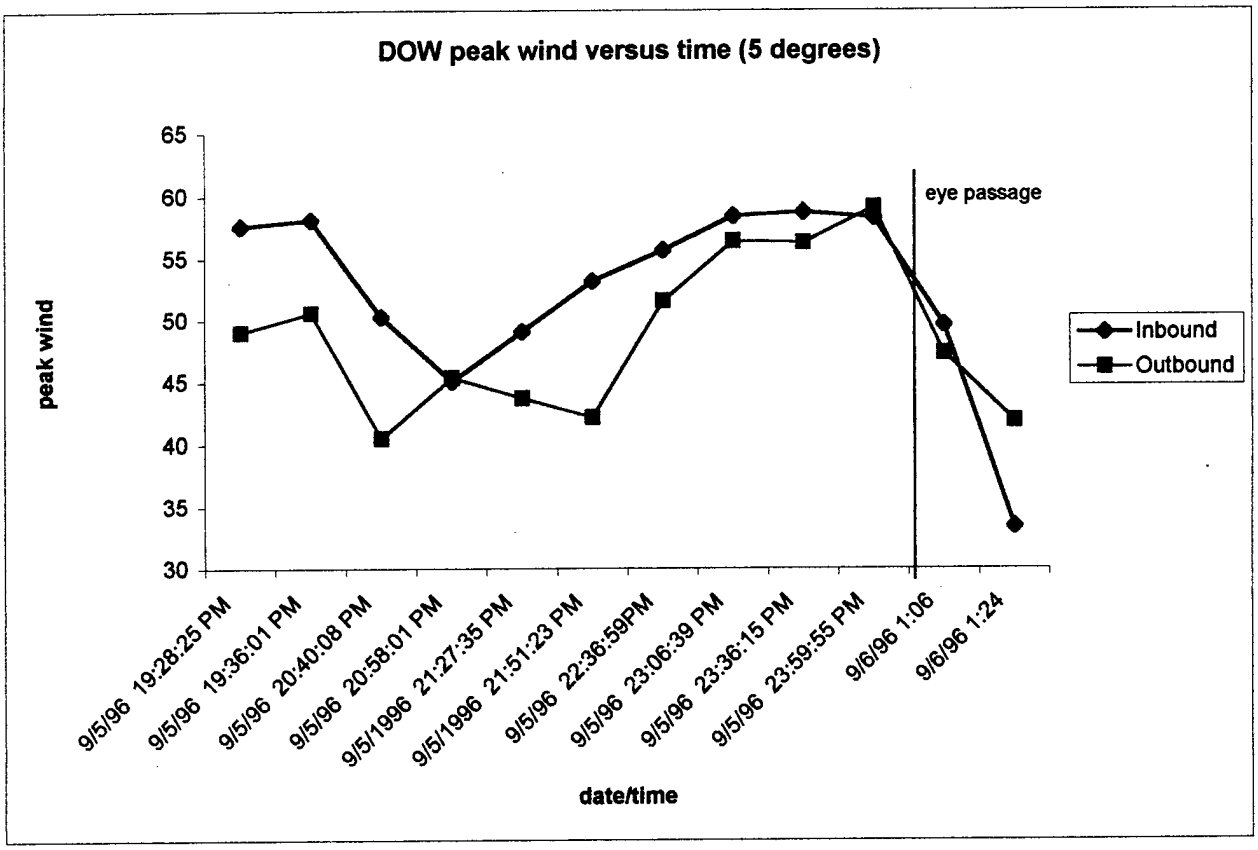


**Figure 2.10** DOW peak wind ($ms^{-1}$) versus time (UTC) for inbound and outbound sides.

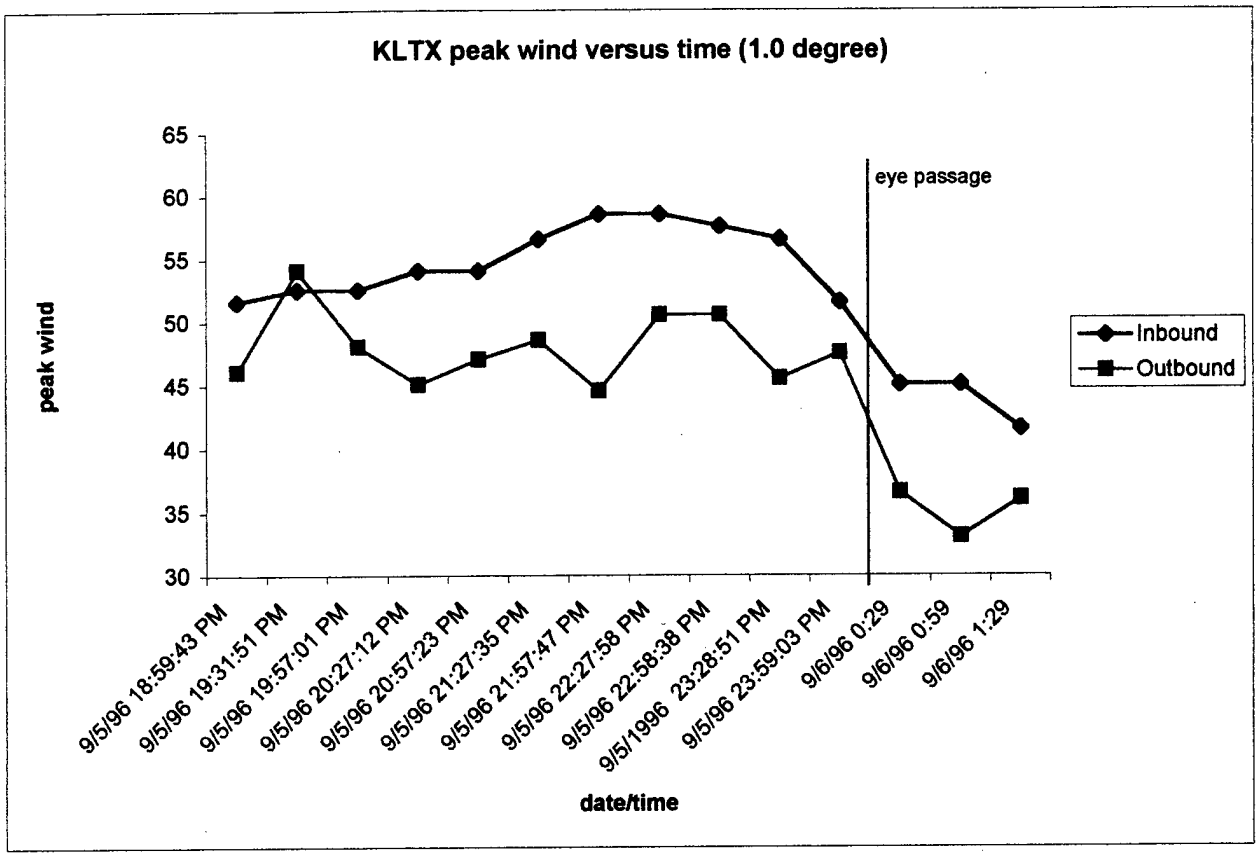


**Figure 2.11** KLTX peak wind ($ms^{-1}$) versus time (UTC) for 1.0 degree elevation angle scan for inbound and outbound sides.

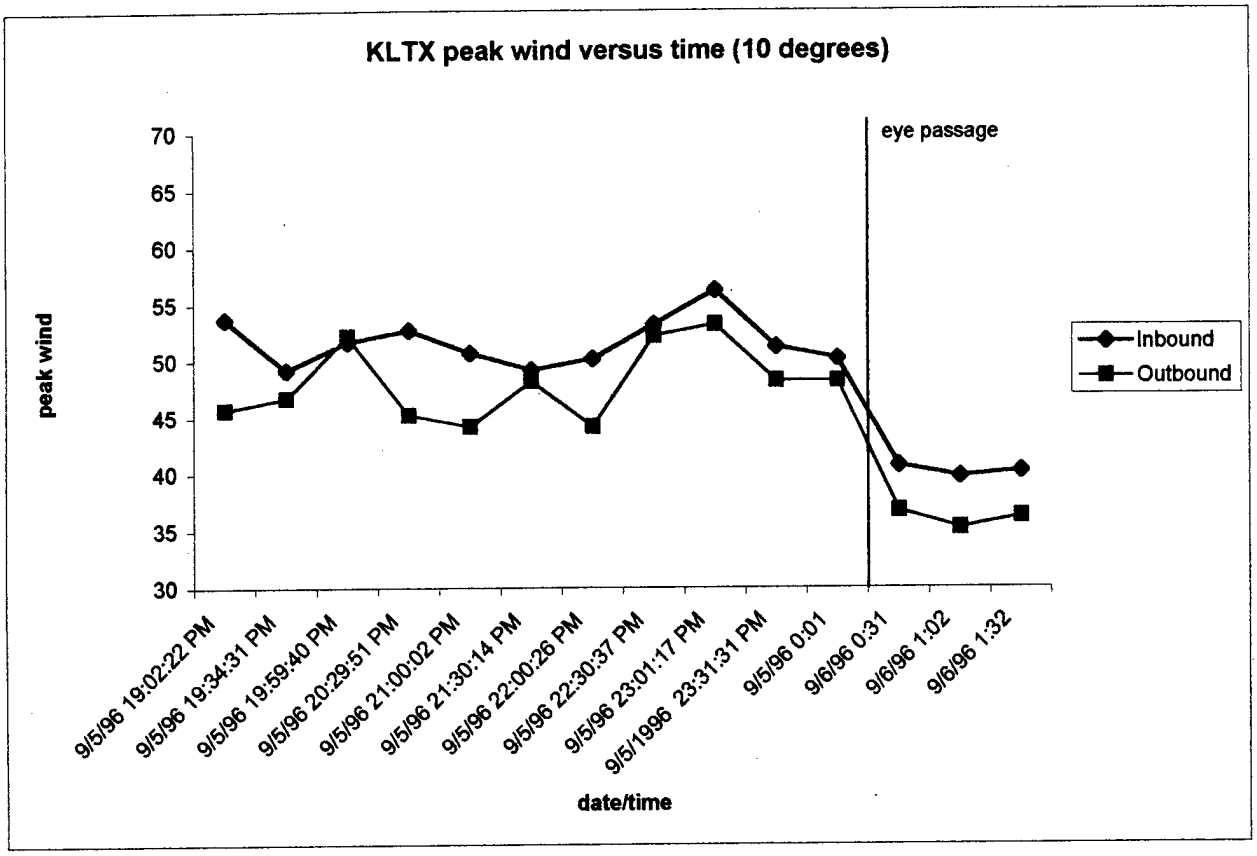


**Figure 2.12** KLTX peak wind ($ms^{-1}$) versus time (UTC) for 10.0 degree elevation angle scan for inbound and outbound sides.

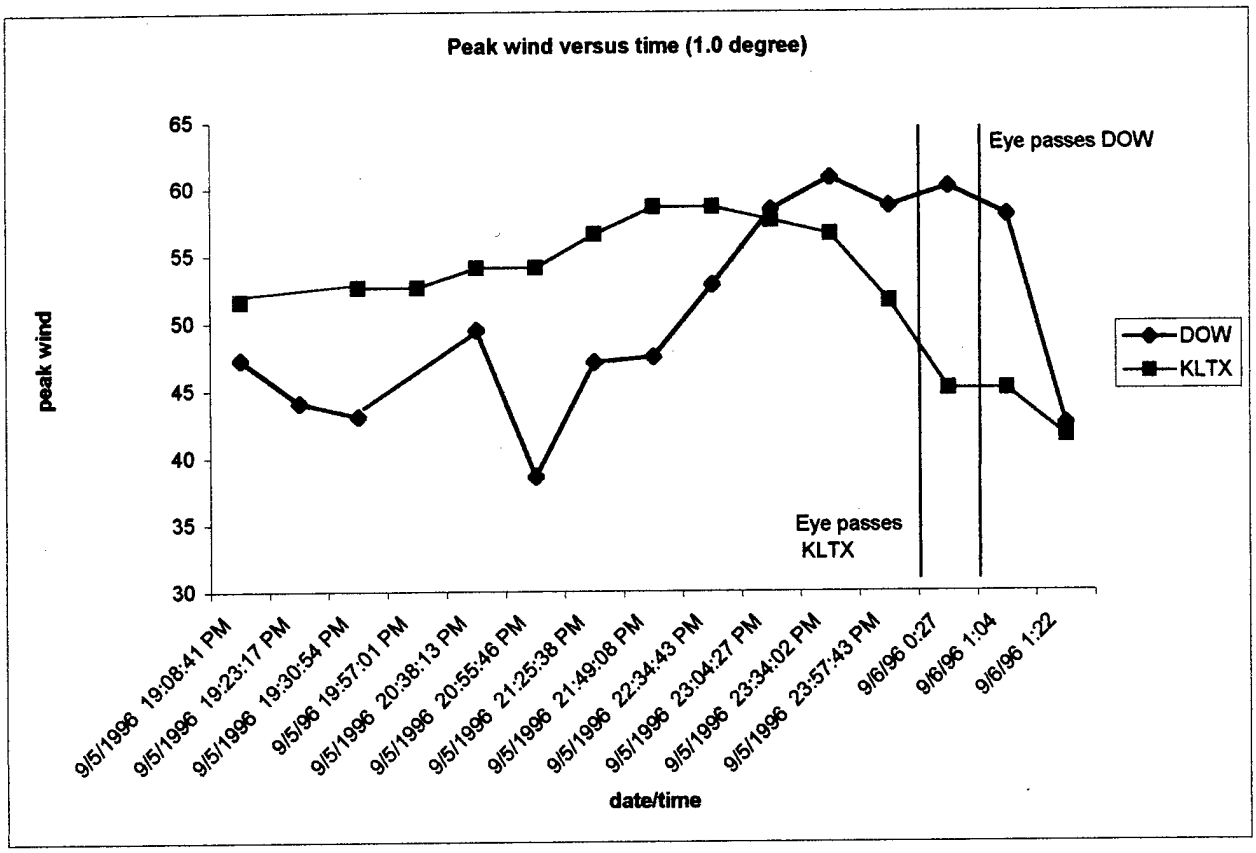


**Figure 2.13** Peak wind ($ms^{-1}$) versus time (UTC) for inbound side of KLTX and DOW using the 1.0 degree elevation angle scan.

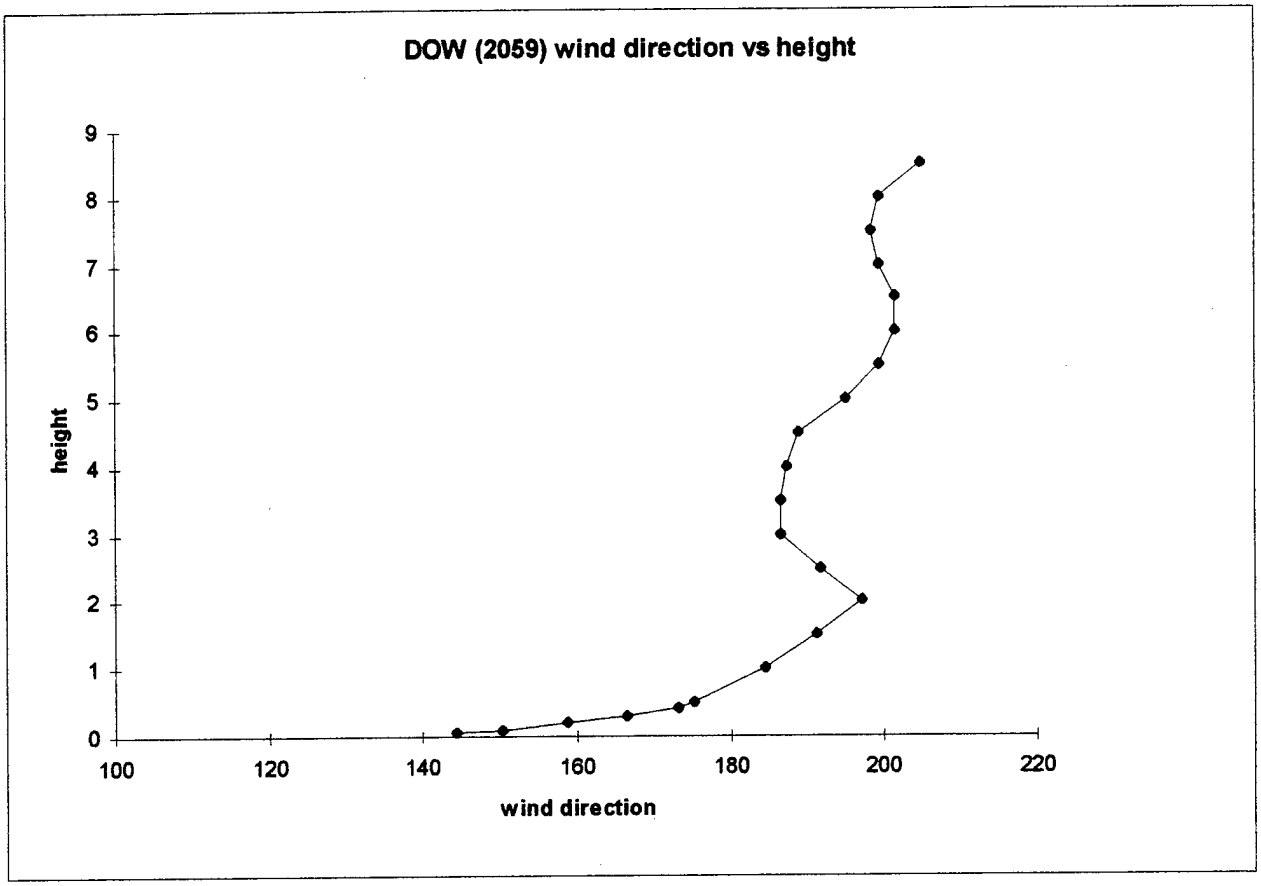


**Figure 2.14** DOW wind direction (degrees) versus height (km) at 2059 UTC.

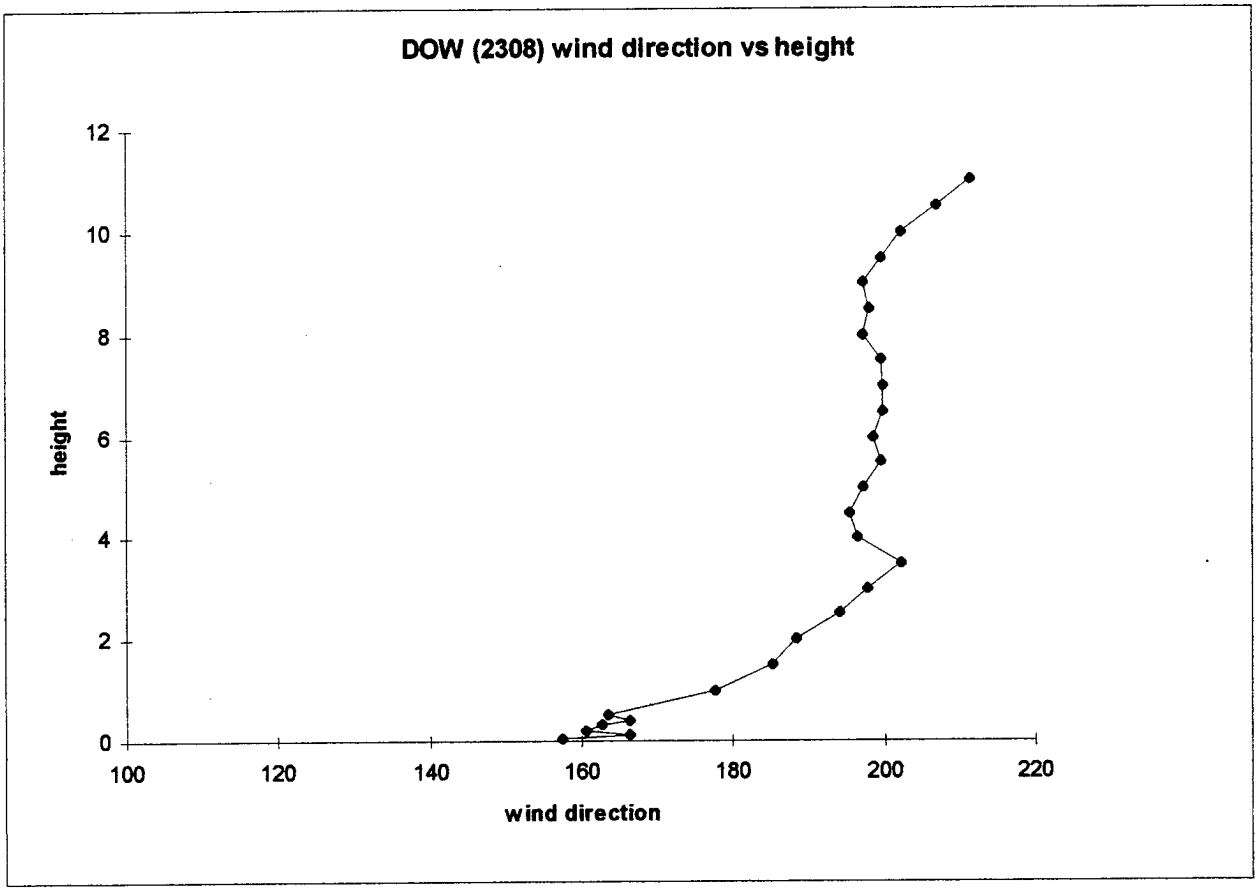


**Figure 2.15** DOW wind direction (degrees) verses height (km) at 2308 UTC

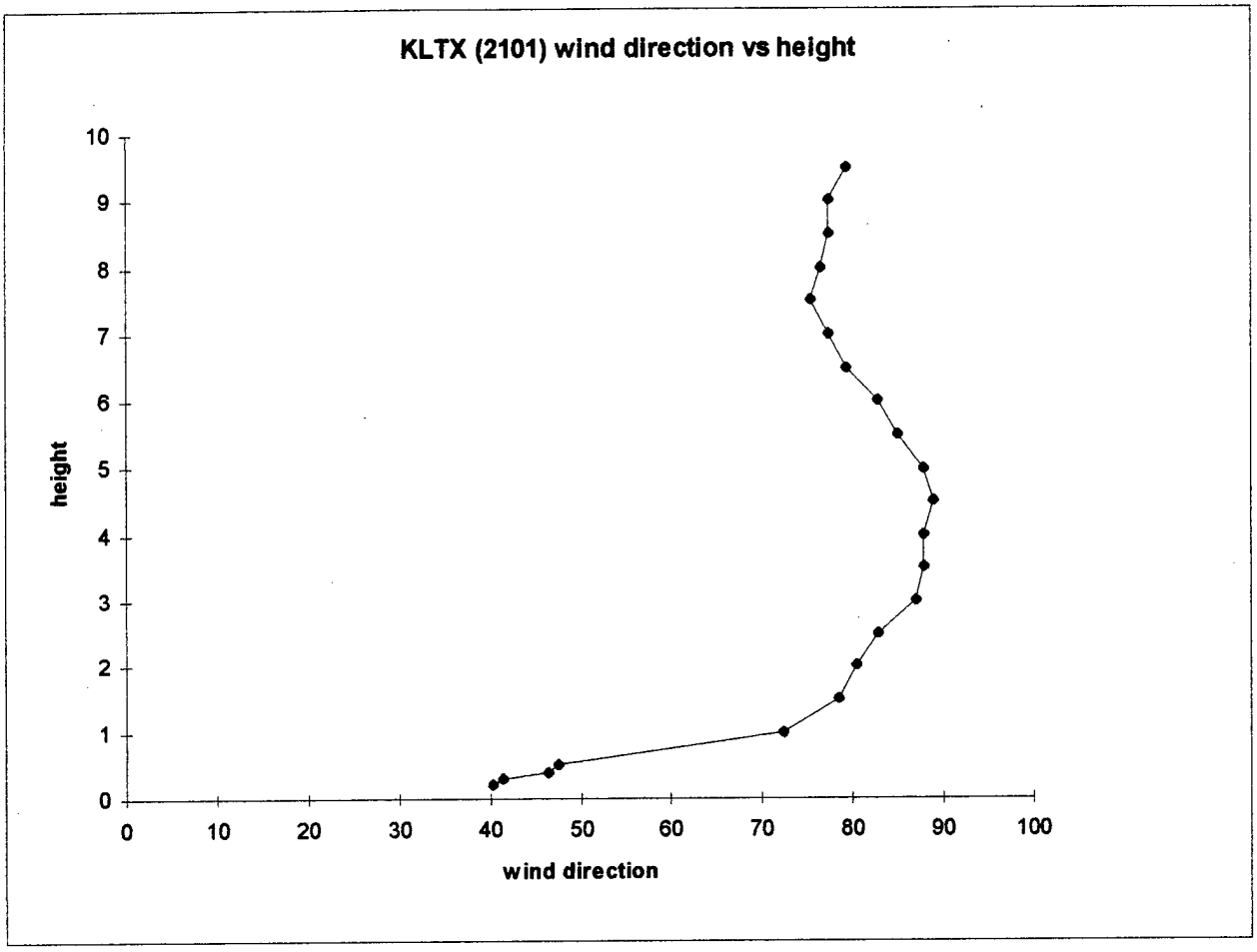


**Figure 2.16** KLTX wind direction (degrees) versus height (km) at 2131.

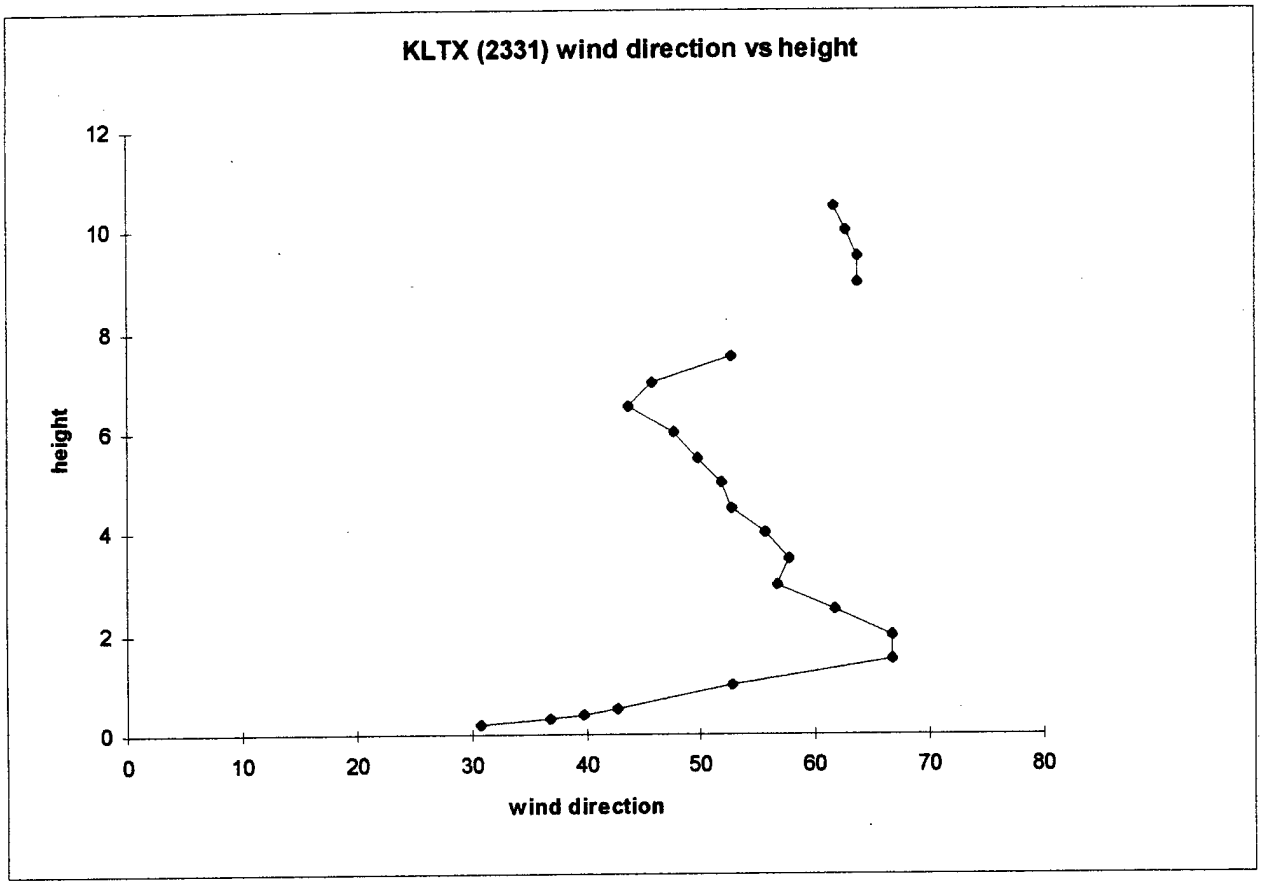


**Figure 2.17** KLTX wind direction (degrees) versus height (km) at 2331 UTC.

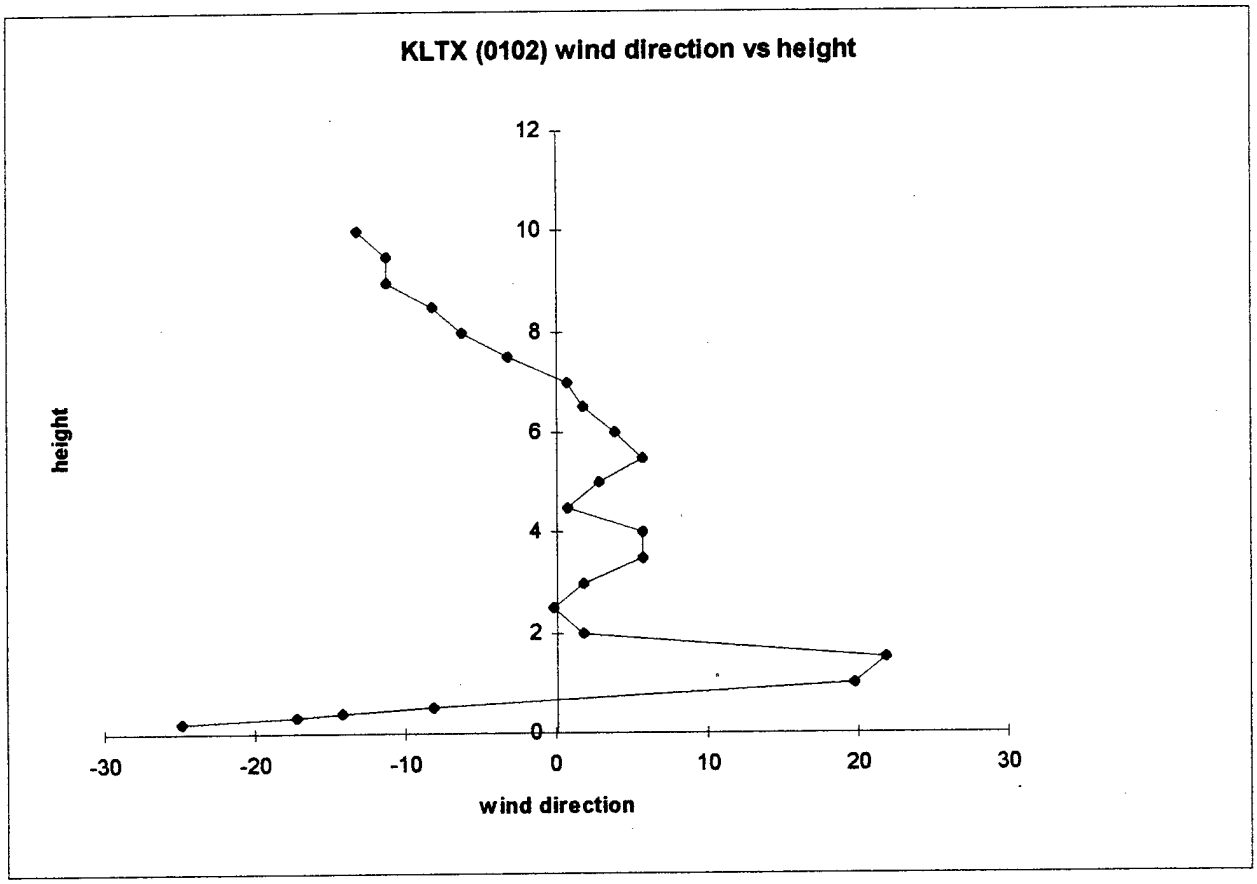


**Figure 2.18** KLTX wind direction (degrees) versus height (km) at 0102 UTC.

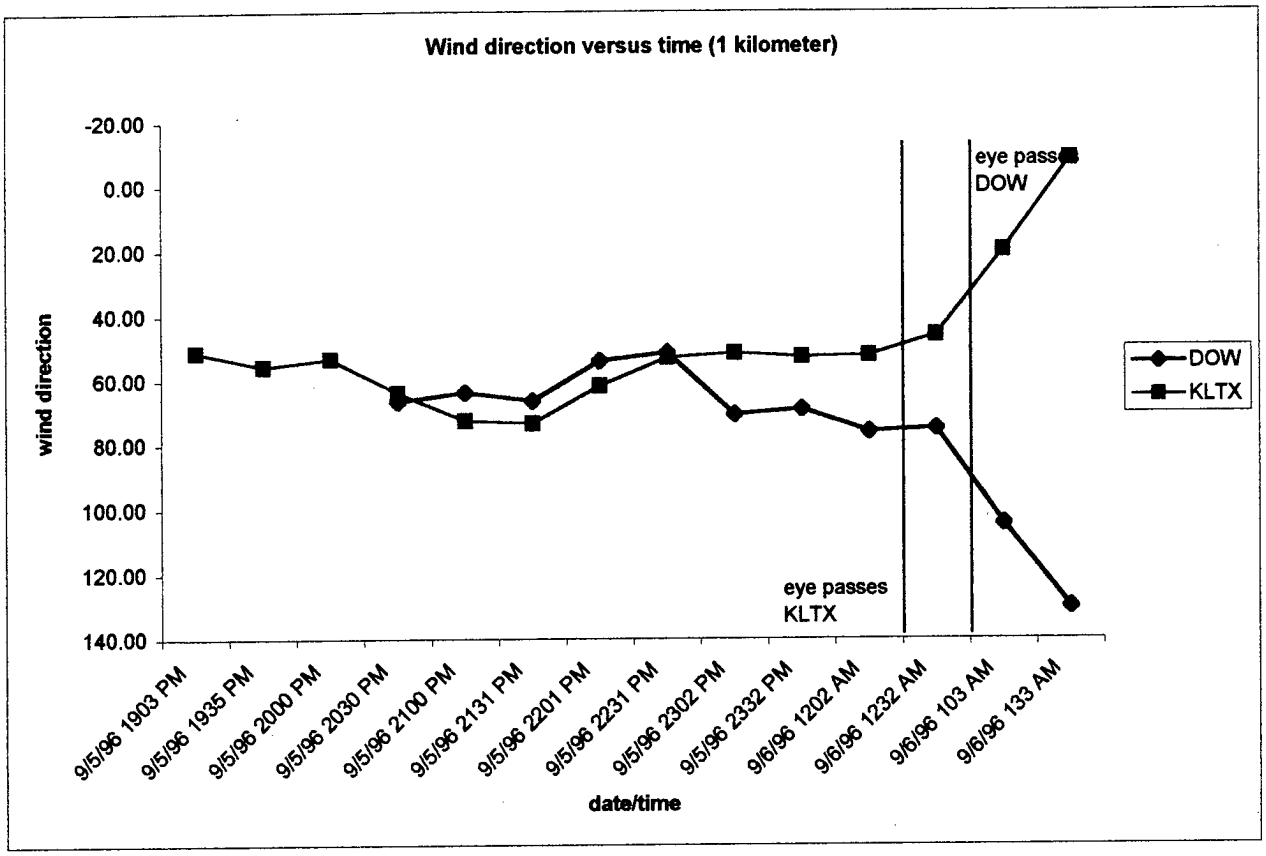


**Figure 2.19** DOW and KLTX wind direction (degrees) versus time (UTC) for 1 kilometer.

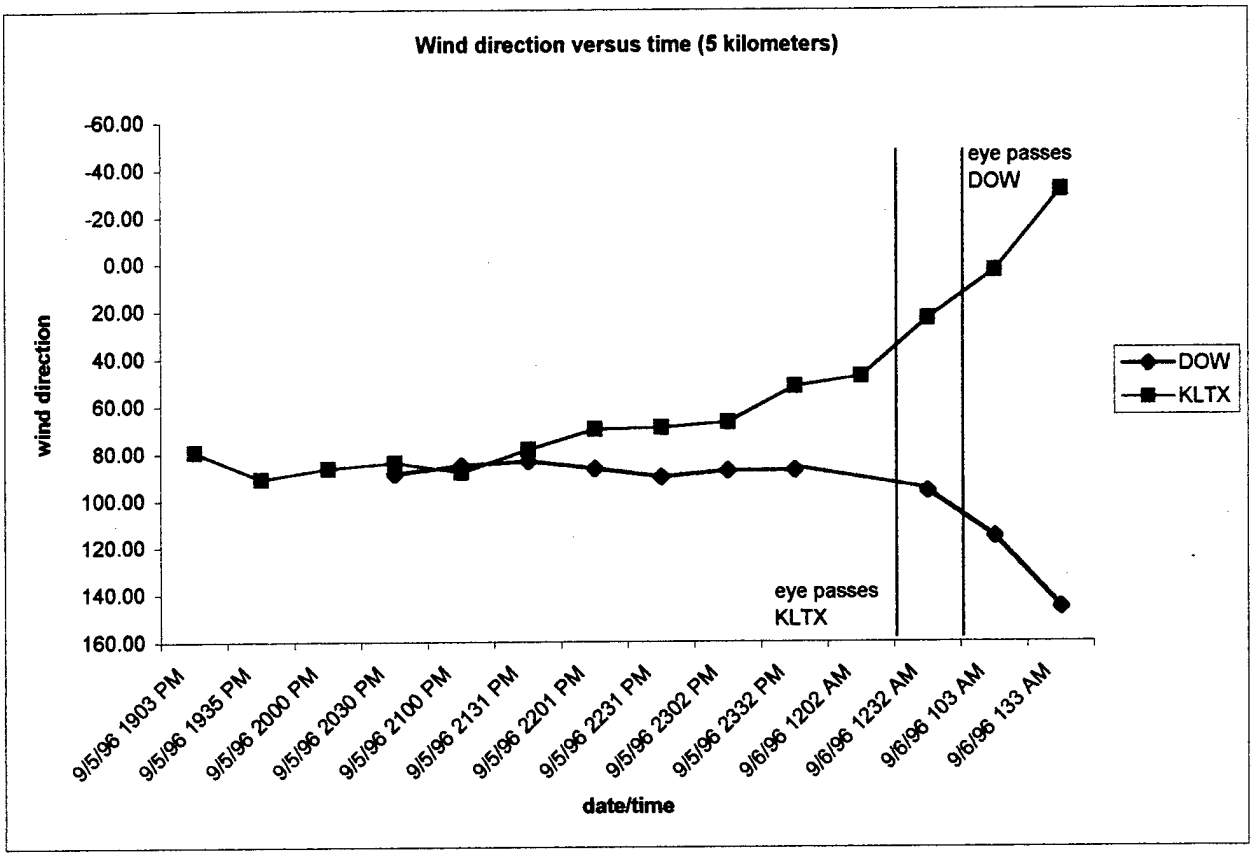


**Figure 2.20** KLTX and DOW wind direction (degrees) versus time(UTC) for 5 kilometers.

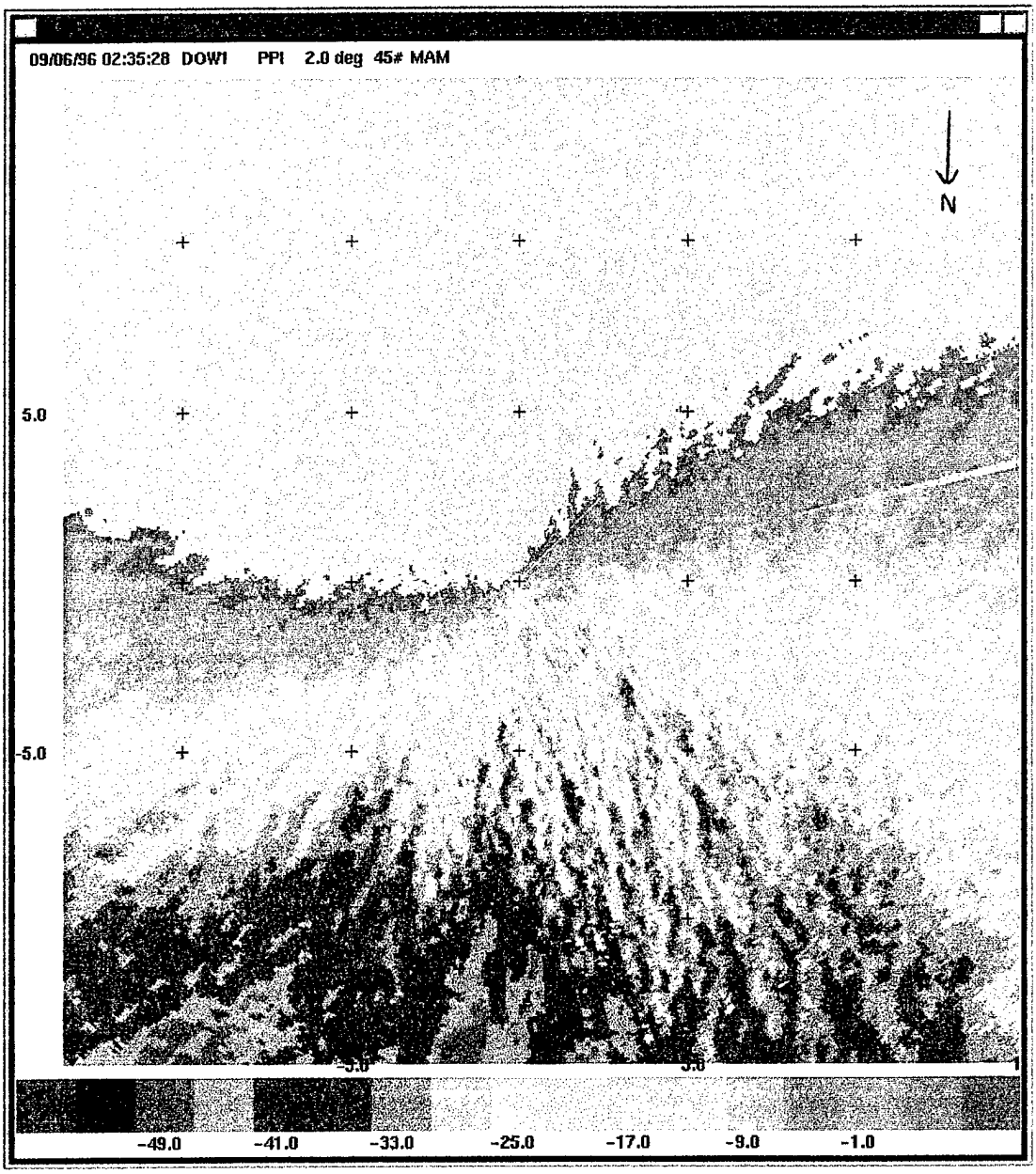


**Figure 2.21** Velocity field (ms $^{-1}$) from the DOW during Hurricane Fran showing the boundary layer rolls.

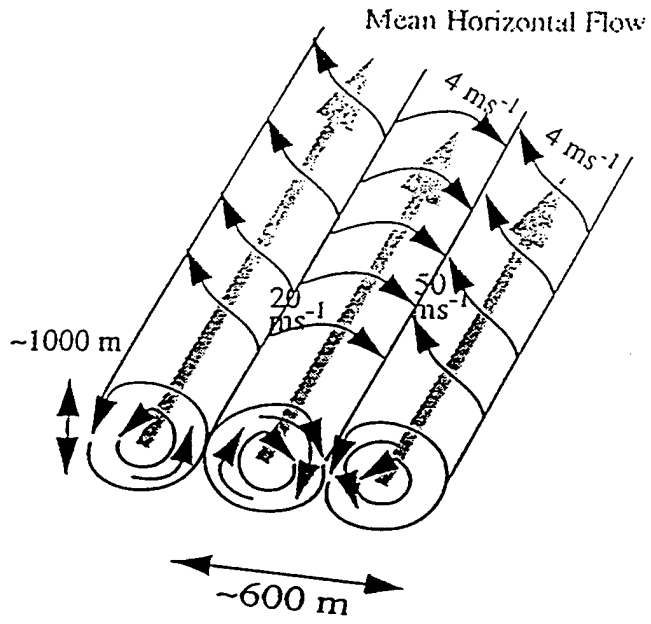


**Figure 2.22** Schematic representation of boundary layer rolls (from Wurman and Winslow, 1998).

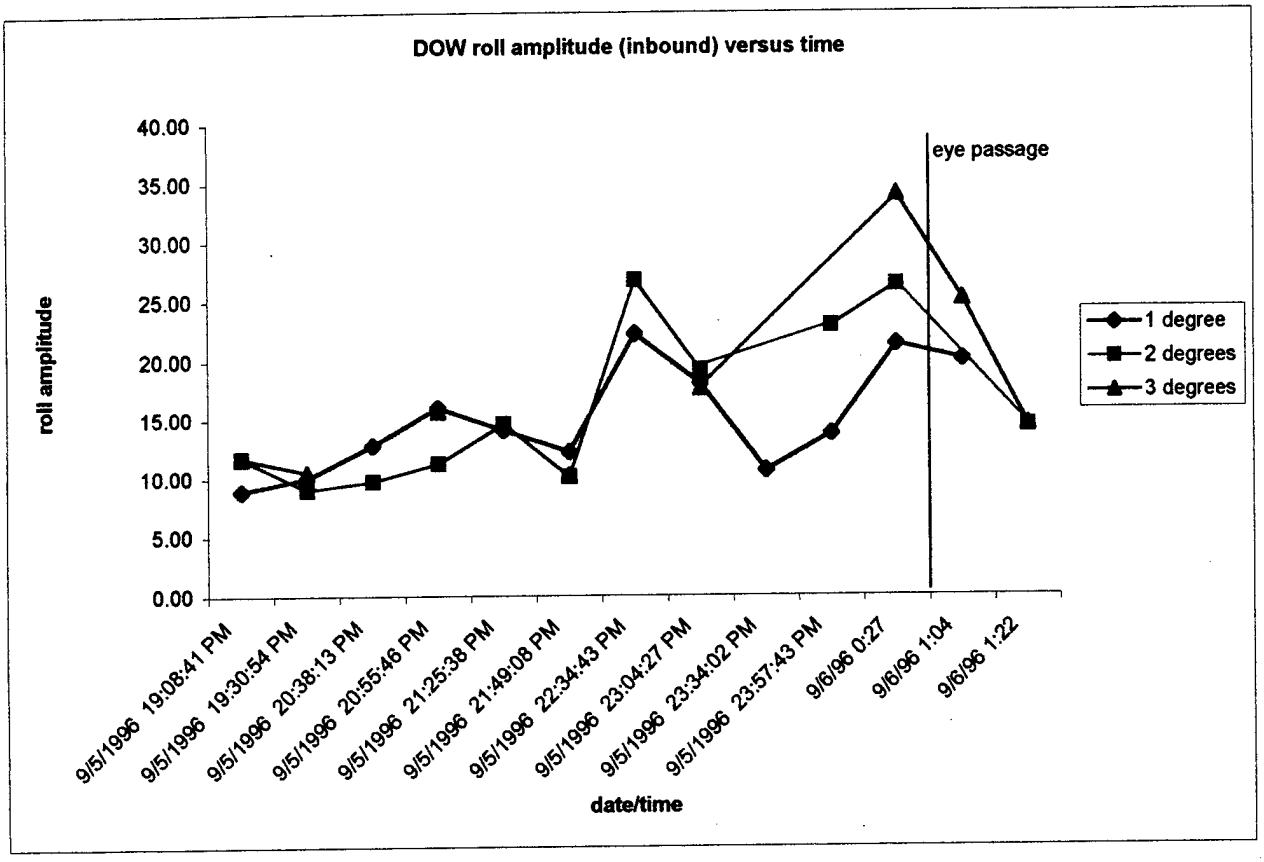


**Figure 2.23** DOW roll amplitude (peak to trough) ($ms^{-1}$) versus time (UTC) for inbound side.

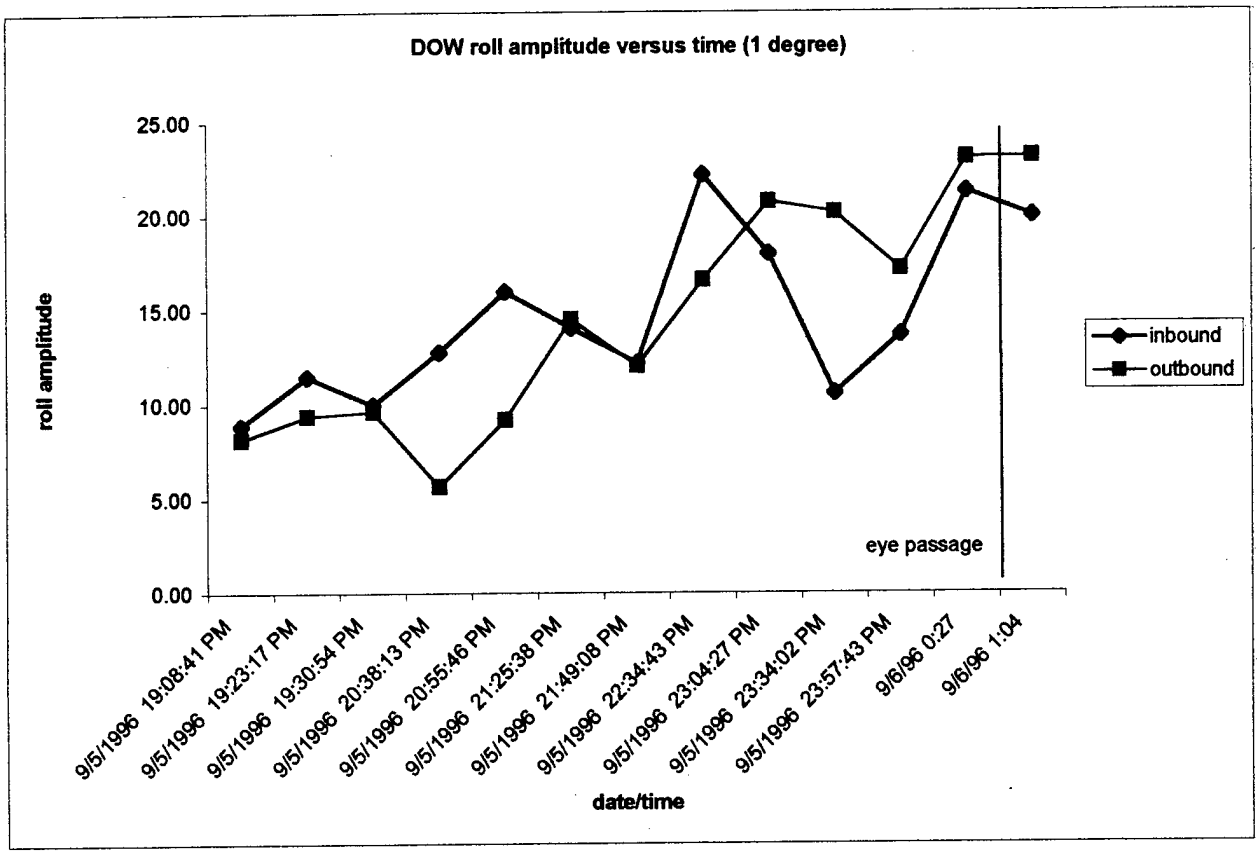


**Figure 2.24** DOW roll amplitude (peak to trough) ($ms^{-1}$) versus time (UTC) for inbound and outbound sides using the 1.o degree elevation angle scan.

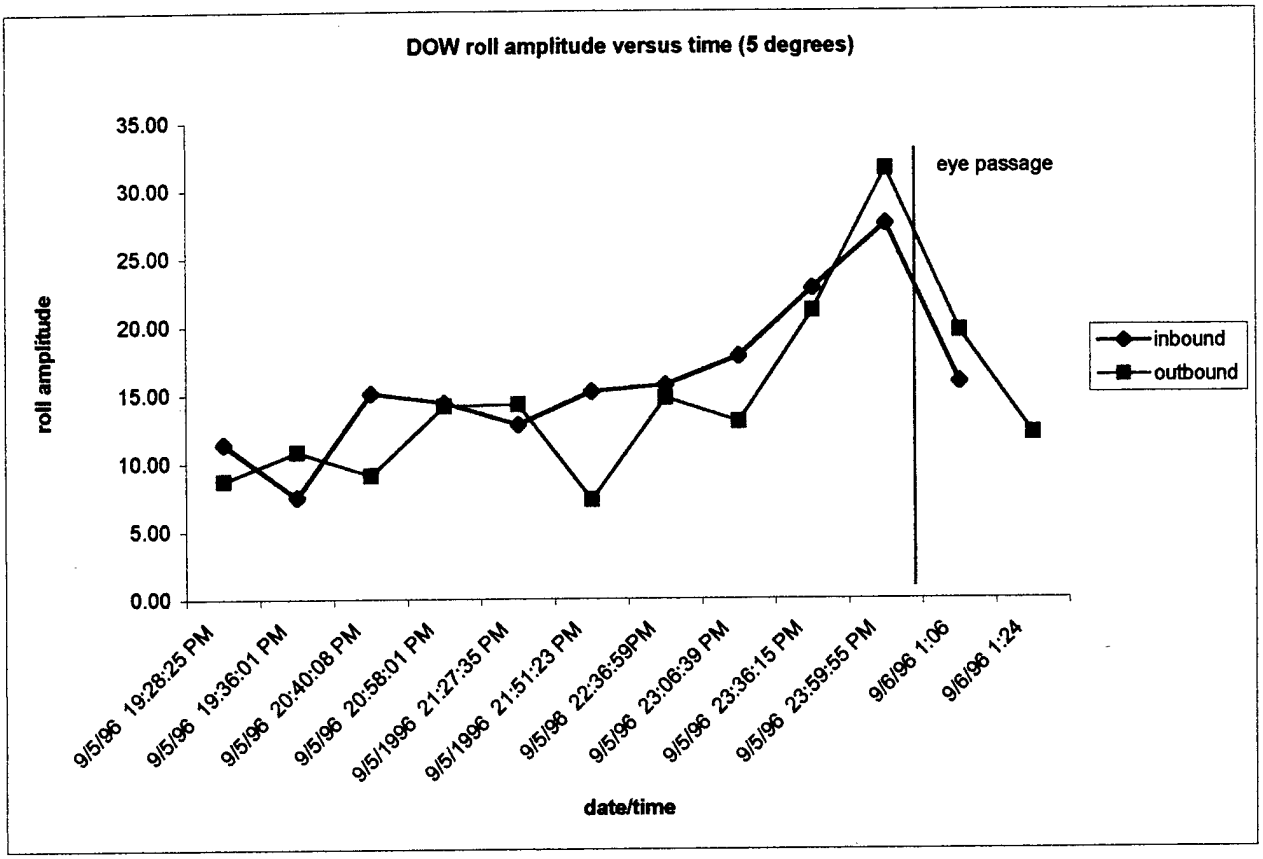


**Figure 2.25** DOW roll amplitude (peak to trough) ($ms^{-1}$) versus time (UTC) for inbound and outbound sides using the 5.0 degree elevation angle scan.

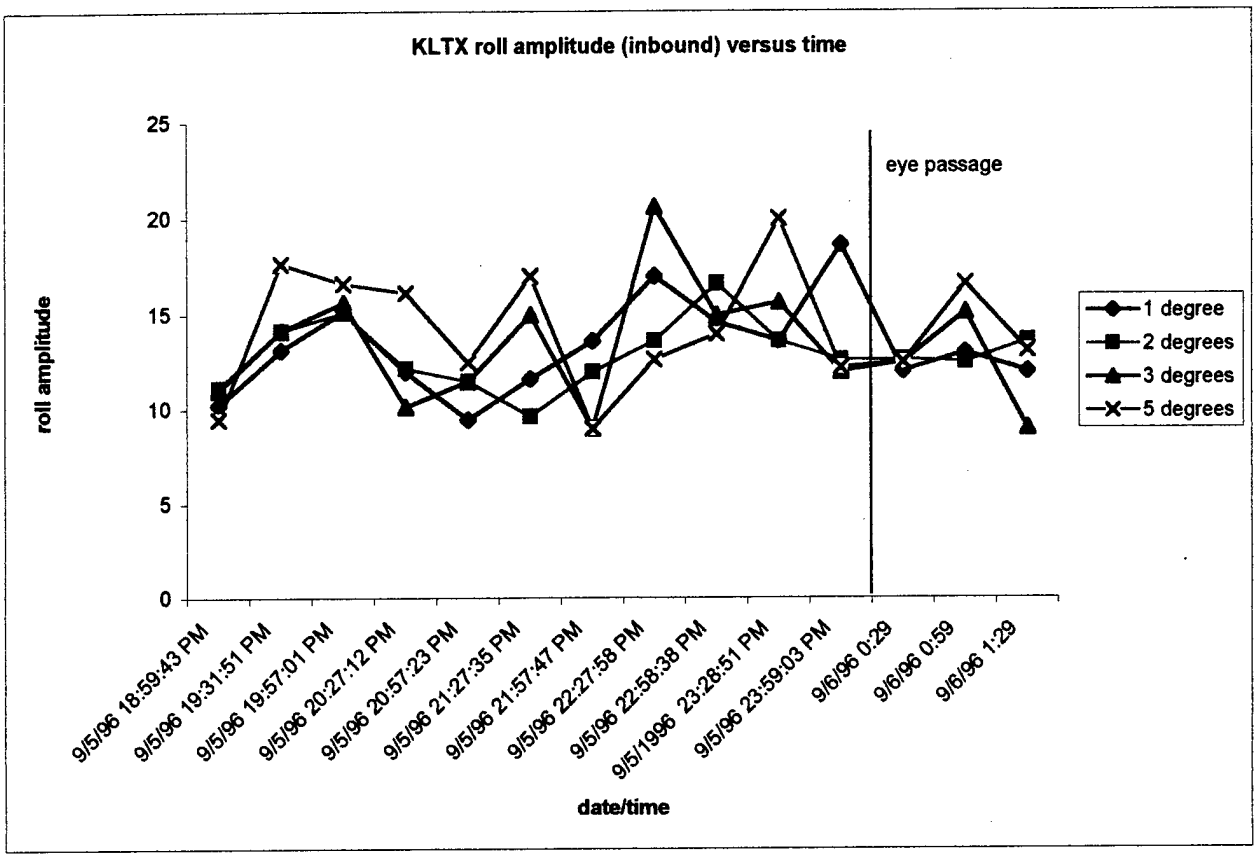


**Figure 2.26** KLTX roll amplitude (peak to trough) ($ms^{-1}$) versus time (UTC) for inbound side.

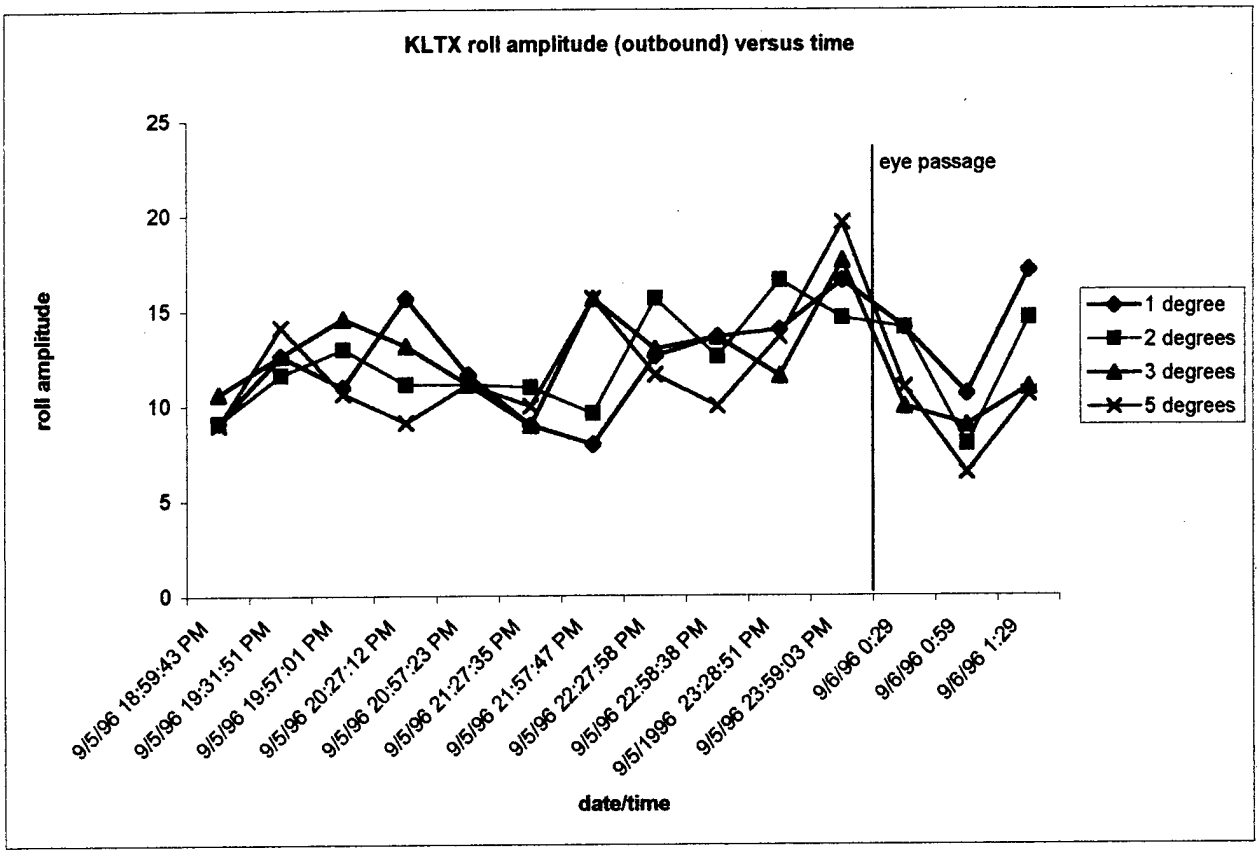


**Figure 2.27** KLTX roll amplitude (peak to trough) ($ms^{-1}$) versus time (UTC) for outbound side.

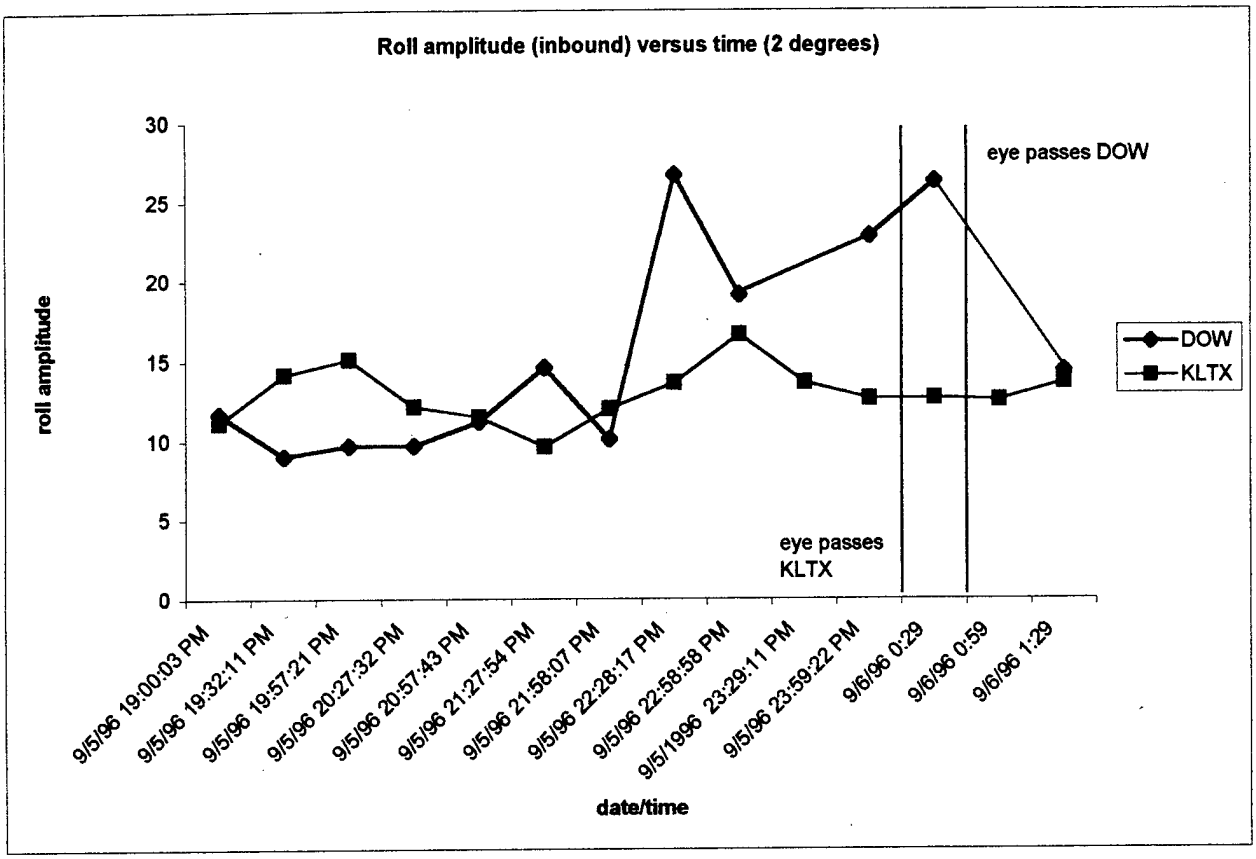


**Figure 2.28** KLTX and DOW roll amplitude (peak to trough) ($ms^{-1}$) verses time (UTC) for inbound side using the 2.0 degree elevation angle scan

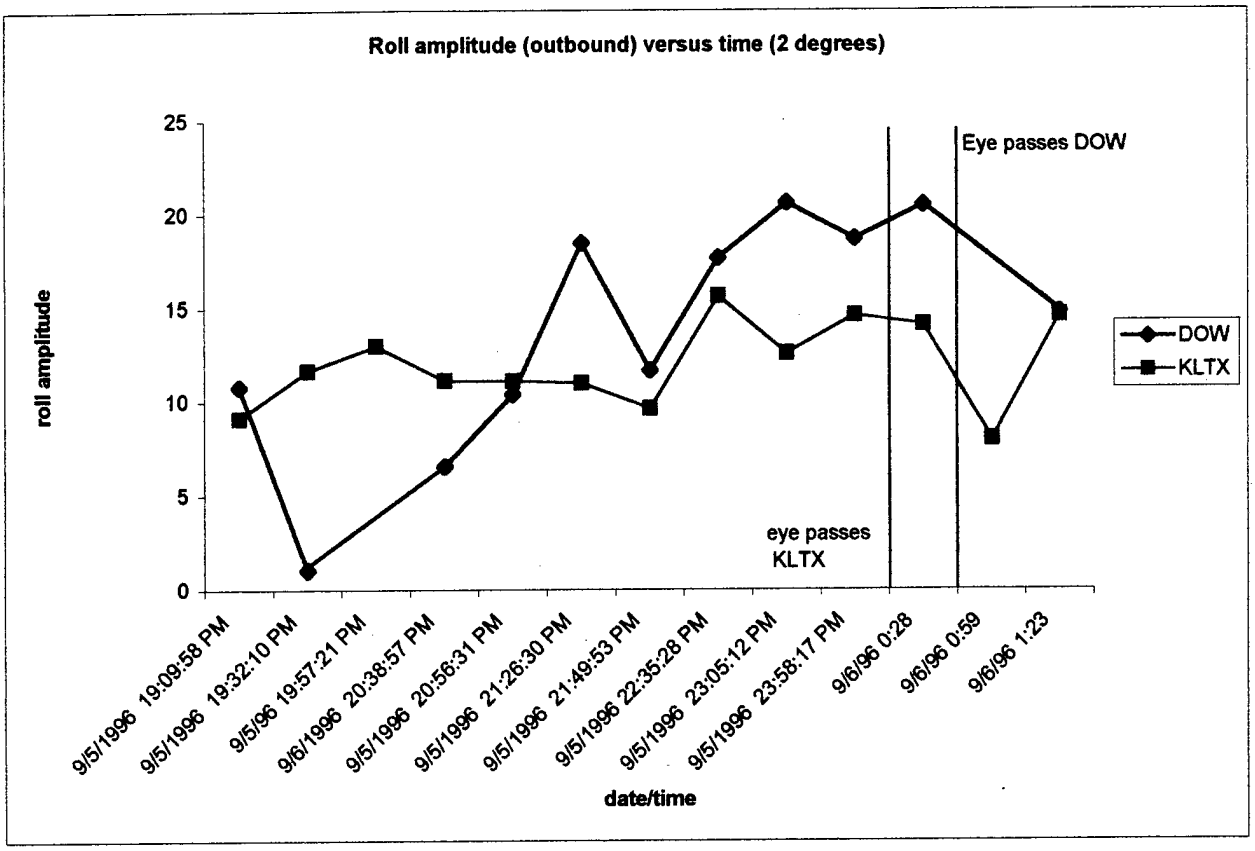


**Figure 2.29** KLTX and DOW roll amplitude (peak to trough) ($ms^{-1}$) versus time (UTC) for outbound side using 2.0 degree elevation angle scan.

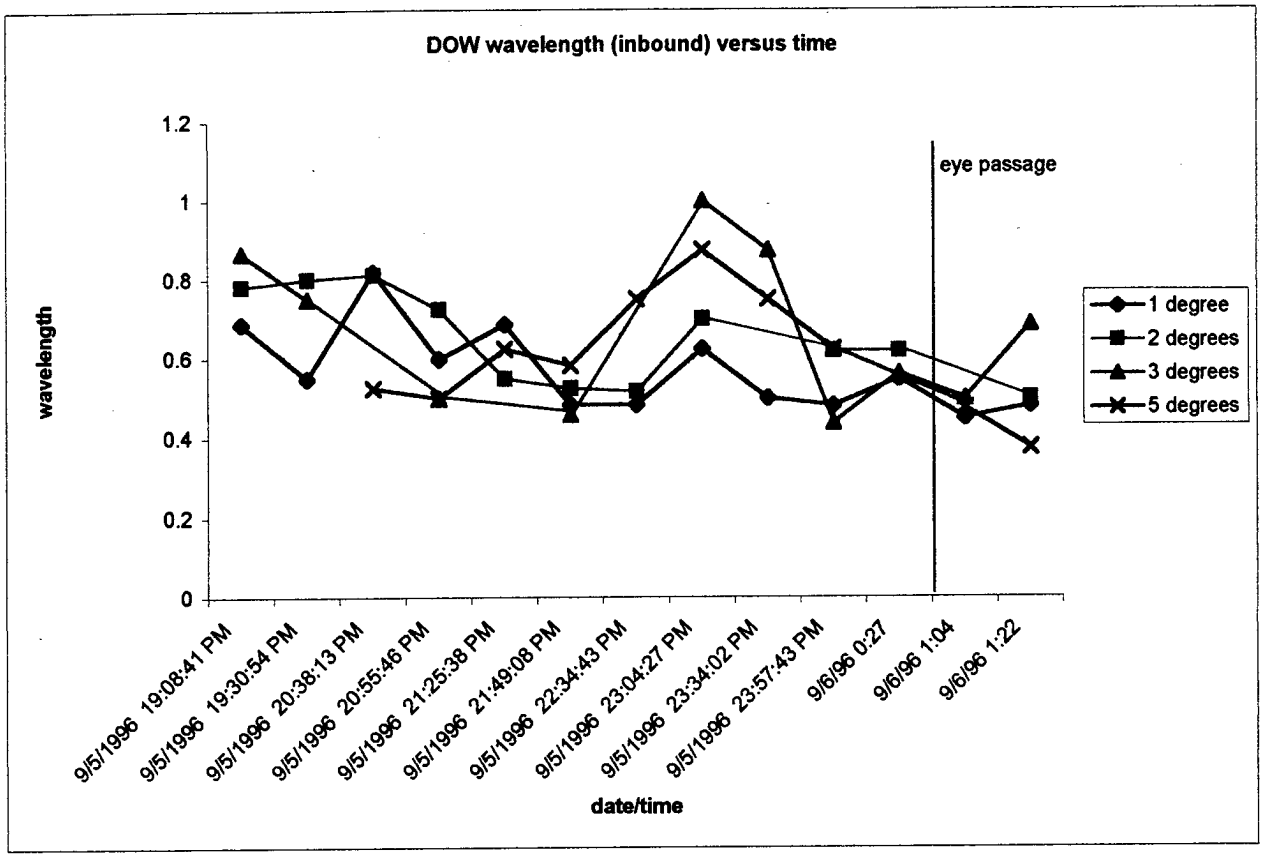


**Figure 2.30** DOW observed roll wavelength (km) versus time (UTC) for inbound side.

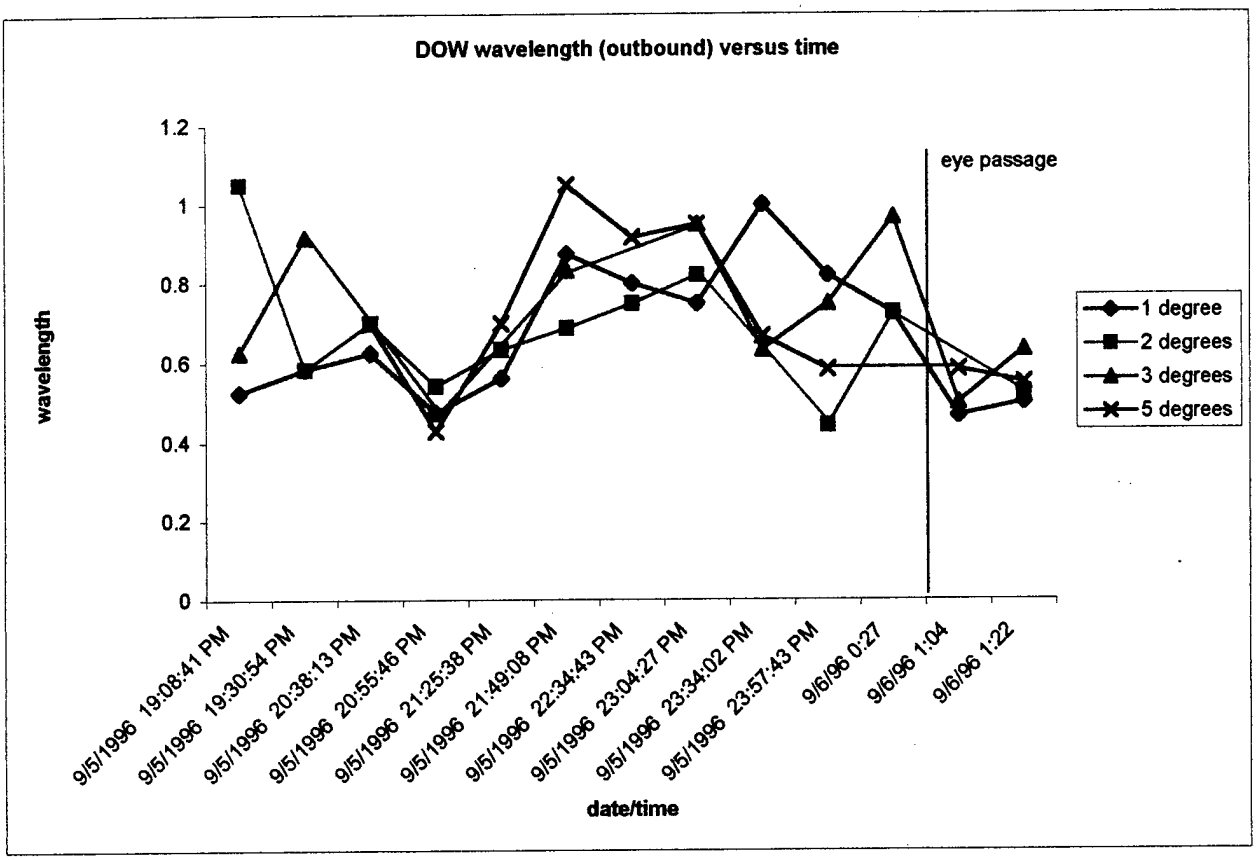


**Figure 2.31** DOW observed roll wavelength (km) versus time (UTC) for outbound side.

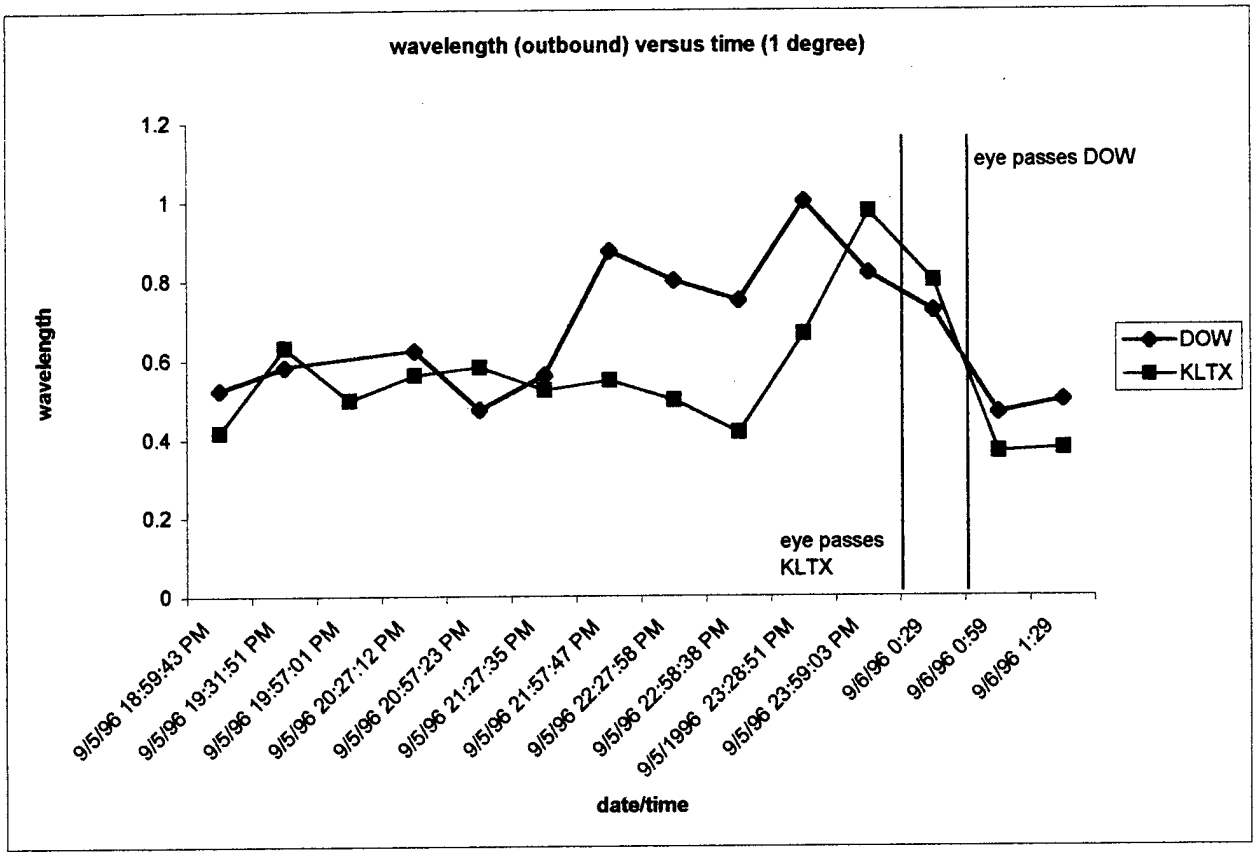


**Figure 2.32** DOW and KLTX observed roll wavelength (km) versus time (UTC) for outbound side using the 1.0 degree elevation angle scan.

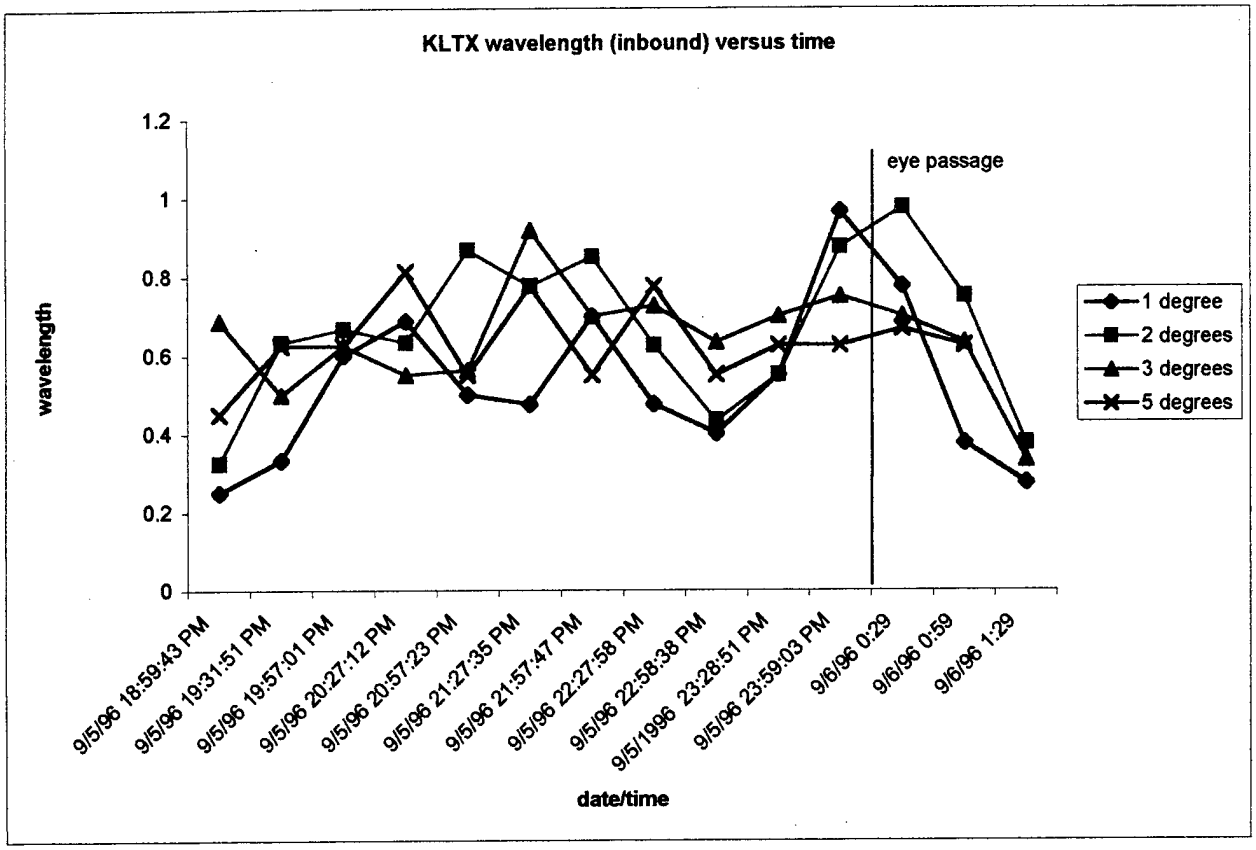


**Figure 2.33** KLTX observed roll wavelength (km) versus time (UTC) for inbound side.

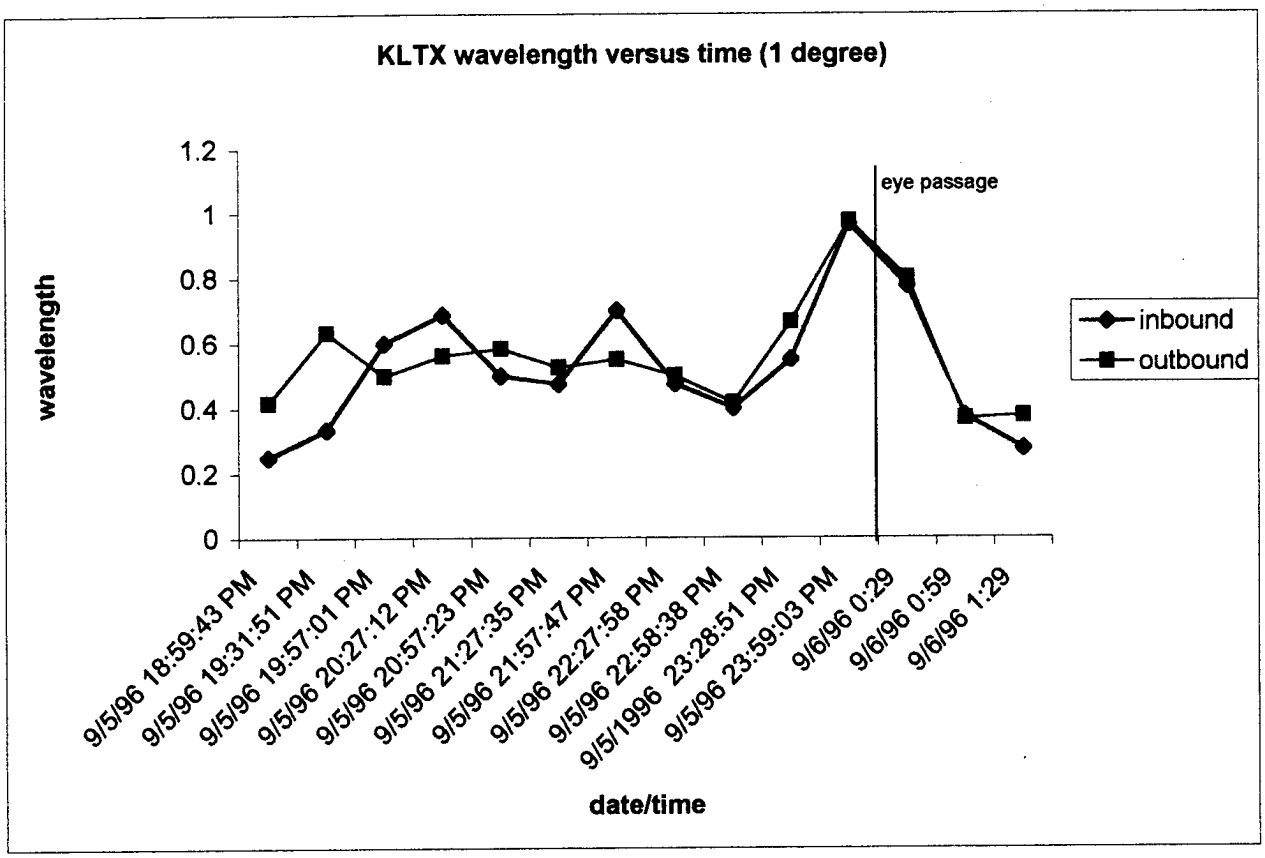


**Figure 2.34** KLTX observed roll wavelength (km) versus time (UTC) for inbound and outbound sides.

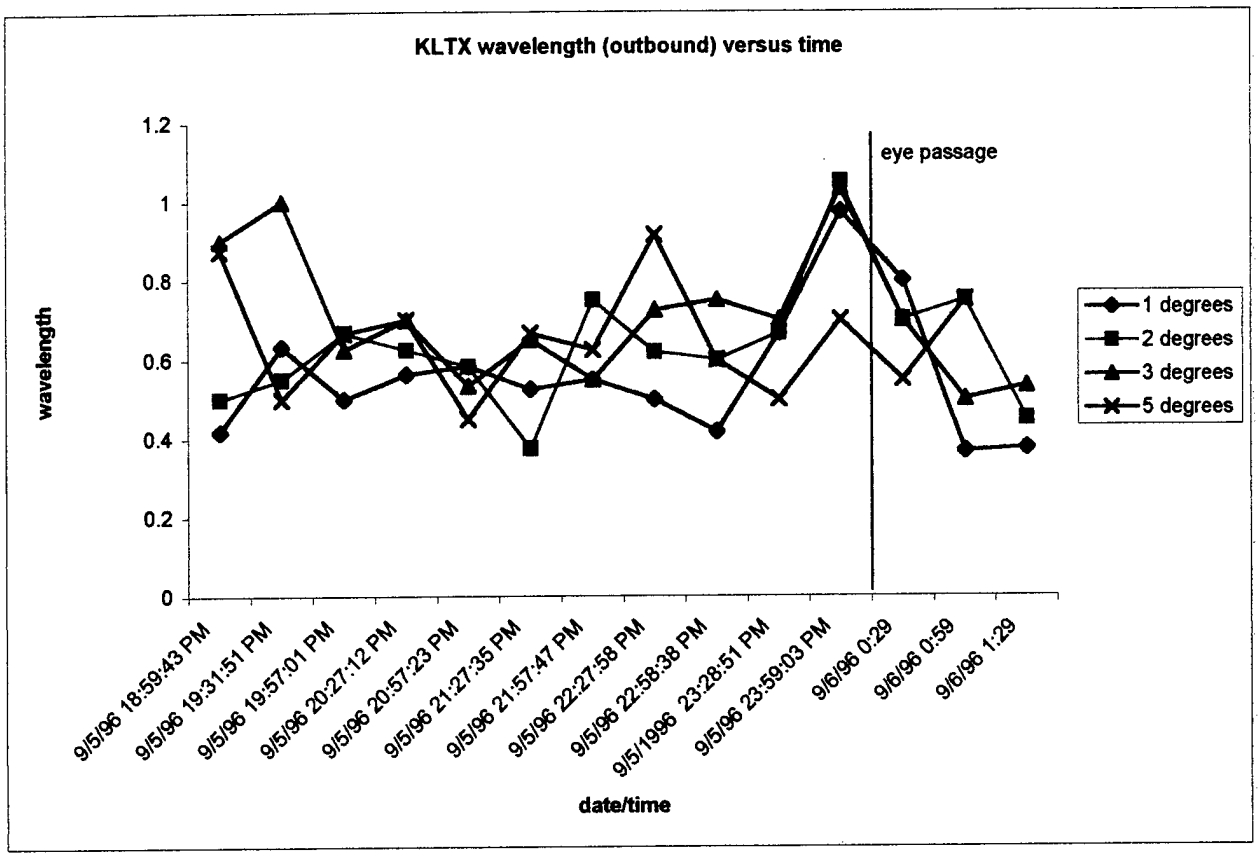


**Figure 2.35** KLTX observed roll wavelength (km) versus time (UTC) for outbound side.

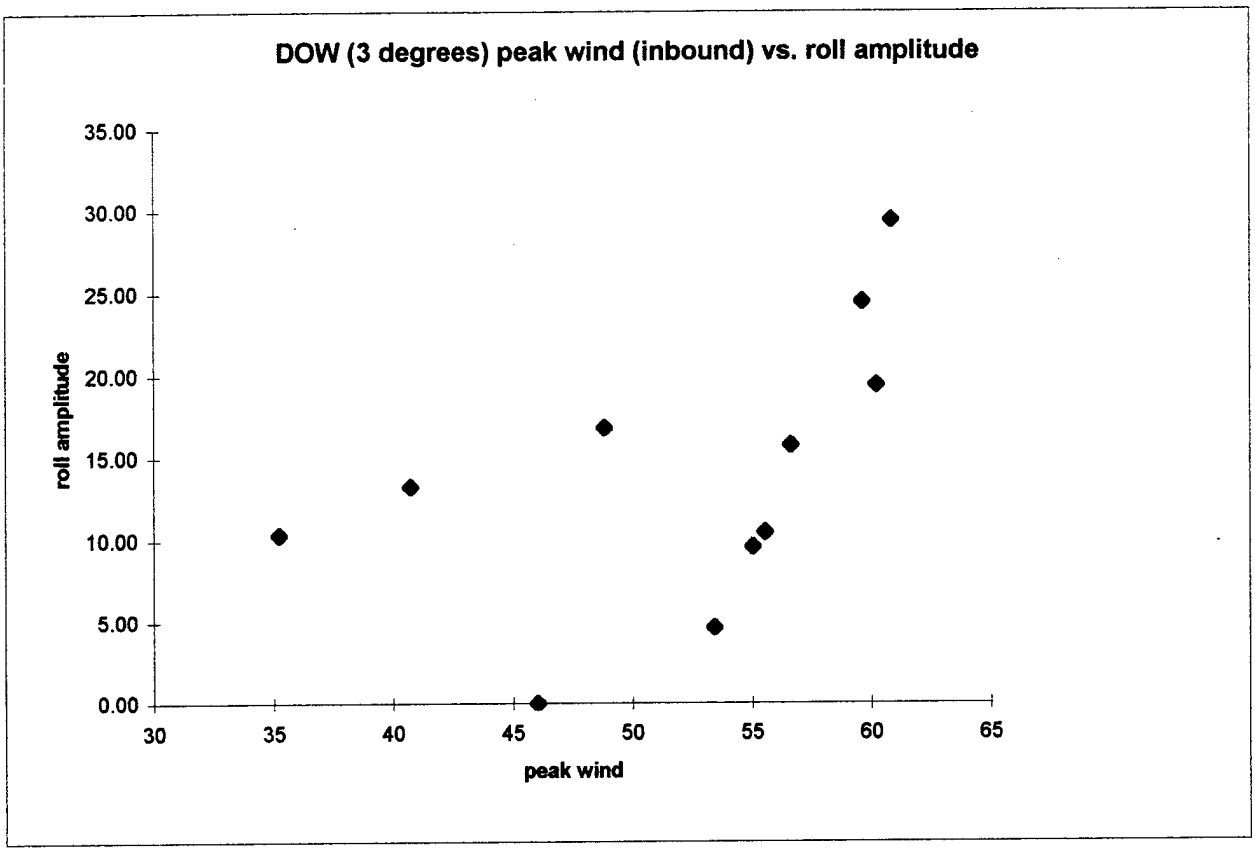


**Figure 2.36** Peak wind ($ms^{-1}$) versus roll amplitude (peak to trough) ($ms^{-1}$) in inbound DOW data from Hurricane Fran using the 3.0 degree scan.

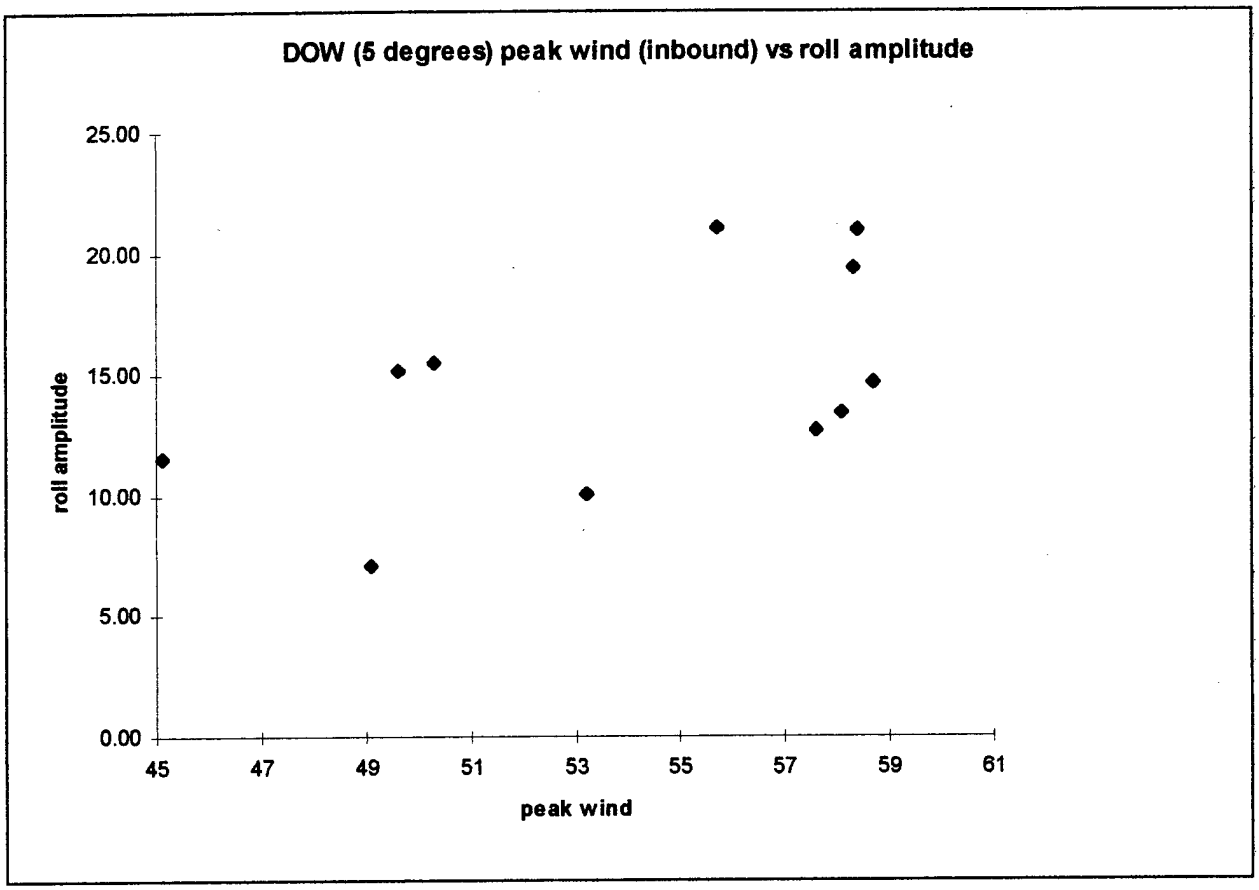


**Figure 2.37** Peak wind ($ms^{-1}$) versus roll amplitude (peak to trough) ($ms^{-1}$) in inbound DOW data from Hurricane Fran using the 5.0 degree scan.

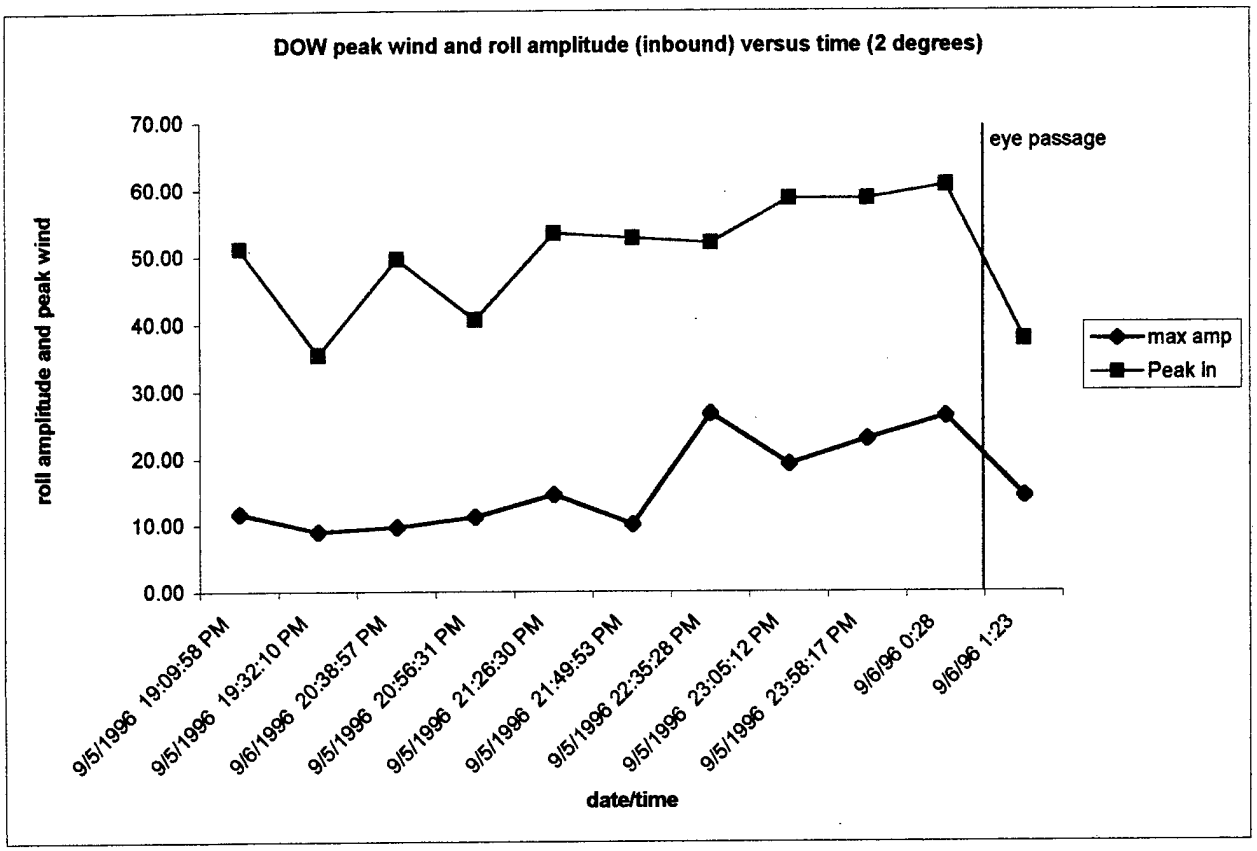


**Figure 2.38** DOW peak wind ($ms^{-1}$) and roll amplitude (peak to trough) ($ms^{-1}$) versus time (UTC) for inbound side using the 2.0 degree elevation angle scan.

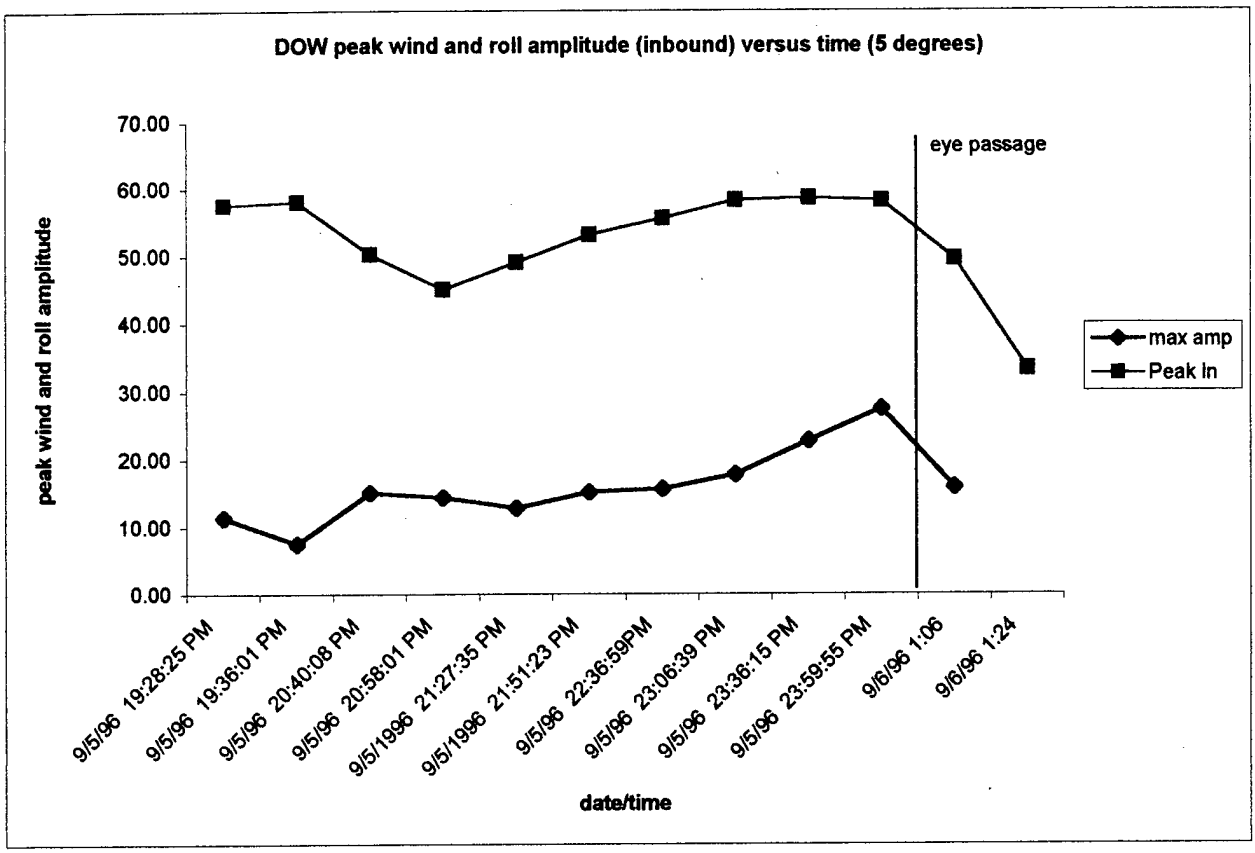


**Figure 2.39** DOW peak wind ($ms^{-1}$) and roll amplitude (peak to trough) ($ms^{-1}$) verses time (UTC) for inbound side using 5.0 degree elevation angle scan.

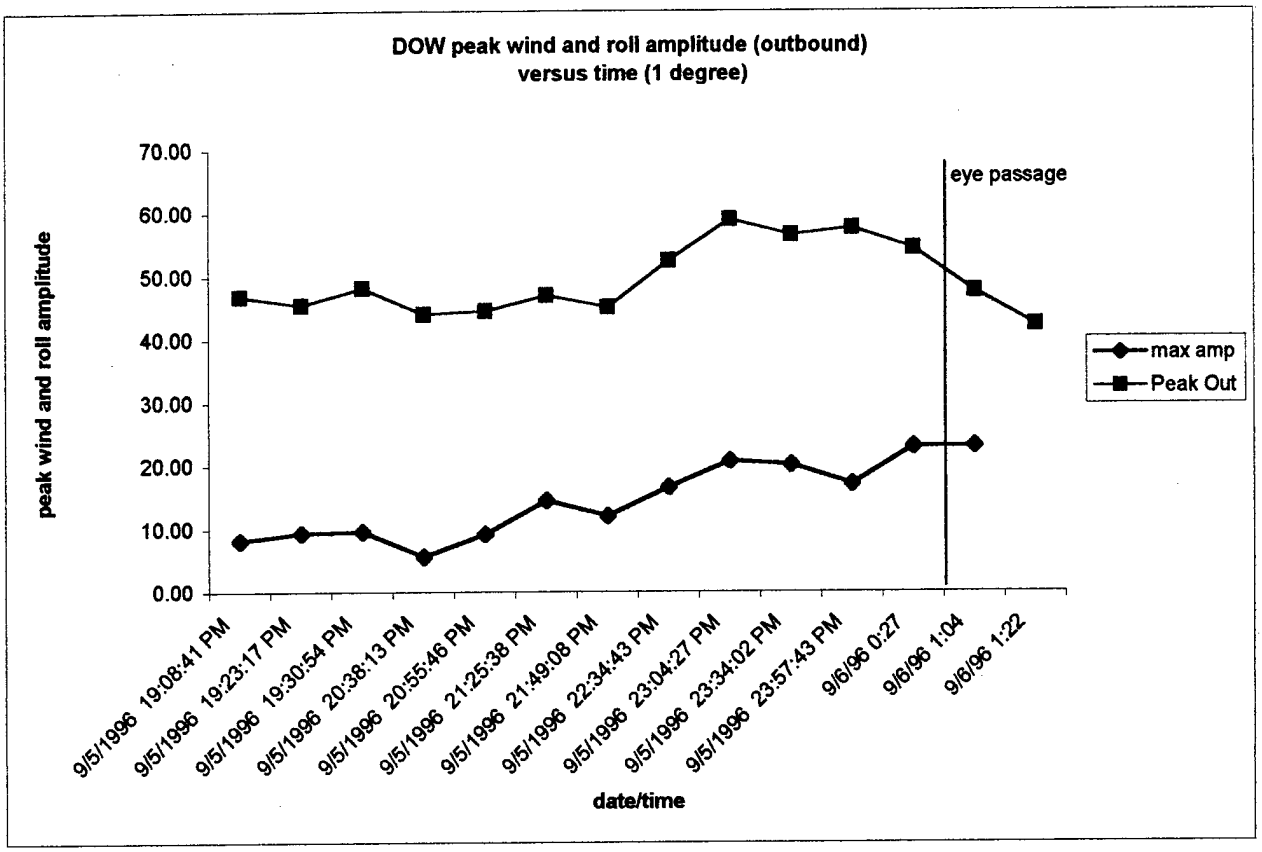


**Figure 2.40** DOW roll amplitude (peak to trough) ($ms^{-1}$) and peak wind ($ms^{-1}$) versus time (UTC) for the outbound side using the 1.0 degree elevation angle scan.

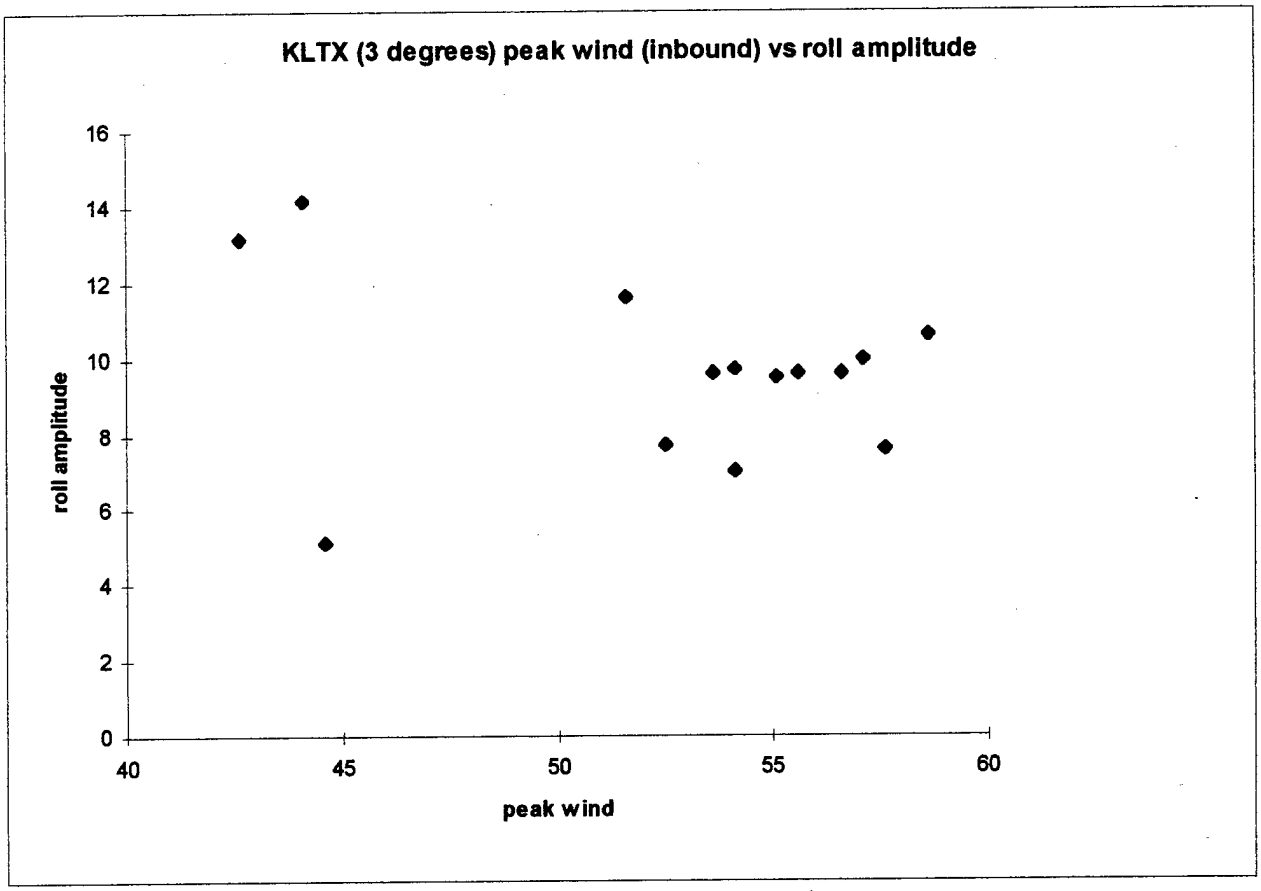


**Figure 2.41** Peak wind ($ms^{-1}$) verses roll amplitude (peak to trough) ($ms^{-1}$) for inbound KLTX data from Hurricane Fran using the 3.0 degree scan.

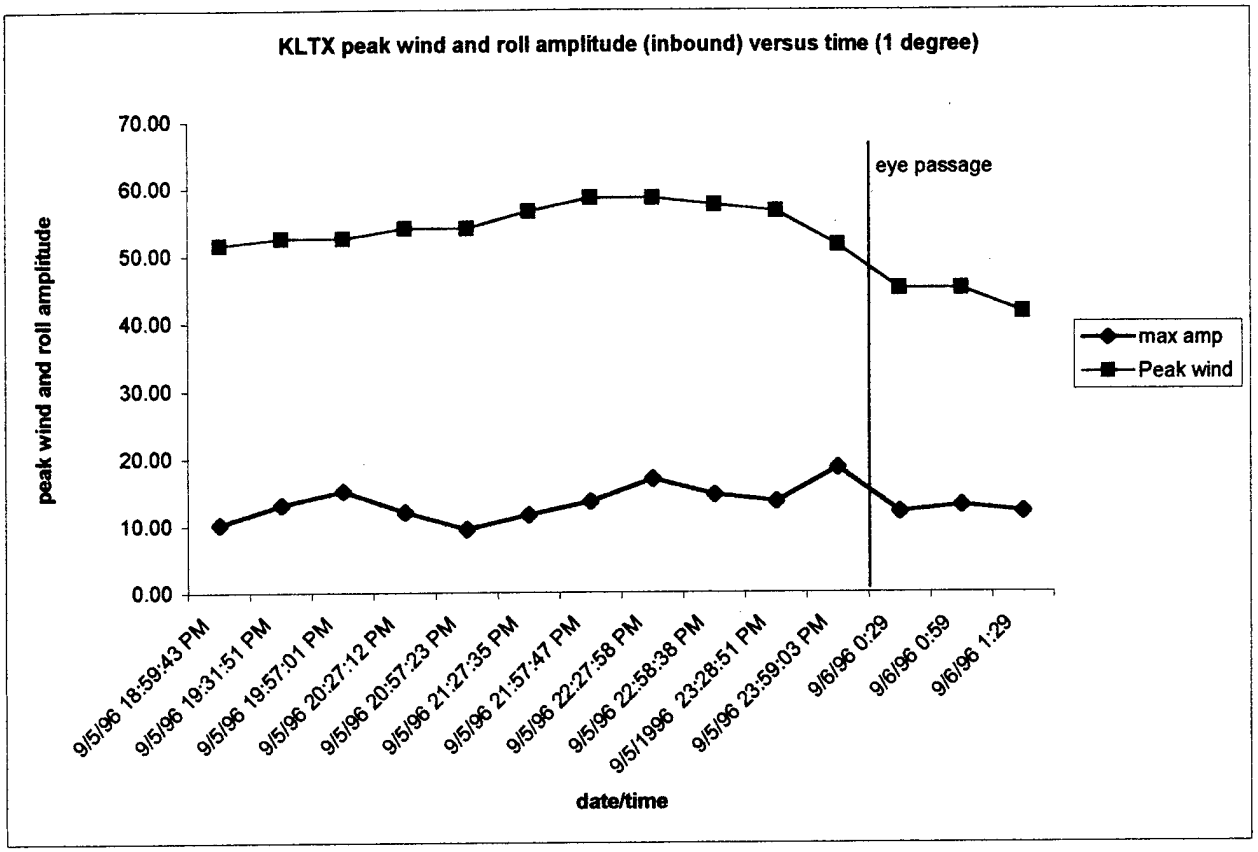


**Figure 2.42** KLTX peak wind ($ms^{-1}$) and roll amplitude (peak to trough) ($ms^{-1}$) verses time (UTC) for inbound side using 1.0 degree elevation angle scan.

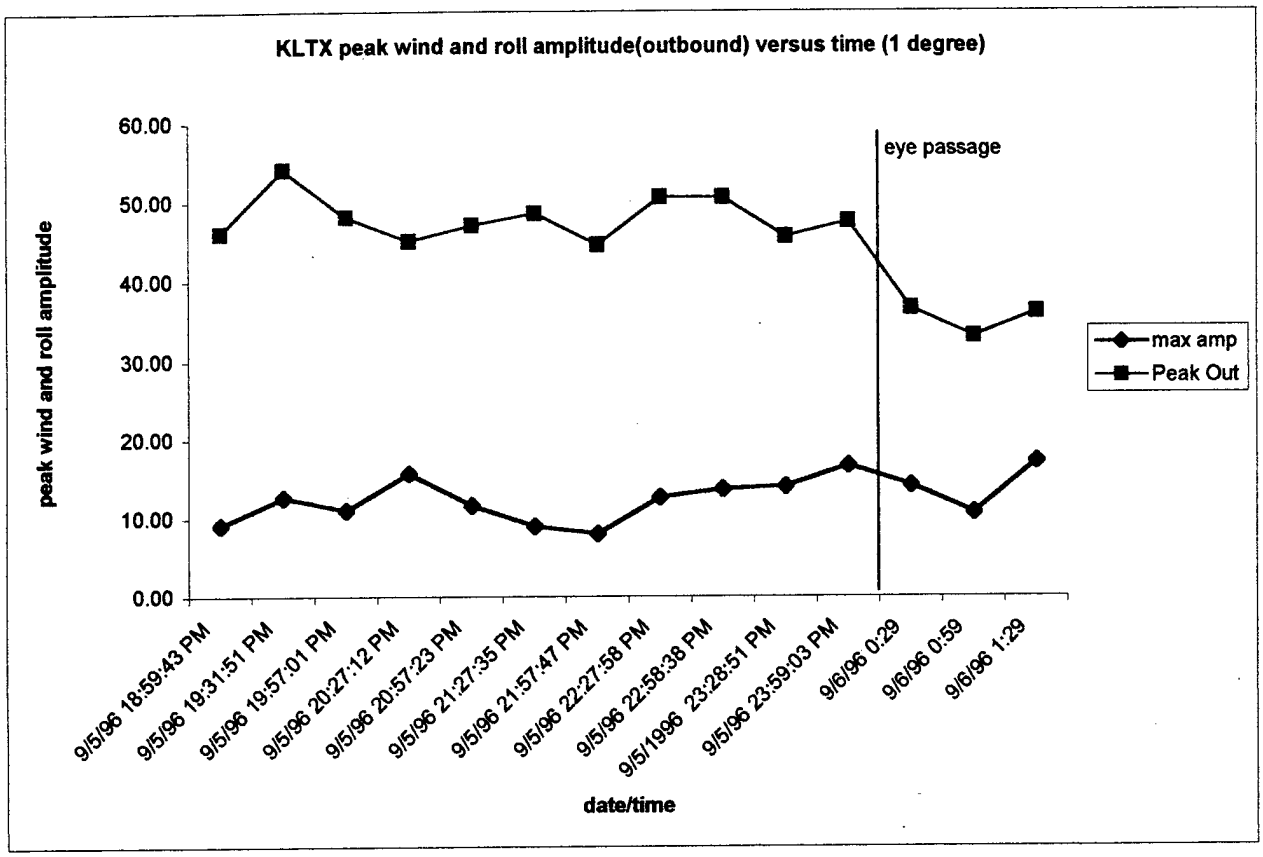


**Figure 2.43** KLTX peak wind ($ms^{-1}$) and roll amplitude (peak to trough) ($ms^{-1}$) verses time (UTC) for outbound side using 1.0 degree elevation angle scan

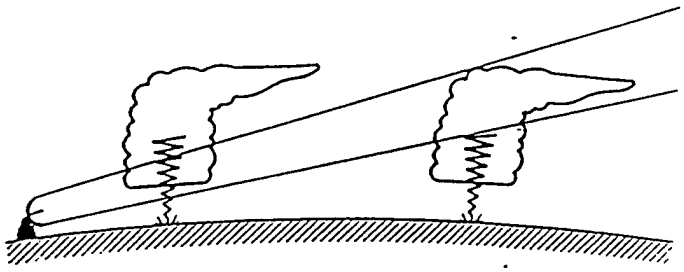

1. Radar Horizon Problem

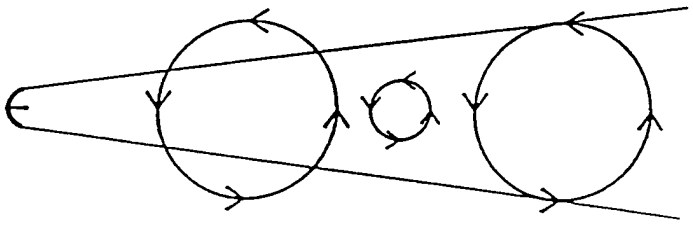

2. Aspect Ratio Problem

**Figure 3.1** An illustration of the Radar Horizon and Aspect Ratio Problems ( from Burgess 1993)
Top: Radar Horizon Problem
Bottom: Aspect Ratio Problem

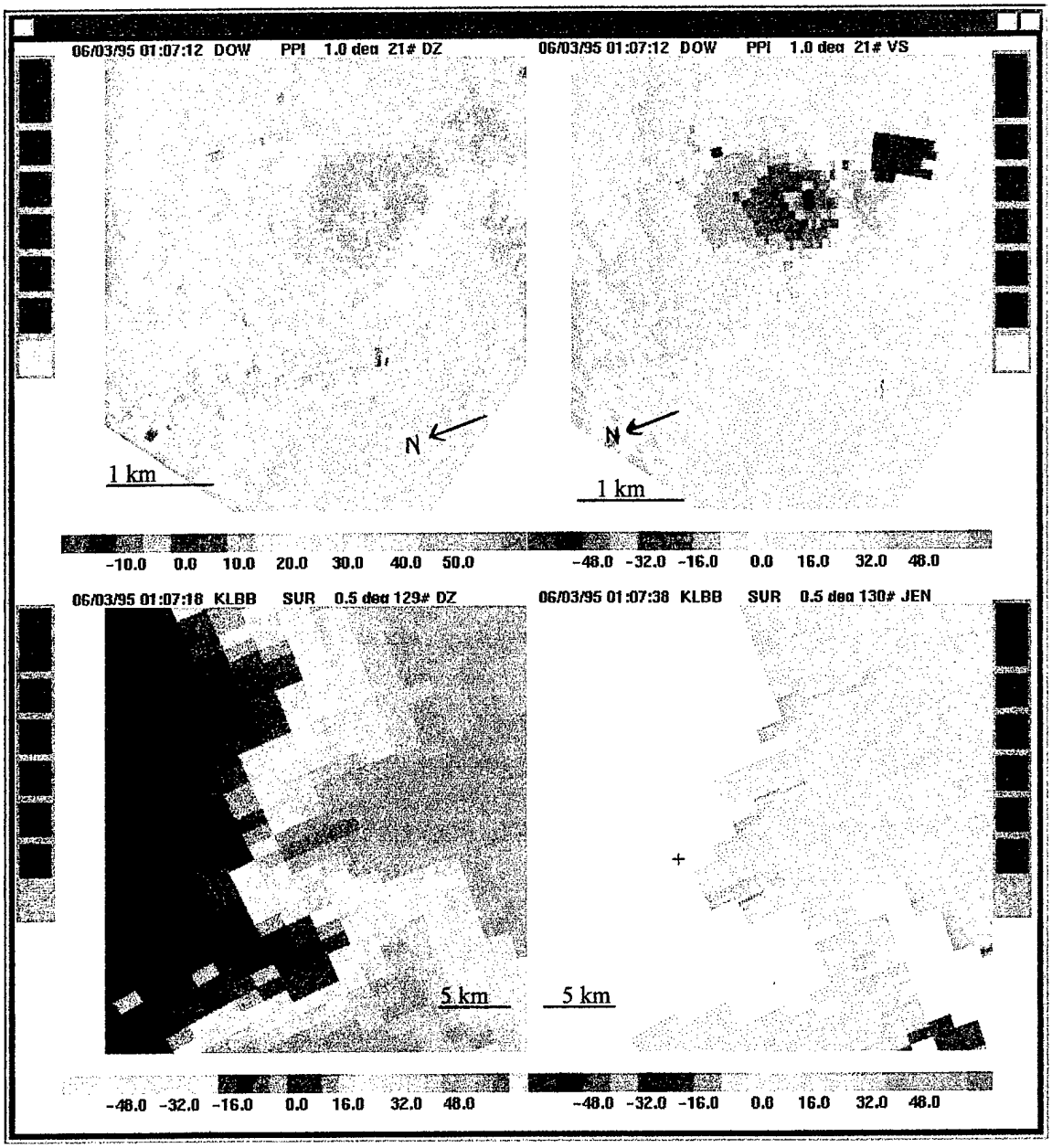


**Figure 3.2** The Dimmit Tornado observed by the KLBB and the DOW (a. is the upper left, b. is the upper right c. is the lower left and d. is the lower right).
a. DOW reflectivity data from the Dimmitt Tornado
b. DOW velocity data from the Dimmitt Tornado.
c. KLBB (Lubbock) reflectivity data from the Dimmit Tornado.
d. KLBB velocity data from the Dimmit Tornado.

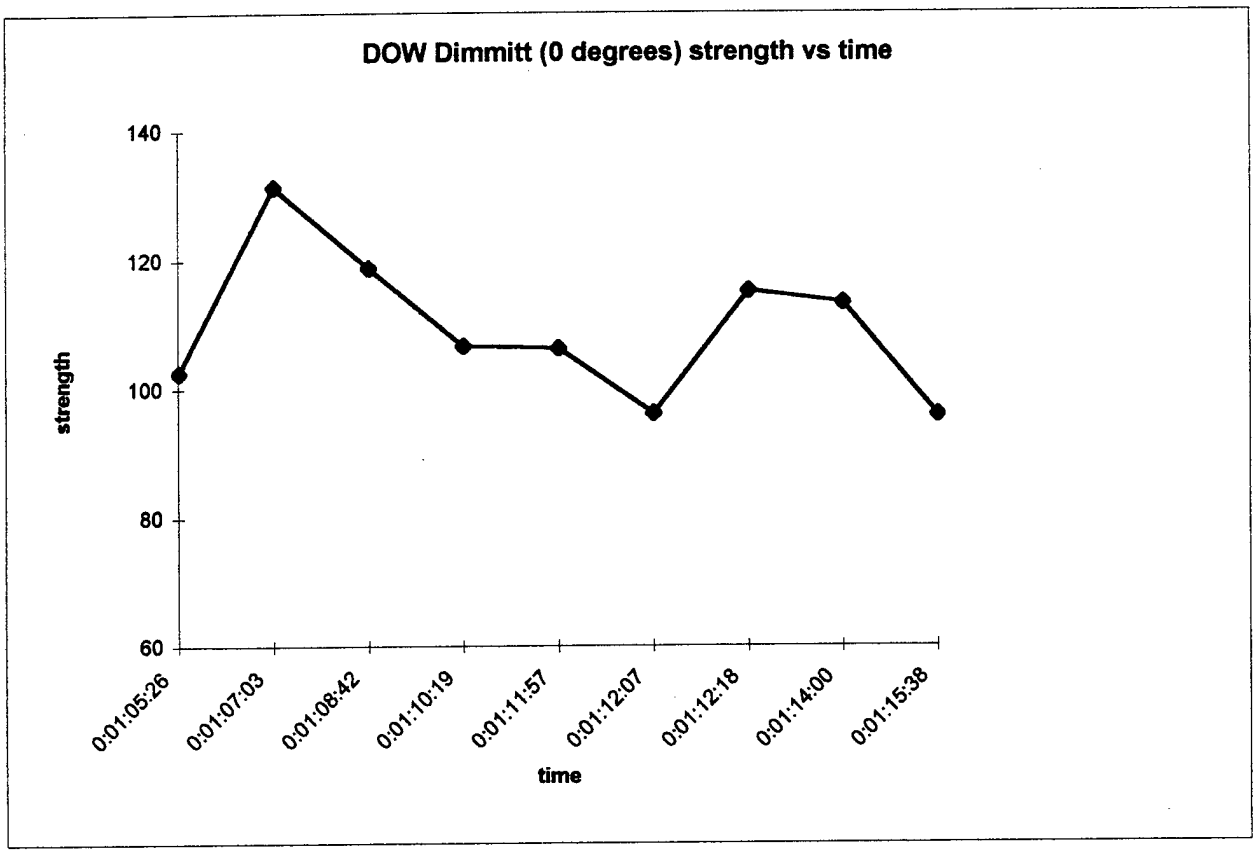


**Figure 3.3** Strength $ms^{-1}$ (difference between the maximum inbound velocity and the maximum outbound velocity) of Dimmit tornado versus time (UTC) taken from DOW data at the 0.0 degree elevation angle.

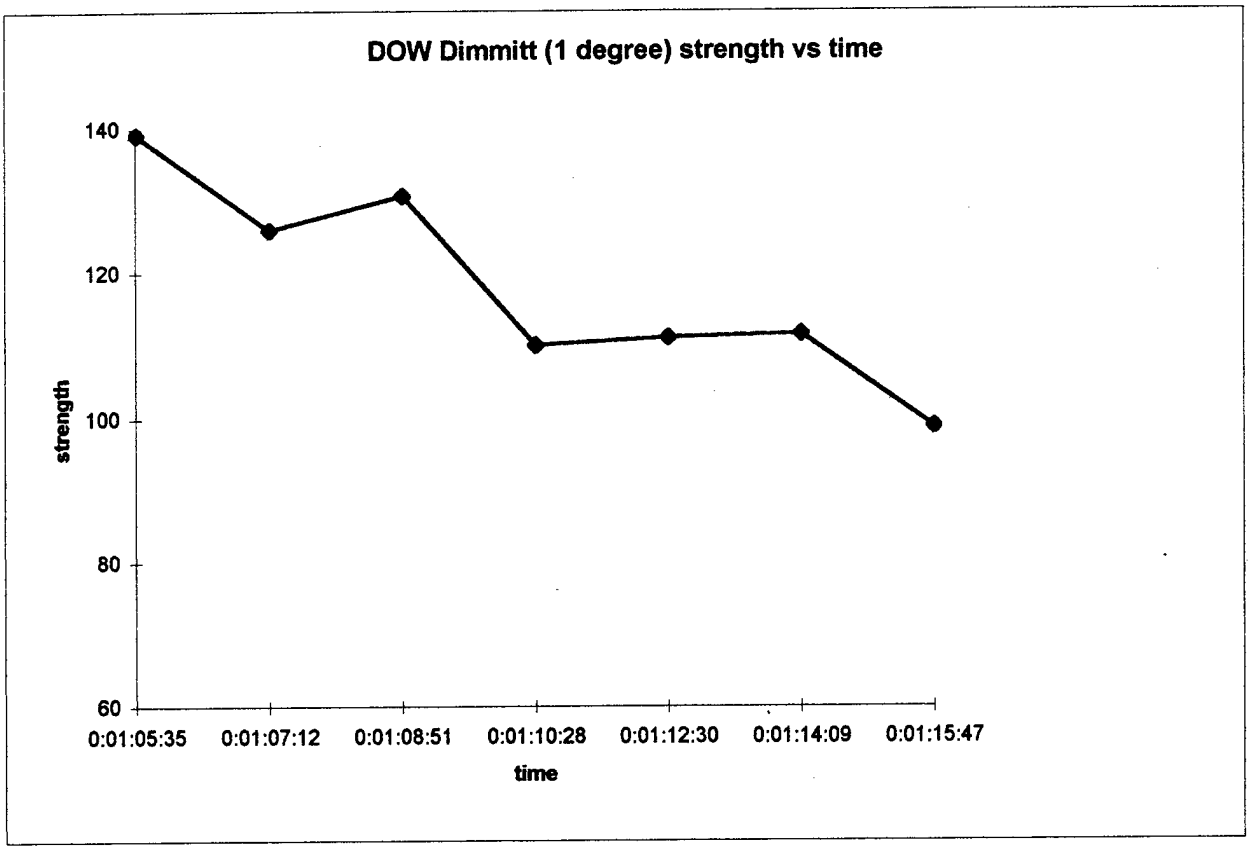


**Figure 3.4** Strength $ms^{-1}$ (difference between the maximum inbound velocity and the maximum outbound velocity of Dimmit tornado versus time (UTC) taken from DOW data at the 1.0 degree elevation angle.

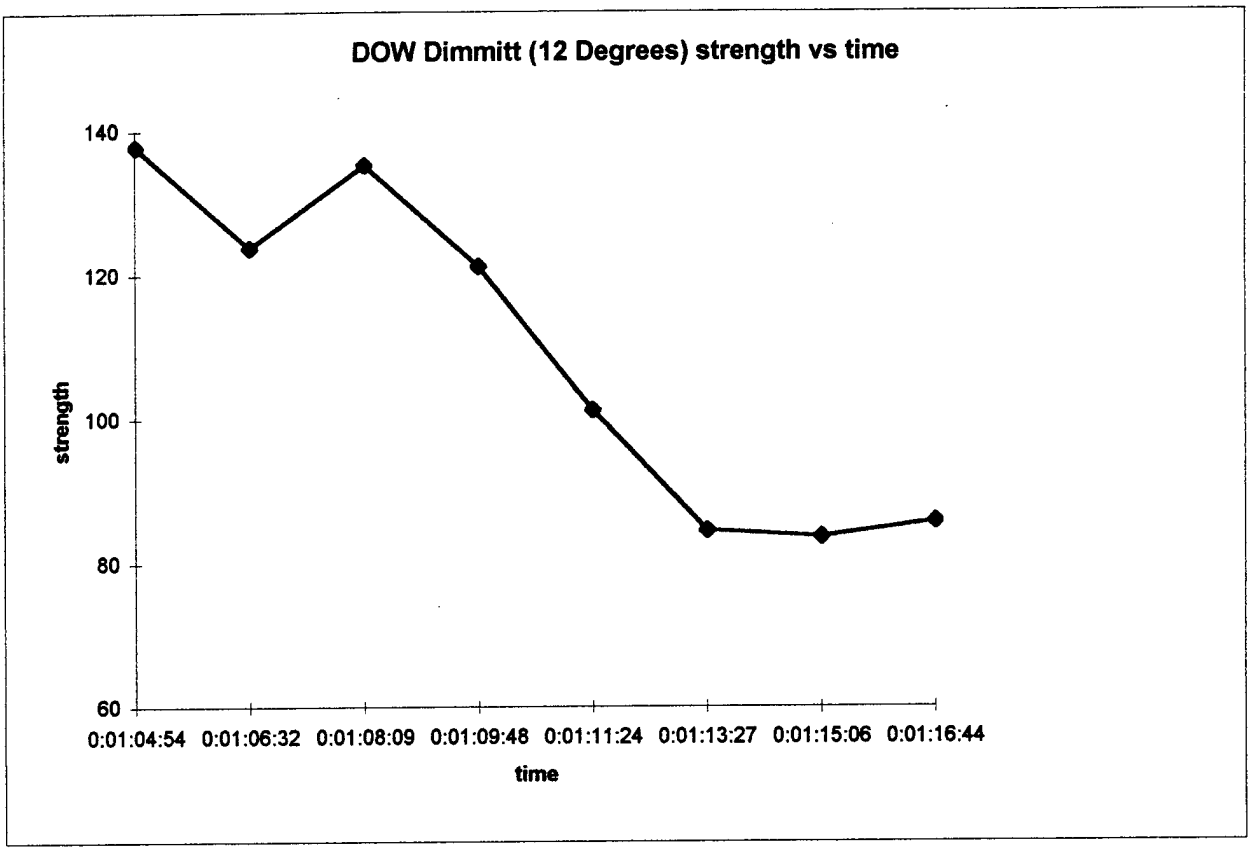


**Figure 3.5** Strength $ms^{-1}$ (difference between the maximum inbound velocity and the maximum outbound velocity) of Dimmit tornado versus time (UTC) taken from DOW data at the 12.0 degree elevation angle.

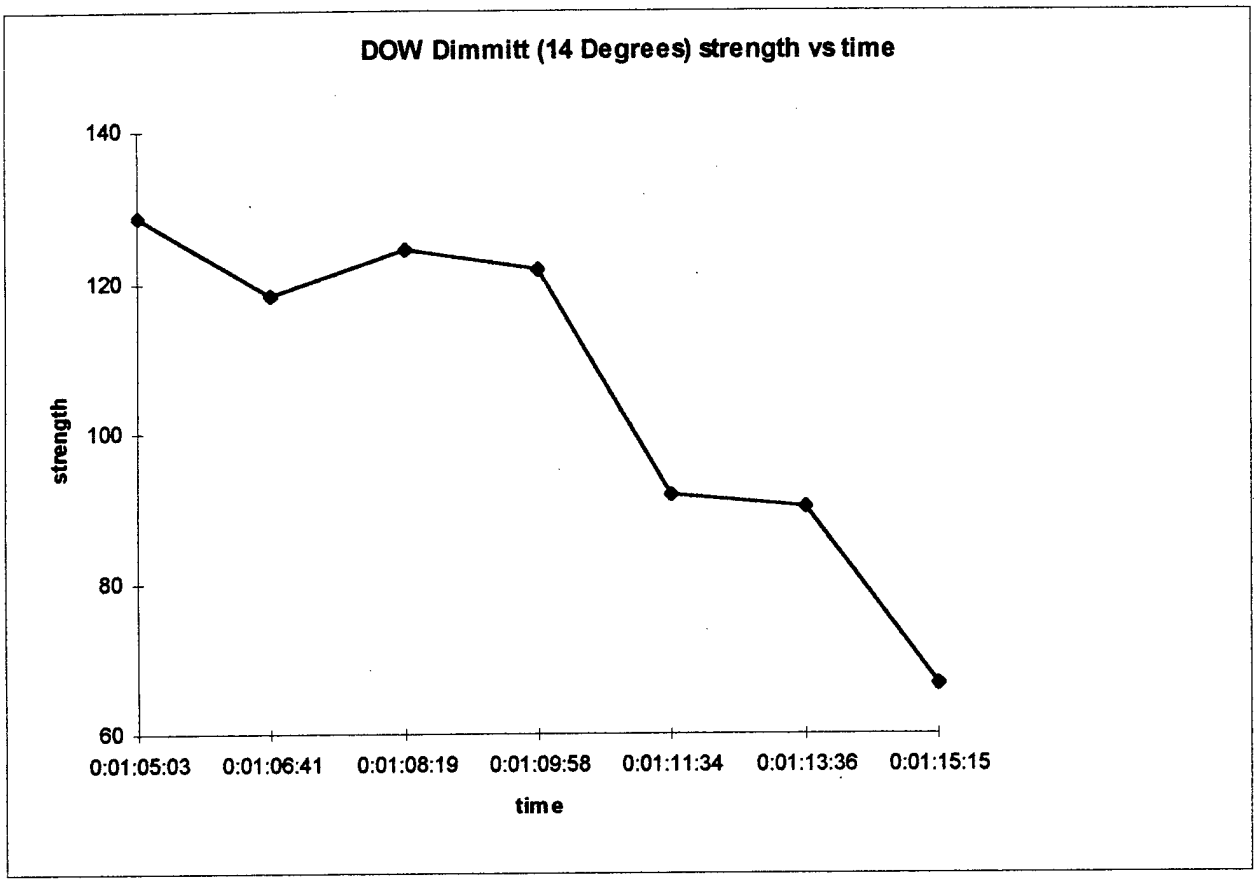


**Figure 3.6** Strength $ms^{-1}$ (difference between the maximum inbound velocity and the maximum outbound velocity) of Dimmit tornado versus time (UTC) taken from DOW data at the 14.0 degree elevation angles.

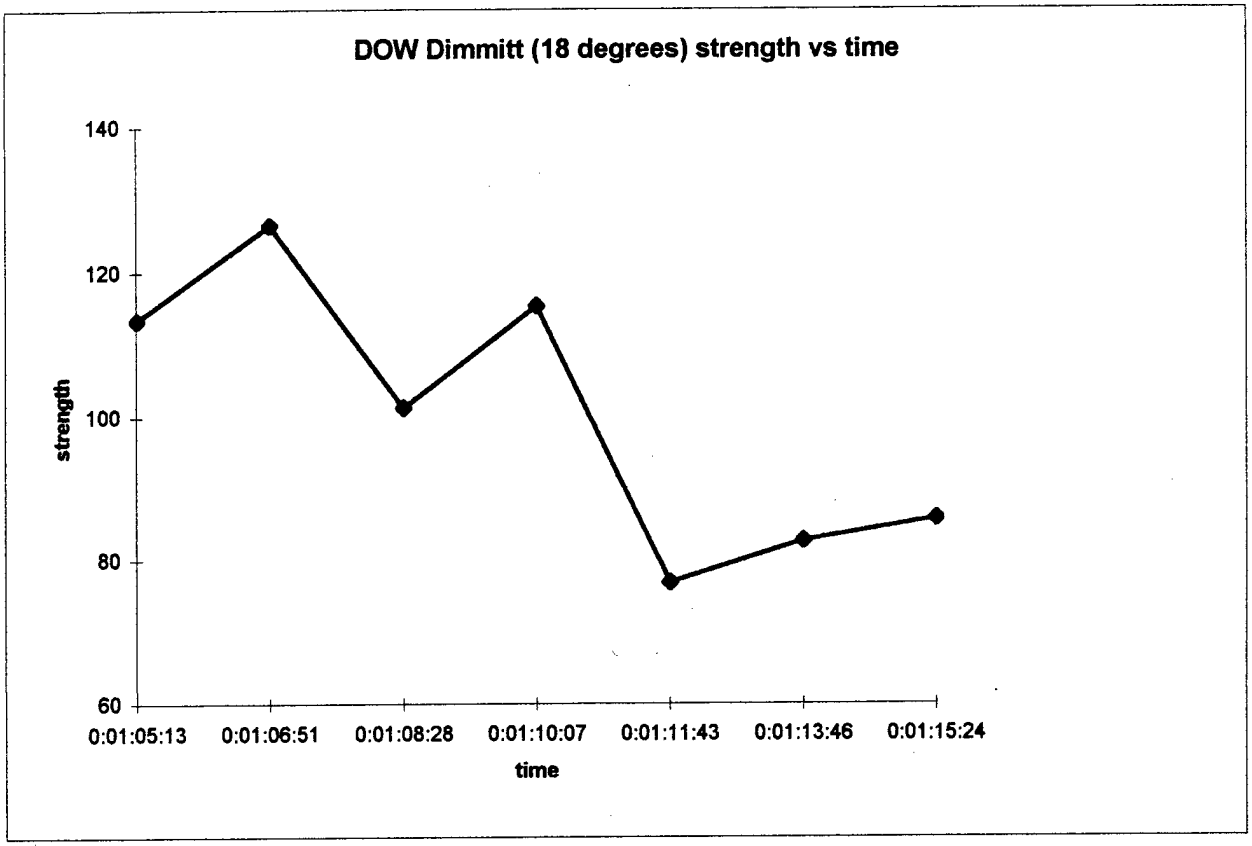


**Figure 3.7** Strength $ms^{-1}$ (difference between the maximum inbound velocity and the maximum outbound velocity) of Dimmit tornado versus time (UTC) taken from DOW data at the 18.0 degree elevation angle.

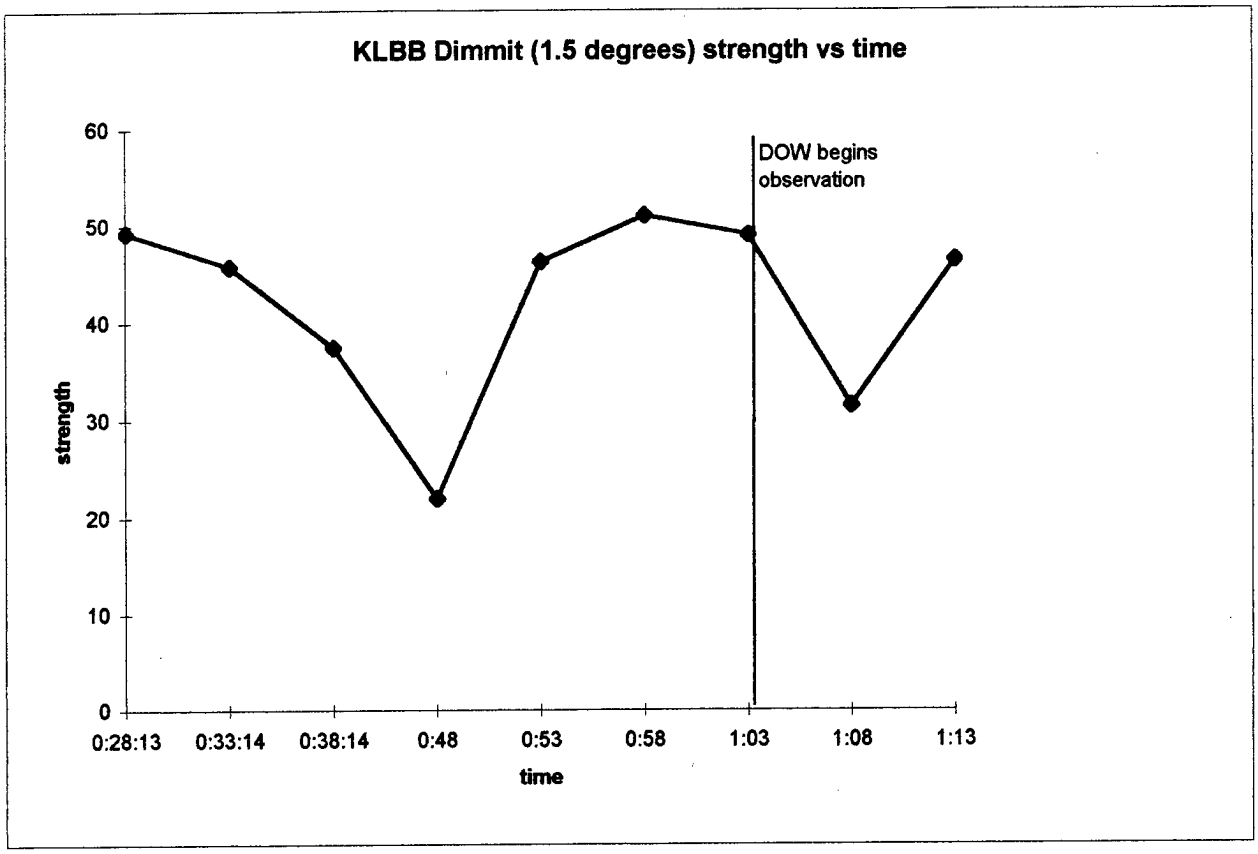


**Figure 3.8** Strength $ms^{-1}$ (difference between the maximum inbound velocities and the maximum outbound velocities) of Dimmit tornado versus time (UTC) taken from KLBB data at the 1.5 degree elevation angle.

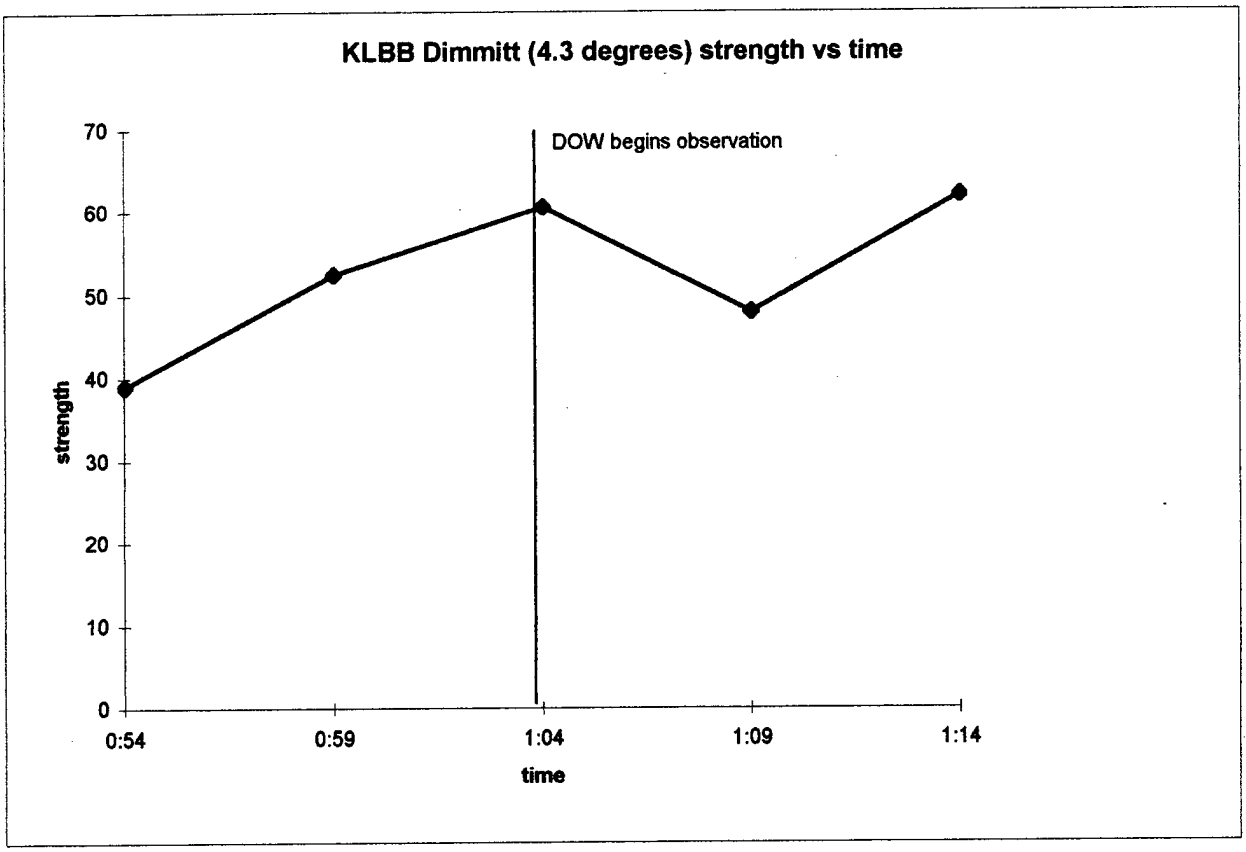


**Figure 3.9** Strength $ms^{-1}$ (difference between the maximum inbound velocity and the maximum outbound velocity) of Dimmit tornado versus time (UTC) taken from KLBB data at the 1.5 degree elevation angle.

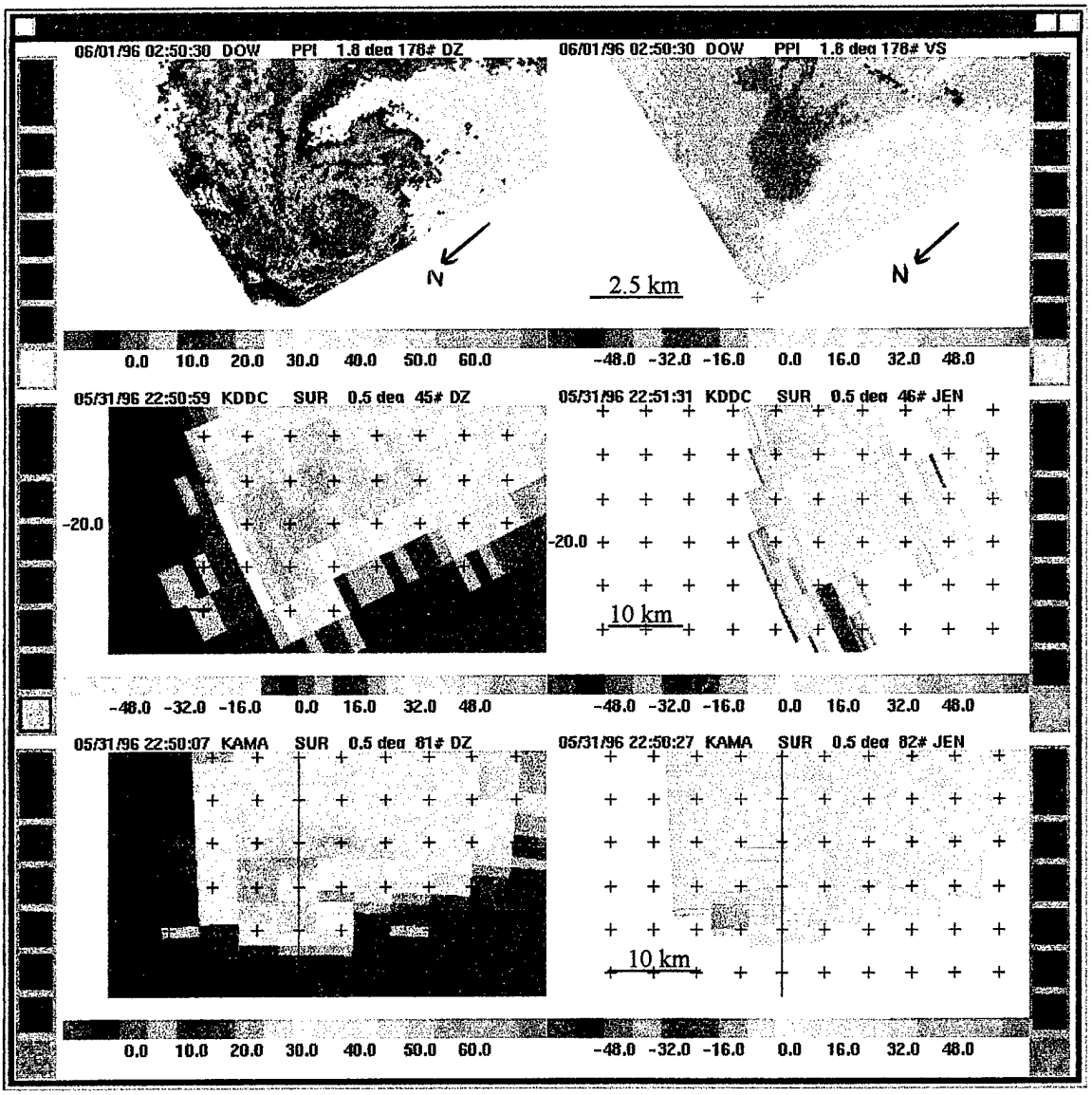


**Figure 3.10** Reflectivity data from the Rolla Tornado (a. is the upper left, b. is the upper right c. is the lower left and d. is the lower right).
a. DOW reflectivity data from the Rolla Tornado.
b. DOW velocity data from the Rolla Tornado.
c. KDDC reflectivity data from the Rolla Tornado.
d. KDDC velocity data from the Rolla Tornado.
e. KAMA reflectivity data from the Rolla Tornado.
f. KAMA velocity data from the Rolla Tornado.

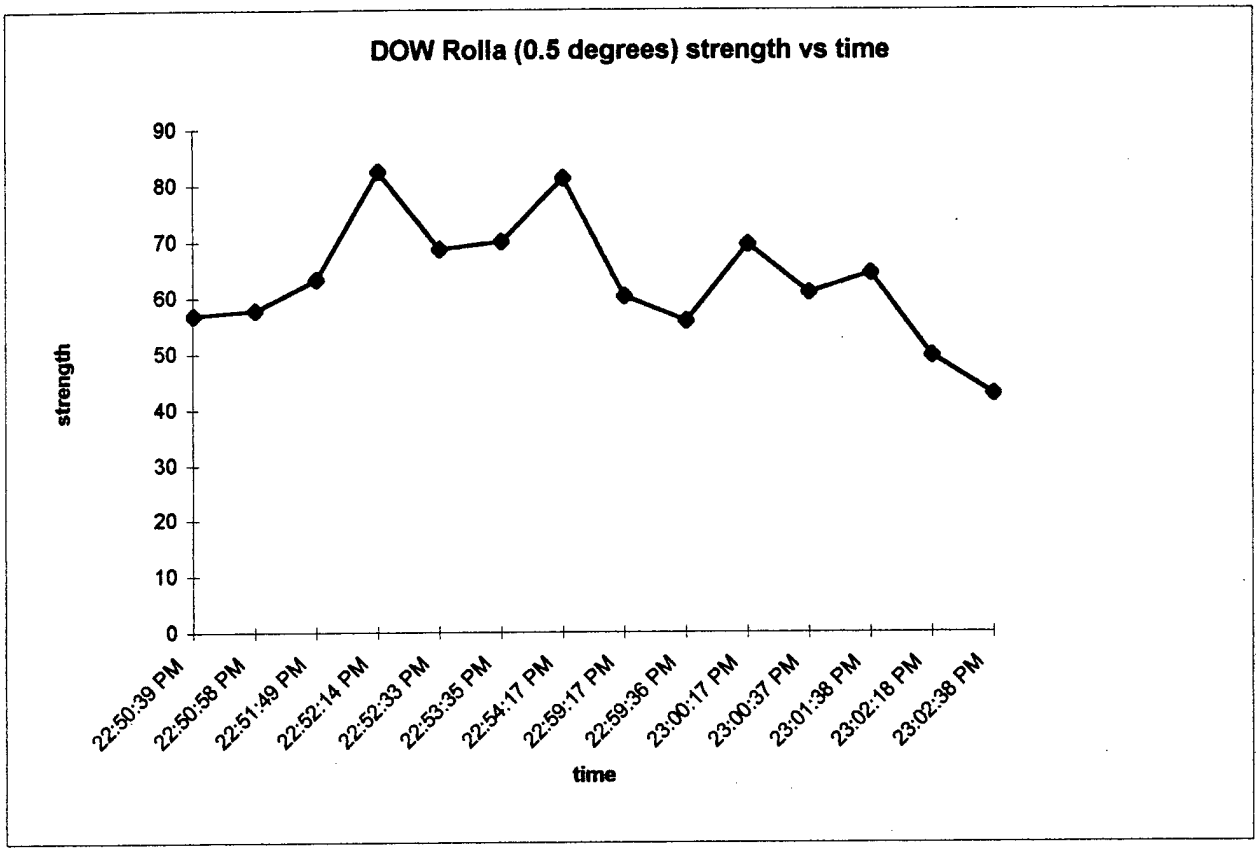


**Figure 3.11** Strength ($ms^{-1}$) (difference between the maximum inbound velocity and the maximum outbound velocities) of Rolla tornado versus time (UTC) taken from DOW data at the 0.5 degree elevation angle.

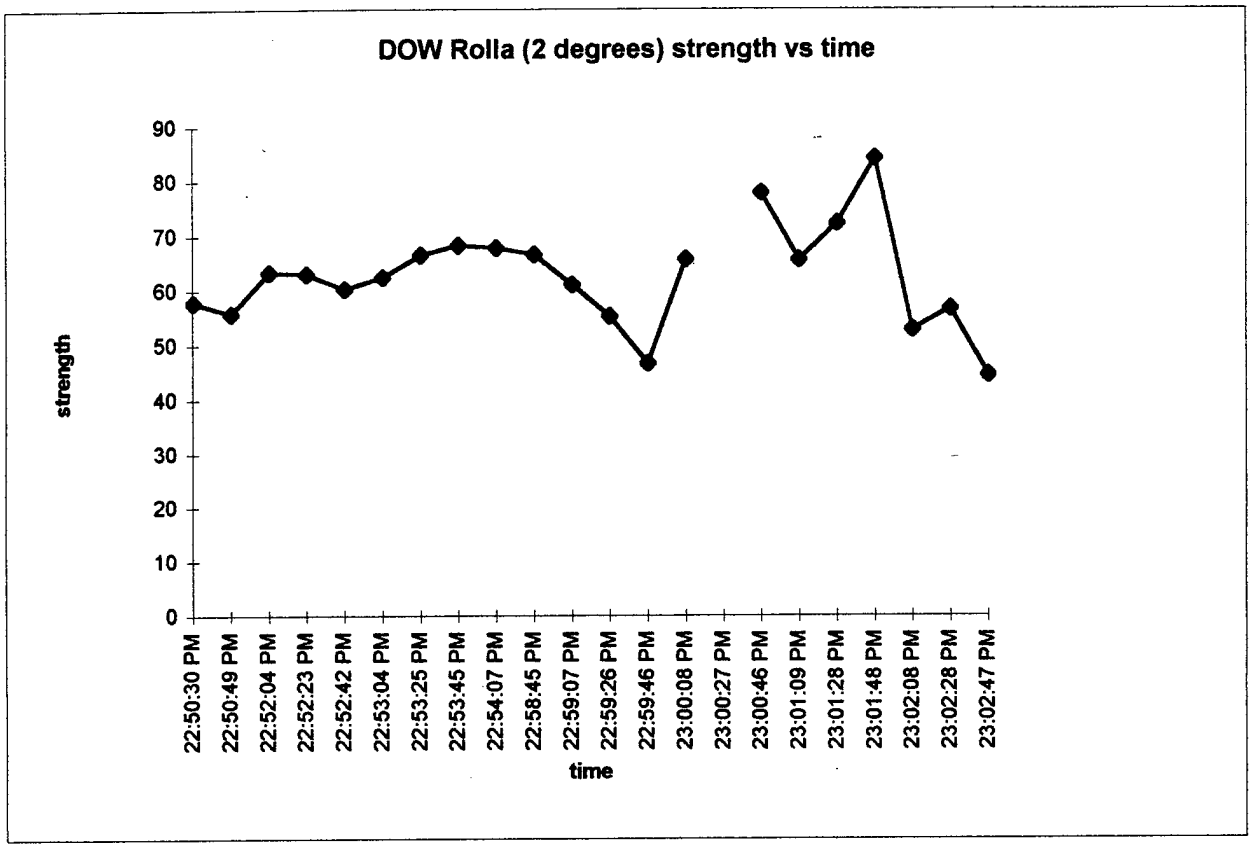


**Figure 3.12** Strength ($ms^{-1}$) (difference between the maximum inbound velocity and the maximum outbound velocity) of Rolla tornado versus time (UTC) taken from DOW data at the 2.0 degree elevation angle.

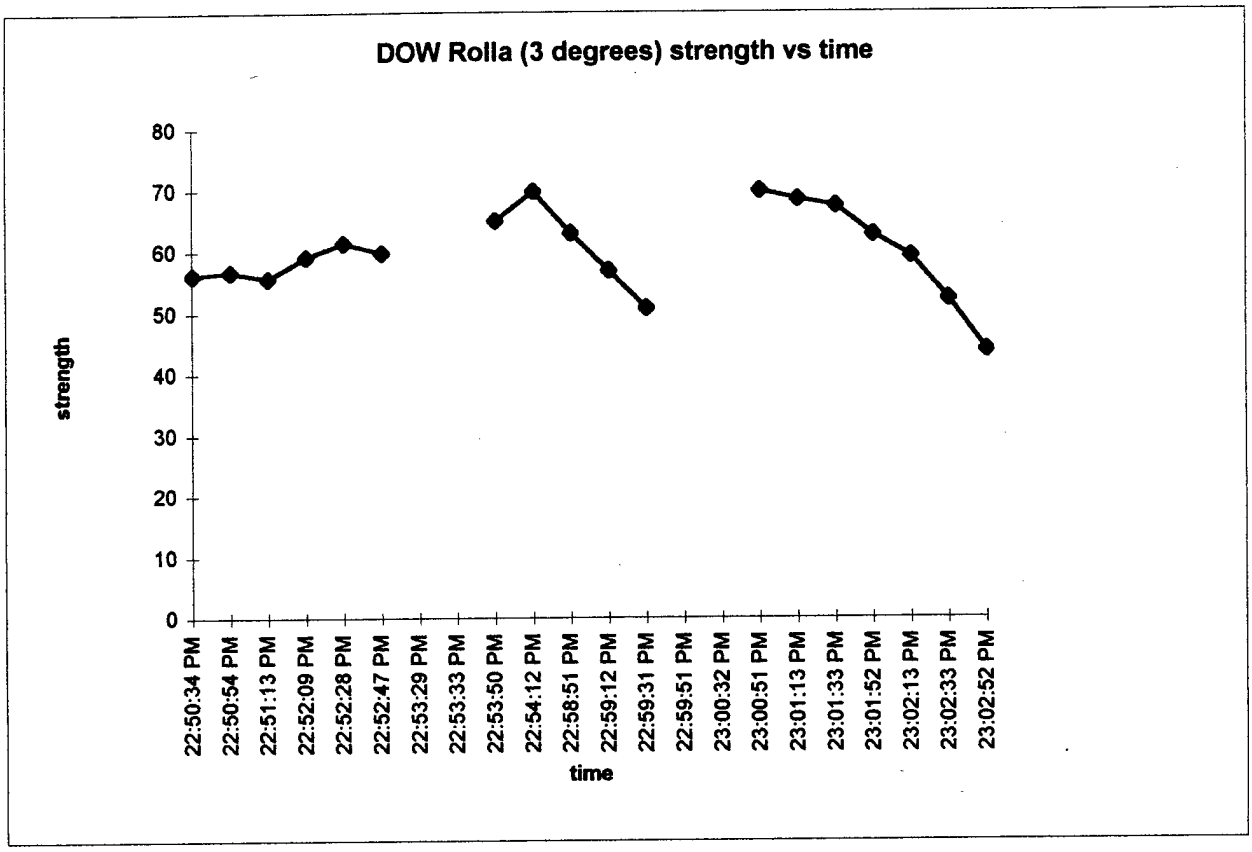


**Figure 3.13** Strength ($ms^{-1}$) (difference between the maximum inbound velocity and the maximum outbound velocity) of Rolla tornado versus time (UTC) taken from DOW data at the 3.0 degree elevation angle.

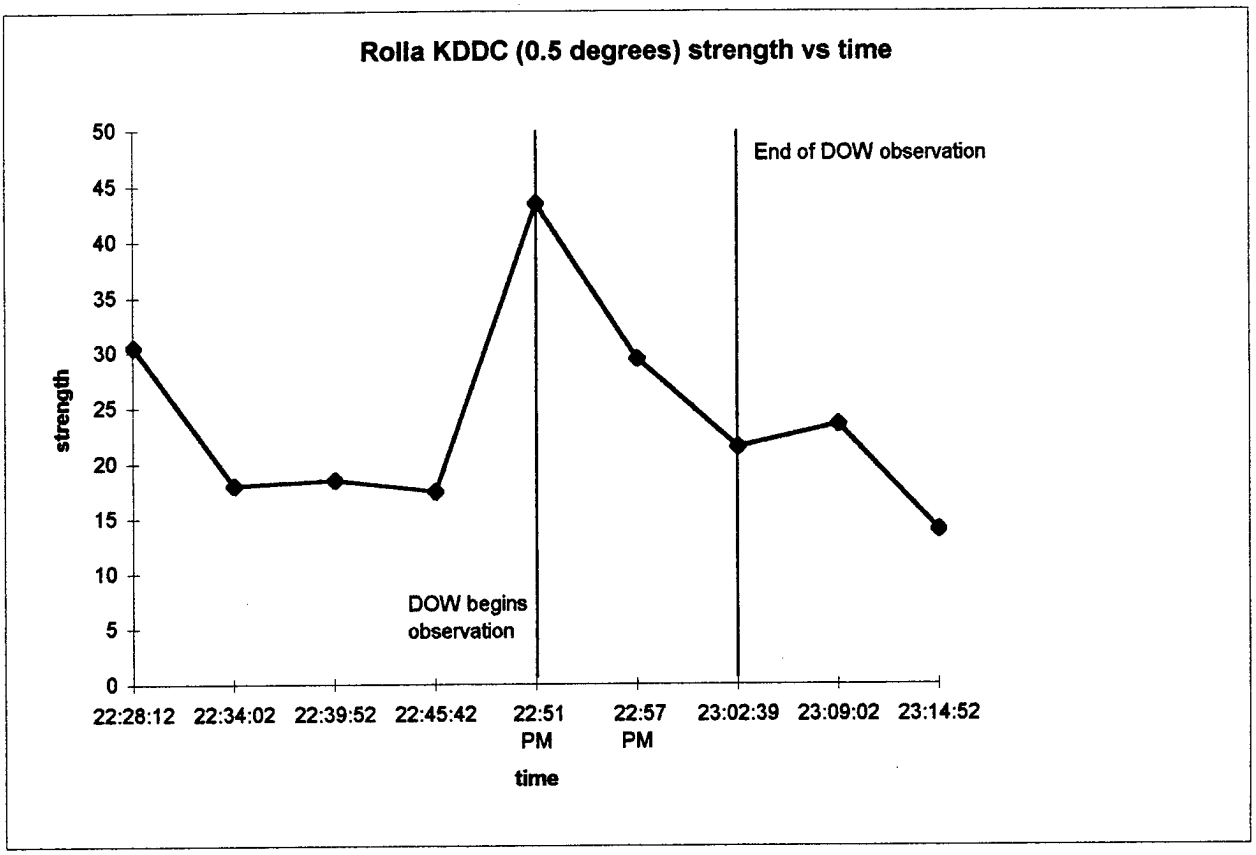


**Figure 3.14** Strength ($ms^{-1}$) (difference between the maximum inbound velocity and the maximum outbound velocity) of Rolla tornado versus time (UTC) taken from KDDC data at the 0.5 degree elevation angle.

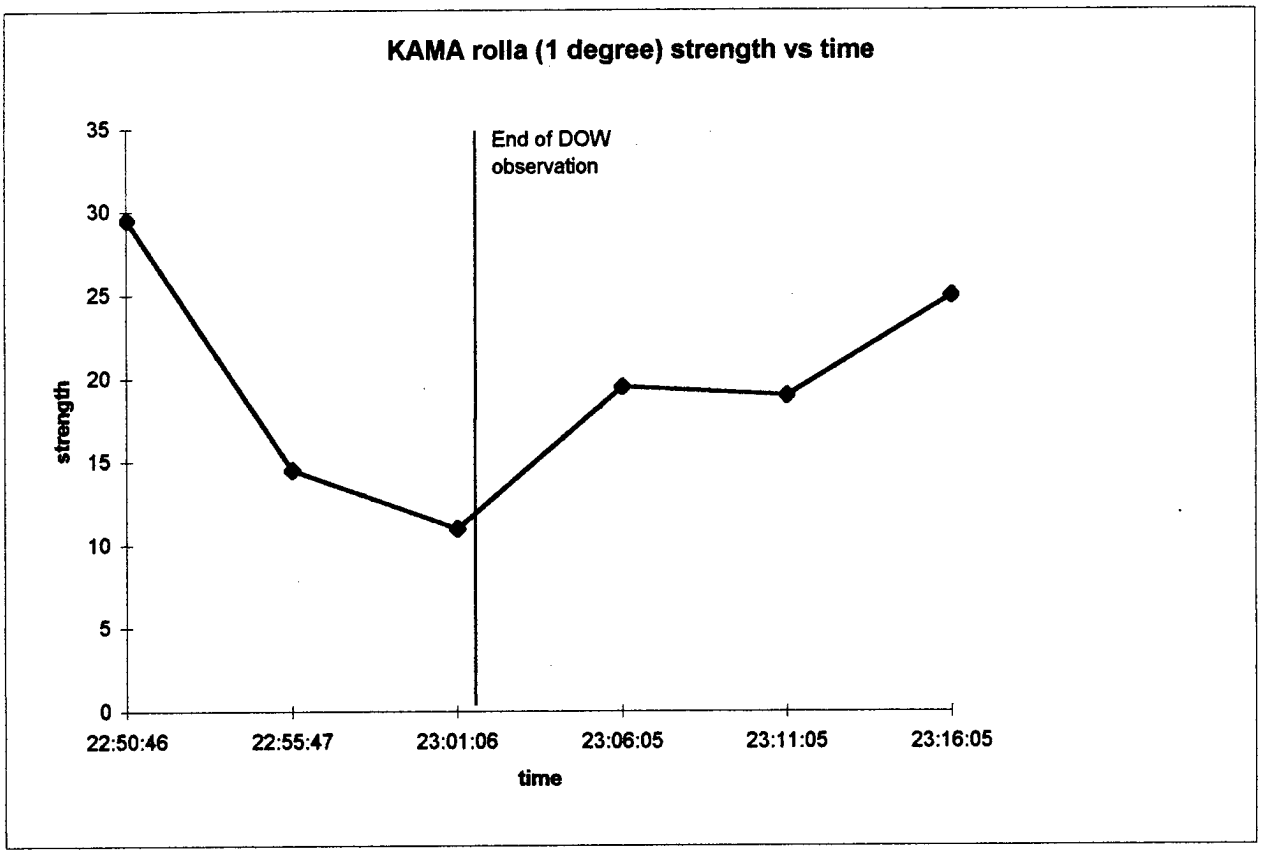


**Figure 3.15** Strength ($ms^{-1}$) (difference between the maximum inbound velocity and the maximum outbound velocity) of Rolla tornado versus time (UTC) taken from KAMA data at the 1.0 degree elevation angle.

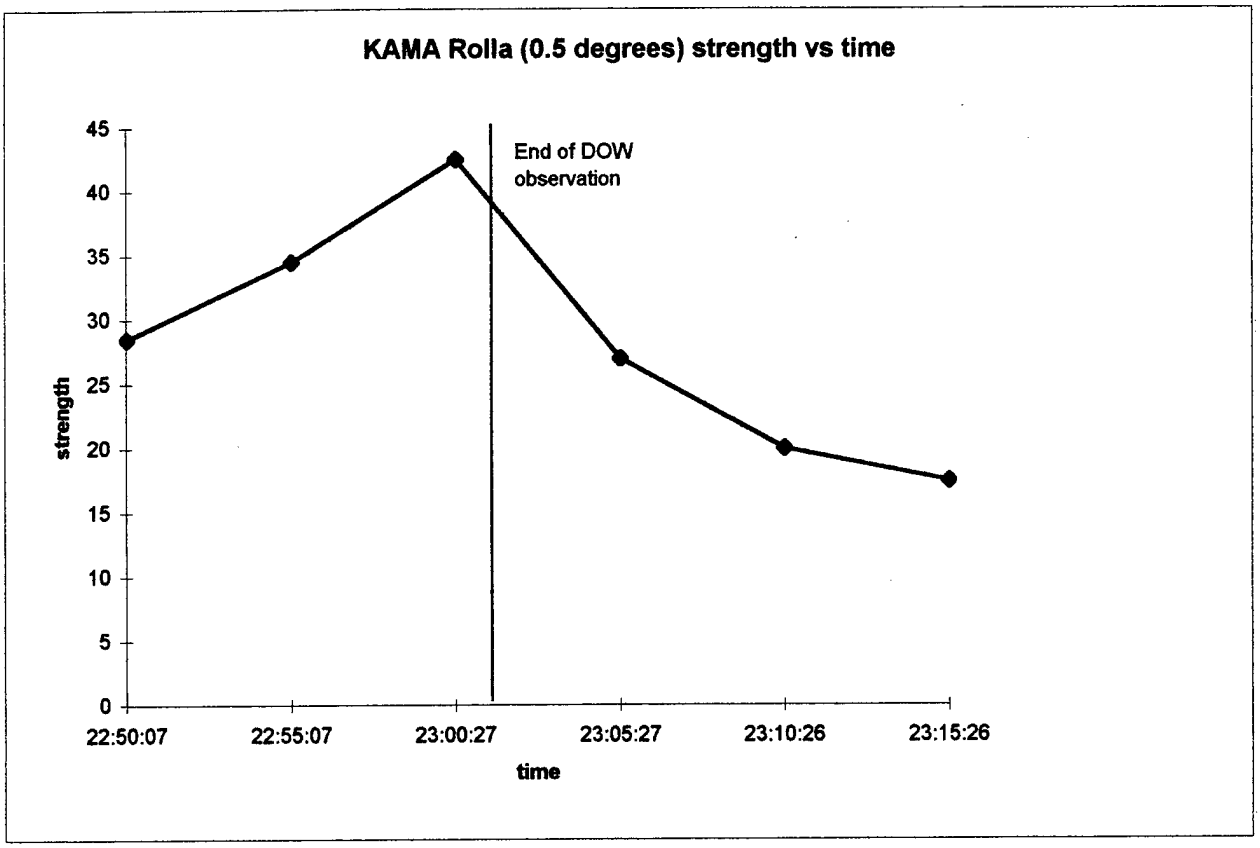


**Figure 3.16** Strength ($ms^{-1}$) (difference between the maximum inbound velocity and the maximum outbound velocity) of Rolla tornado versus time (UTC) taken from KAMA data at the 0.5 degree elevation angle.

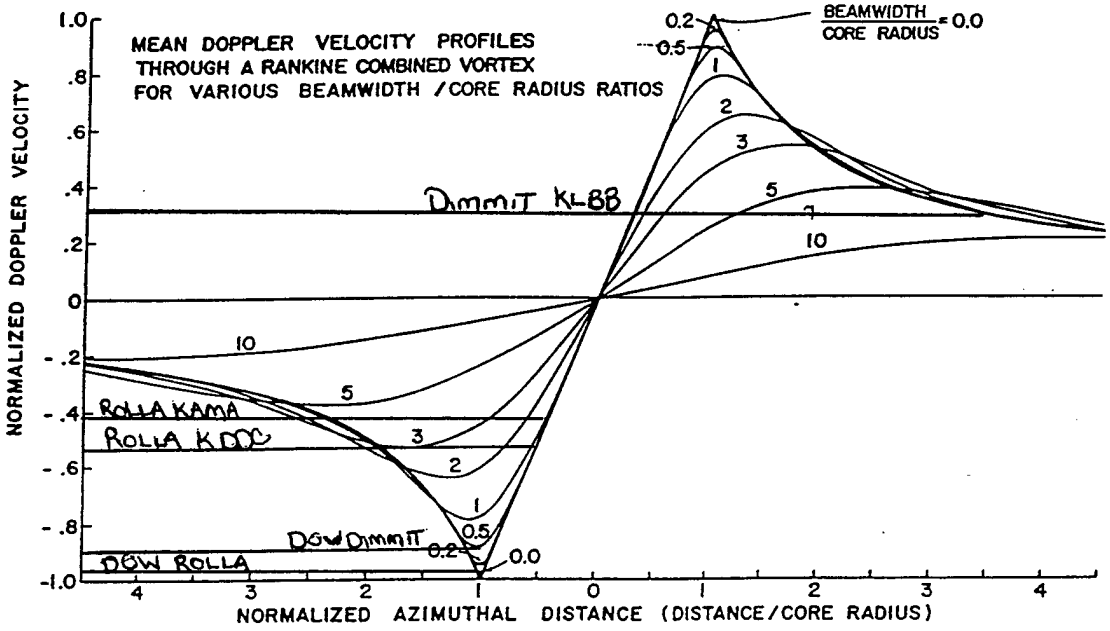


**Figure 4.1** Relation of beam width to vortex size (from Burgess, 1993)

# REFERENCES


Alberty, R., and T. Crum, Lt. Col., 1991: The NEXRAD program: past, present and future; a 1991 perspective. *Preprints, 25th International Conference on Radar Meteorology*, Paris, Amer. Met. Soc., 123-126.

Ahrens, C. D., 1994: *Meteorology Today an introduction to weather, climate and the environment fifth edition.* West Publishing Company, 418-444

Bennett, S. P.,1997:An overview of Hurricane Hortense and its aftermath. *Preprints, 22nd conference on Hurricanes and Tropical Meteorology.* Ft Collins, Amer. Met. Soc., 109-110.

Burgess, D.W., R. J. Donaldson, Jr., and P. R. Desroches, 1993: Tornado detection andwarning by Radar. *The Tornado: Its Structure, Dynamics, Prediction and Hazards, Geophys. Monograr.*, No. 79, Amer. Geophys Union. 203-221.

Cline, J. W., 1997: Surface-based wind and pressure fields in Hurricane Fran over North Carolina. *Preprints, 22nd conference on Hurricanes and Tropical Meteorology.* Ft Collins, Amer. Met. Soc., 643-644.

Dodge, P., S. Houston, and J. Gamache, 1997: Three dimensional windfields in Hurricane Fran (1996) at landfall. *Preprints, 22nd conference on Hurricanes and Tropical Meteorology.* Ft Collins, Amer. Met. Soc.,115-116.

Gamache, J. F., H. E. Willoughby, M. L. Black, and C. E. Samsury, 1997: Wind shear, sea surface temperature, and convection in hurricanes observed by airborne Doppler radar. *Preprints, 22nd conference on Hurricanes and Tropical Meteorology,* Ft Collins, Amer. Met. Soc. 121-122

Gentry, C. R., 1983: Genisis of tornadoes associated with hurricanes. *Mon. Wea. Rev.,* **40**, 1793-1805

Gill, S., 1998: High resolution radar observations of a tornado vortex: a study of Dimmitt, Texas 3 June 1995 UTC, and the Rolla Kansas tornado 1 June 1996 UTC. A Thesis for the School of Meteorology, University of Oklahoma.

Holton, J. R., 1992: *An introduction to Dynamic Meteorology Third Edition.* AcademicPress, 66-69.

Hondanish, S., S. Spratt, and D. Sharp, 1997: WSR-88d Characteristics of tornado Producing Convective Cells Associated with Tropical Cyclones. *22nd conference on Hurricanes and Tropical Meteorology.* pp 675-676.

Houston, S., M. D. Powell, and P. P. Dodge, 1997: Surface wind fields in 1996 Hurricanes Bertha and Fran at Landfall. *22nd conference on Hurricanes and Tropical Meteorology,* 92-93

Jorgensen, D. P., 1985: Vertical Motions in Intense Hurricanes. J. Atmos. Sci., 42, 839-856.

Jorgensen, D. P., 1984: Masoscale and convective-scale chracteristics of mature hurricanes. Part I: general observations by research aircraft. *J. Atmos. Sci.,* **41** 1268-1285.

Lee, W.,1997: Structure of Typhoon Herb (1996) observed by WSR-88D in Taiwan. *22nd conference on Hurricanes and Tropical Meteorology*, 670-671.

Marks, F. D. Jr., and P. P. Dodge, 1997: Hurricane concentric eyewall characteristics as revealed by airborne Doppler radar analyses. *Preprints, 22nd conference on Hurricanes and Tropical Meteorology,* 102-103.

National Climatic Data Center 1996: *Storm Data*, **38**, 78 Asheville NC

Schneider, D.G., L. Xie, and S. Raman, 1997: An investigation of the mesoscale and convective features or Hurricane Opal, *Preprints, 22nd Conference on Hurricanes andTropical Meteorology*, 119-120.

Wurman, J., J. M. Straka and E.N. Rasmussen, 1996: Fine Scale Doppler radar observations of tornadoes. Science, 272, 1774-1777

Wurman, J., J.M. Straka, E.N. Rasmussen, M. Randall, and A. Zahrai, 1997: Design and deployment of a portable, pencil beam, pulsed, 3-cm Doppler Radar. *J. Atmos. And Ocean. Tech.,* **14** 1502-1512

Wurman, J., and J. Winslow, 1998: Intense sub-kilometer boundary layer rolls in Hurricane Fran. *Science* **280** 555-557.

http://www.nhc.noaa.gov/fran.html